UNIVERSIDADE FEDERAL DO PARANÁ

LEDIANE MARCON

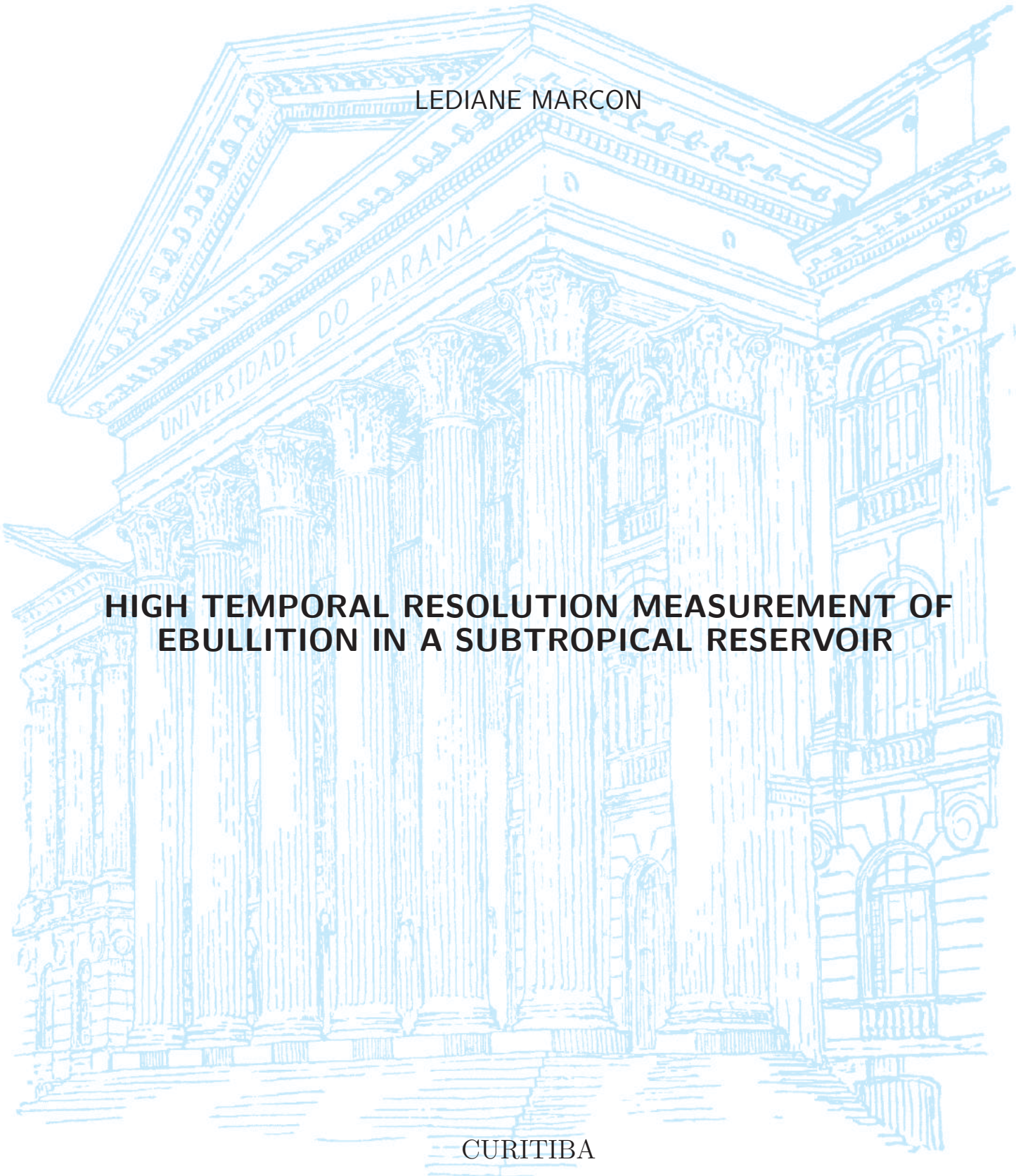


# HIGH TEMPORAL RESOLUTION MEASUREMENT OF EBULLITION IN A SUBTROPICAL RESERVOIR

CURITIBA

2018

LEDIANE MARCON

# HIGH TEMPORAL RESOLUTION MEASUREMENT OF EBULLITION IN A SUBTROPICAL RESERVOIR

Dissertação apresentada ao Programa de Pós-Graduação em Engenharia de Recursos Hídricos e Ambiental da Universidade Federal do Paraná, como requisito parcial à obtenção do grau de Mestre.

Universidade Federal do Paraná

Setor de Tecnologia

Programa de Pós-Graduação em Engenharia de Recursos Hídricos e Ambiental

Supervisor: Dr.-Ing Tobias Bleninger

Co-supervisor: D.Sc. Michael Männich

CURITIBA

2018

FICHA CATALOGRÁFICA ELABORADA PELO SISTEMA DE BIBLIOTECAS/UFPR
BIBLIOTECA DE CIÊNCIA E TECNOLOGIA

M321h Marcon, Lediane
High temporal resolution measurement of ebullition in a subtropical reservoir / Lediane Marcon. – Curitiba, 2018.
93 f. : il. color. ; 30 cm.

Dissertação - Universidade Federal do Paraná, Setor de Tecnologia, Programa de Pós-Graduação em Engenharia de Recursos Hídricos e Ambiental, 2018.

Orientador: Tobias Bleninger.
Coorientador: Michael Männich.

1. Variação temporal. 2. Armadilha automática para bolhas. 3. Emissão de metano. I. Universidade Federal do Paraná. II. Bleninger, Tobias. III. Männich, Michael. IV. Título.

CDD: 628.11

Bibliotecária: Romilda Santos - CRB-9/1214

MINISTÉRIO DA EDUCAÇÃO
SETOR TECNOLOGIA
UNIVERSIDADE FEDERAL DO PARANÁ
PRÓ-REITORIA DE PESQUISA E PÓS-GRADUAÇÃO
PROGRAMA DE PÓS-GRADUAÇÃO ENGENHARIA DE RECURSOS HÍDRICOS E AMBIENTAL

# TERMO DE APROVAÇÃO

Os membros da Banca Examinadora designada pelo Colegiado do Programa de Pós-Graduação em ENGENHARIA DE RECURSOS HÍDRICOS E AMBIENTAL da Universidade Federal do Paraná foram convocados para realizar a arguição da Dissertação de Mestrado de **LEDIANE MARCON**, intitulada: **HIGH TEMPORAL RESOLUTION MEASUREMENT OF EBULLITION IN A SUBTROPICAL RESERVOIR.**, após terem inquirido a aluna e realizado a avaliação do trabalho, são de parecer pela sua aprovação no rito de defesa. A outorga do título de Mestre está sujeita à homologação pelo colegiado, ao atendimento de todas as indicações e correções solicitadas pela banca e ao pleno atendimento das demandas regimentais do Programa de Pós-Graduação.

Curitiba, 16 de Fevereiro de 2018.

TOBIAS BERNWARD BLENINGER(UFPR)
(Presidente da Banca Examinadora)

CRISTOVÃO VICENTE SCAPULATEMPO FERNANDES(UFPR)

STEPHAN HILGERT(KIT)

MICHAEL MANNICH(UFPR)

MARCO AURELIO DOS SANTOS(UFRJ)

À um grande filósofo. *In memoriam.*

# Acknowledgements

It was a hard but gratifying way to conclude this stage. The knowledge is something incredibly interesting, fascinating, and dingy. The most astonishing thing is that it is not a lonely pathway, in fact, this dissertation was a result of several contributions of surrounding people. Each contribution (scientific and emotional) was extremely appreciated.

I would like to express my deep gratitude to my supervisor professor Tobias Bleninger, for been a very optimistic person, for showing that the world is a place where changes are possible, and for being very patient. Thank you for trusting in my work and for the support. I enjoyed listening to your experiences. I have learned a lot, and I include, of course, how to drive a boat.

I am very grateful to my co-supervisor professor Michael Mannich. For all the field campaigns. Were tiring days of hard work, full of field surprises (some of them not so good), but always with very interesting discussions. Thank you for sharing your ideas and for keeping me always motivated, even after those initial months of no data.

All professors from the Department of Hydraulics and Sanitation (DHS). Especially the coordinator and professor Cristóvão. Your character, dedication, and concern for each one of us are admirable. You have a great soul. I will never be able to thank enough for your kind words, they made a huge difference for me.

This study was possible due to the collaboration of several people and institutions. I kindly thanks the company SENECT who developed the Automated Bubble Traps and Andreas Maeck by providing the continuous support for the equipment; The Karlsruhe Institute of Technology (KIT) for the support and supervision, specially Dr. Stephan Hilgert ; The sanitation company Sanepar which manages the Passaúna reservoir and allowed the study to be conducted in the reservoir; The Coordination for the Improvement of Higher Education Personnel (CAPES) by the financial support through a master scholarship; the project NoPa-SeWaMa for financial support for material and field campaigns; and institutions as Smart Energy - TecPar and Instituto das Águas do Paraná by the available data.

I thank my family, above all my parents and siblings for their love and trust. My niece Laura and nephews Jonas, Vinícius, and Josué for all the happy moments; Josué your young age and your brilliant mind inspire me.

I am glad I have met very nice colleagues at the PPGERHA, who have made the work environment lighter and the work more enjoyable. I also thank all the university's employees. Our secretary Celmar for your dedication and for all solved issues.

Friends have an important role in our life. I thank them all, old and new ones. Especially my dear friend Cristina from who I learned a lot, and for being so helpful, and a good listener.

# Resumo

Corpos d'água, tanto natural quanto artificial, são fontes de metano para a atmosfera. O metano é formado no sedimento de reservatórios a partir da decomposição da matéria orgânica em condições anóxicas. Apesar do metano ser liberado para a atmosfera por três processos principais: ebulição, difusão e através de plantas com raiz, a ebulição é o caminho predominante. A ebulição é um processo complexo. Depende espacialmente de fatores que atuam sobre grandes distâncias (mudanças de pressão atmosférica, incidência de ventos, entre outros), fatores que agem localmente (características do sedimento, produção de gás, biota, etc.) e varia temporalmente devido às oscilações dos parâmetros com o tempo. O objetivo principal desta pesquisa foi obter medições contínuas de ebulição em um reservatório de água localizado em Curitiba - PR, Brasil, avaliar a variabilidade temporal das emissões e investigar possíveis correlações com condições ambientais. Três armadilhas automáticas de captura de gás (ABT), que são funis invertidos que permanecem submersos na coluna d'água, foram utilizados para realizar medições contínuas do fluxo de gás com registros em intervalos de 15 segundos. Dados auxiliares foram obtidos com medições realizadas diretamente no reservatório ou a partir de estações instaladas nas proximidades da área de estudo. Os resultados obtidos pelos ABTs estiveram de acordo com medições feitas com funis convencionais. A serie temporal de dados de ebulição evidenciou a grande variabilidade temporal existente, os fluxos com menor intensidade ocorreram com maior frequência e predominando intervalo entre eventos menor que 10 minutes. As emissões variaram espacialmente, sendo os maiores fluxos registrados no ponto de média profundidade (P2). Foi observado nos fluxos uma forte variação sazonal. O fluxo médio registrado durante o verão no ponto P2 foi 16 vezes superior ao fluxo médio que ocorreu durante final do outono e início do inverno. Essas variações foram atribuídas a uma combinação de alterações das condições químicas da coluna d'água e às características de armazenamento do gás no sedimento. Além disso, fluxos de maior intensidade estiveram correlacionados à períodos de redução na pressão atmosférica e à incidência de ventos com maior intensidade. Por fim, foi mostrado que medições realizadas durante curtos períodos tendem a subestimar o fluxo médio de gás.

**Palavras-chaves**: Variação temporal. Armadilha automática para bolhas. Emissão de metano.

# Abstract

Water bodies, either natural or man-made impounded areas, are sources of methane to the atmosphere. Methane can be formed in the anoxic region at bottom sediments of reservoirs by decomposition of organic matter. Although there are three main ways through which methane reach the atmosphere: ebullition flux, diffusion flux and through rooted plants, the ebullition flux is the dominant pathway. Ebullition is a complex process spatially dependent on factors acting over large distances (atmospheric pressure changes, wind, so forth) and factors acting locally (sediment characteristics, gas production, biota, etc), and temporal variable due to parameters' oscillation with time. As a consequence, the temporal resolution of measurements and their sampling time have an effect on understanding the process and in determining ebullition rates. The main objective of this research was to obtain continuous measurements of ebullition in a freshwater reservoir located in Curitiba - PR, Brazil, to evaluate its temporal variability, and to investigate possible correlation with ambient conditions. Three Automated Bubble Traps (ABT), which are inverted funnels that stay submerged in the water column, had been used for continuous measurement of gas flux in time steps of 15 seconds. Auxiliary data were obtained either through direct measurement in the reservoir or from stations nearby the study site. ABTs measurements agreed with measures from conventional funnels. The time series data showed the large temporal variability in ebullition, the less intense fluxes occurred with higher frequency and prevailing a time interval between events smaller than 10 minutes. Emissions fluxes varied spatially; the largest mean fluxes were recorded from the middle depth location (P2). A strong seasonal variation was observed in the fluxes. The mean gas emission recorded during summer time at P2 was sixteen-fold the mean flux of late fall and beginning of winter period. The variations were attributed to a combination of changes in the water column chemical conditions and sediment characteristics of gas storage. In addition, high flux events were correlated with reductions in the atmospheric pressure and increased winds intensities. Lastly, it is showed that short-period of sampling time tends to underestimate the mean gas emission flux.

**Key words**: Temporal variability. Automated Bubble Trap. Methane emission.

# List of Figures

# List of Tables

# Contents

# Introduction

Reservoirs of different sizes have been constructed worldwide with various purposes as for water supply, energy generation, flood control, agriculture use and recreation. In a survey performed to identify large dams, Lehner et al. (2011) pointed out that there are 6862 dams with its reservoirs around the world, yet a number of reservoir might not be included in the list due to lack of information. In Brazil, for instance, data published by the National Agency of Water (ANA) showed a number of 6928 man-maid reservoirs with surface area greater than 20 ha, this number includes all sorts of reservoirs such the ones used for aquaculture or irrigation purposes (FUNCEME, 2008).

In addition to a large number of existing reservoirs, a considerable number of new dams are expected to be constructed due to the increase in water demand. Zarfl et al. (2014) found that in 2014, 3700 dams for hydropower generation were under construction or planned mainly in countries with emerging economies, such as Brazil. Brazil has faced severe water crisis, mainly in the biggest economic centres, as São Paulo and Rio de Janeiro located in the Southeast region of the country. A period of drought, which started in 2014, caused a reduction in reservoirs water levels and lead to temporary cessation of water supply in some regions and reduction of the minimum flow rate. In Paraíba do Sul river, for example, the minimum flow rate was shortened to 58% of the regular flow rate (BRITTO; JOHNSSON; CARNEIRO, 2016). In this scenario, reservoirs play an important role in water supply and in some cases they have a relevant share for the total amount of water delivered for public use. The Passaúna reservoir located near to Curitiba-PR supplies water for 22% of the population in the metropolitan region.

Nonetheless, damming of rivers for reservoir construction changes the riverine characteristics of the impounded water body to a lentic system. The alterations are manifold such as reduced flow velocity, increased sediment retention (VÖRÖSMARTY et al., 2003), reduced vertical mixing, modification of the vertical distributions of substances and their concentration in the water column and in the sediment (FRIEDL; WÜEST, 2002), as well as biological impacts mainly on the diversity and abundance of aquatic organisms upstream and downstream of the dam due to alterations in the transfer of nutrients (MAAVARA et al., 2015).

A more recent topic related to reservoirs are their potential contribution to greenhouse gases (GHG) emissions. After Rudd et al. (1993), who based on previous measurements of carbon dioxide and methane fluxes tested the hypothesis that hydropower reservoirs contribute to greenhouse gas emissions, several studies, some of which will be mentioned throughout the text, have investigated this topic, however, some processes are still not totally understood. Studies conducted and published by IPCC (2013) have shown tendencies regarding changes on global climate and the contribution of greenhouse gases to these changes strengthening, in this way, the importance of understanding and quantifying gas emissions from reservoirs.

The organic matter retained in the reservoir becomes available for bacterial decomposition. Water column thermal and chemical stratification, in addition to high rates of dissolved oxygen consumption by bacterial activity causes the formation of anoxic zones, which provide conditions for methane formation. Methane is a potent greenhouse gas and its concentration in the atmosphere increased by 150% compared to pre-industrial concentrations (MYHRE et al., 2013). This gas has a global warming potential (GWP) 34 times greater than $CO_2$ for a 100-years time scale (MYHRE et al., 2013). Ongoing research aims at investigating the magnitude of freshwater methane emissions and the contribution of man-made water bodies.

The total amount of gas emitted by water bodies is still not a consensus. Teodoru et al. (2012) measured carbon dioxide and methane emissions for pre-flood and post-flood situations of Eastmain-1 reservoir located in Quebec - Canada. The main findings were that the flux of carbon dioxide to the atmosphere was higher in the first years after flooding even after three years past impoundment the flux was still threefold the mean flux for water bodies in the region. In the case of methane, there wasn't a large variation comparing before and after flooding conditions, mainly because emissions through gas bubbles were not considered in the study. Nevertheless, such behavior for gas flux may be quite different for reservoirs located in tropical regions as for these cases reservoirs do not have an ice covered period.

ST. LOUIS et al. (2000) compiled data of reservoir area from the International Commission on Large Dams (ICOLD) with carbon dioxide and methane fluxes and estimated that for tropical regions methane emissions from reservoirs is $300\,\mathrm{mg\,m^{-2}\,d^{-1}}$, this flux is fifteenfold the flux estimated for temperate reservoirs. Following ST. LOUIS et al. (2000)' work Deemer et al. (2016) gathered additional information from both diffusion and ebullition gases emissions from reservoirs worldwide. The authors estimated global carbon emission due to methane from reservoirs as $120\,\mathrm{mg\,m^{-2}\,d^{-1}}$ which is higher than the emissions calculated for other water bodies. According to ST. LOUIS et al. (2000) on a global scale methane emission from reservoirs can represent 20% of the anthropogenic sources for atmospheric methane.

Although several researches have attempted to estimate the contribution of reservoir on greenhouse gas emissions, information is still missing. Processes such as gas bubble formation and its eventual release from sediment is reported to have a large spatial and temporal variability implying that obtaining accurate results requires measurements over long periods of time covering large area (Del SONTRO, 2011). This large variability on fluxes and strategies that could be used to handle it are still a challenge faced by researchers, mainly when costs are taken into account.

Among the existing methods for fluxes measurements, ebullition is commonly obtained by the use of inverted funnels that are placed submerged in the water column or by floating chambers which also measures diffusion flux. Both mentioned methods remain in water for short periods of time (minutes to hours, maximum for a few days) and fluxes are not recorded in discrete time intervals, but an integrated value for the entire period is obtained instead. New alternatives of measurement have been developed such as automated bubble traps, which are a version of the conventional funnels with the advantage of performing automatic measurements with high temporal resolution (VARADHARAJAN; HERMOSILLO; HEMOND, 2010; MAECK; HOFMANN; LORKE, 2014).

With respect to the emissions from subtropical reservoirs, not many studies have measured ebullition flux and none with high temporal resolution measuring over long periods were found in Brazil This research is the first to present measurement results of ebullition from a Brazilian reservoir obtained by automated bubble traps. In addition to the large number of reservoirs already constructed, there are many reservoirs planned to meet either water supply or electric generation needs. A report produced by the Ministry of Mines and Energy (MME) pointed that nowadays Brazil is the second largest hydroelectric producer supplying 75% of the electricity consumed through hydro resources and does not have full capacity installed (MINISTÉRIO DE MINAS E ENERGIA, 2015).

Brazil had committed to developing actions towards sustainable development. The National Plan on Climate Change (COMITÊ INTERMINISTERIAL SOBRE MUDANÇA DO CLIMA, 2008) establishes goals including reduction of greenhouse gases emissions and development of national programs to mitigate and adapt to climate change. A most recent is the Paris agreement, in which the country pledged to reduce greenhouse gases emissions. In this scenario, studies that assess emissions might contribute with the knowledge to be used in developing mitigating measures and to provide decision makers

with additional information to be considered in the impact analysis of new reservoirs constructions.

# Objective

The main objective of this dissertation was to address the temporal variability of ebullition flux in a freshwater reservoir by measuring gas flux with a high temporal resolution during several months and to investigate the possible relation of this events with environmental forcings.

## Specific objectives

- Defining the prototype operational configuration of the Automated Bubble Traps by establishing laboratory test and operational analysis;
- Obtaining continuous gas flux records from Passaúna reservoir by installing and maintaining the equipment in the field;
- Complementing flux records with records of environmental data by installation of environmental sensors, and elaboration of in-situ measurements;
- Identifying potential environmental forcings, triggering ebullition, by processing data records using statistical methods and correlation techniques.

# Dissertation structure

This dissertation is divided into four main sections. In the first section is presented a brief literature overview including aspects of the carbon cycle and methane formation, followed by the ebullition process and the techniques that are currently applied to gas measurement in water bodies. Sections 2 and 3, which are entitled materials and methods respectively, present details about the study site, all the equipment used for measurements, how measures were conducted and how data was processed. In the last section are shown the results obtained and the analysis done compared with information from the literature. It was also added to the section the main conclusions of this research and an overview of field activities conducted.

# 1 Greenhouse gas emission measurements from inland waters

This chapter covers a brief description of carbon forms found in water bodies as reservoirs and its main sources. In addition, it is presented in detail how gas bubbles are formed in sediment and the processes that have an effect on its release to the atmosphere. Lastly, it is given an overview of techniques applied for ebullition measurement.

## 1.1 Carbon cycle in reservoirs

The biogeochemical cycles refer to the dynamics of chemical components and matter within 'reservoirs' or compartments of the environment. A compartment can be either a biotic or an abiotic component through which chemical substances and matter flows in different forms (ODUM; BARRETT, 2007).

There are several biogeochemical cycles widely studied that play an important role for the organisms and for the environmental conditions. As examples are the cycles of water, carbon, nitrogen, phosphorus, and so forth. Carbon is present in water in the form of different components and its cycle is characterized by complex processes which may vary from one place to another (LAMPERT; SOMMER, 2007).

Carbon in water is divided into an organic fraction and an inorganic fraction, Figure 1. In the organic fraction carbon is present dissolved in the water (DOC) or particulate (POC). The DOC, which comes from the decomposition of plants and animals and also from organisms excretion, can be grouped in distinct substances such as proteins, humic substances, and carbohydrates (ESTEVES, 1998). The POC portion includes carbon sources from suspended organic matter, detritus, biota and from suspended sediment (ESTEVES, 1998). Thus, the DOC and the POC are formed from either allochthonous matter that enters the water body or from autochthones sources.

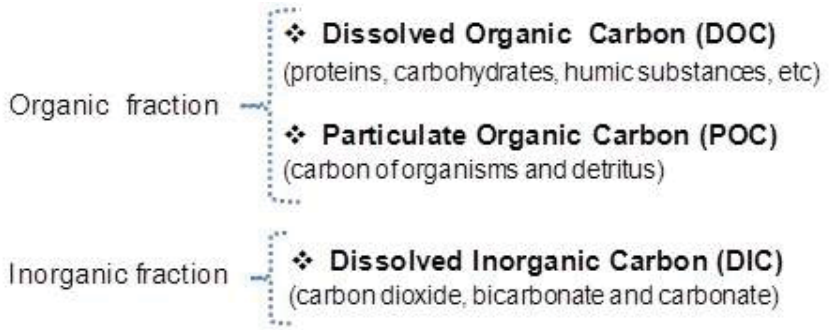


Figure 1: Main fractions of carbon encountered in water bodies.

According to Lampert and Sommer (2007), the inorganic fraction of carbon is found dissolved (DIC) as carbon dioxide, bicarbonate, and carbonate. The main sources of DIC are gaseous exchange with the atmosphere and through biologic activities as respiration and decomposition. The authors also

point that comparing DOC, POC, and DIC with respect to the amount of each form the DIC usually prevails followed by DOC and lastly by the POC.

The main carbon supplies for the reservoirs are organic matter from the catchment, from autochthones sources and from the flooded area (International Hydropower Association (IHA), 2010). Reservoirs have the characteristics of lentic environments where the biogeochemical processes, as well as the vertical distribution of substances and biotic components, differs from riverine conditions. The load of organic matter can either settle in the reservoir or stay suspended in the water column, for both cases its decomposition by bacterial activities results in gas production such as methane ($CH_4$) and carbon dioxide ($CO_2$). As mentioned by Sobek et al. (2012) sedimentation rates that occur in the reservoir can provide enough organic matter for methane production which will be available for oxidation or might reach the atmosphere.

The flooded area characteristics such as vegetation and soil type may have a large contribution to emissions and gas formation mainly in the first years after flooding. This behavior is noticed with the tendency of emissions to decline over the years (TEODORU et al., 2012). ST. LOUIS et al. (2000) point that gas formation relies on the amount of carbon that is contained in the flooded area. According to the authors, a portion of the inundated matter is labile carbon which is easily decomposed in the first years while older organic carbon from tree boles and soil are not readily decomposable and will take longer to be decomposed. Nonetheless, in the case of methane, it wasn't verified a variation on emissions over the years, owning to missing measurements from gas bubbles (ST. LOUIS et al., 2000; TEODORU et al., 2012). Another aspect that should be considered is that unlike in river conditions, reservoir creates a barrier for sediment and matter coming from the catchment which in anoxic conditions such as in the bottom sediment is favorable to methane formation and might contribute to maintaining methane emissions not so variable over the years.

## 1.2 Methane emissions and processes

Greenhouse gases have dropped the attention due to its radiative forcing on climate and mainly in their potential to increase the earth temperature. Methane is reported to have a global warming potential 34 times greater than carbon dioxide for 100-year time frame and its concentration in 2011 exceeded pre-industrial levels by 150% (MYHRE et al., 2013), thus methane and its sources have been the subject of many studies. ST. LOUIS et al. (2000) reported that on a global scale methane emission from reservoirs can represent 20% of other sources of anthropogenic methane.

Four processes account for methane formation in natural systems: biogenesis, thermogenesis, geogenesis and ignigenesis (VALENTINE et al., 2004). Valentine et al. (2004) summarizes that among all processes biogenesis, also called methanogenesis, which results from microbial metabolism, can occur at temperatures from 0 to 100°C and account for more than 85% of the methane produced. According to Smith et al. (2003) methane formation from decomposition of organic matter will start after complete reduction of $O_2$, $NO_3^-$, $Fe^{3+}$, $Mn^{4+}$, and $SO_4^{2-}$. Such anoxic and low redox conditions are commonly found in the bottom sediment of reservoirs.

There are different methanogenic pathways that result in methane formation, however, the two most important transformations are the carbon dioxide reduction (Equation 1.1) and the aceticlastic reaction (Equation 1.2), as presented by Valentine et al. (2004). According to Lampert and Sommer (2007) two-thirds of the methane is formed by the acetate pathway.

$$CO_2 + 4H_2 \rightarrow CH_4 + 2H_2O \tag{1.1}$$

$$CH_3COO^- + H^+ \rightarrow CH_4 + CO_2 \tag{1.2}$$

Although it was widely supported that in anoxic conditions prevails methane while in oxic environments carbon dioxide predominates (ESTEVES, 1998; LAMPERT; SOMMER, 2007), the so-called "methane paradox" highlighted situations in which saturation of dissolved methane were verified in oxic layers of water (KEPPLER et al., 2009; TANG et al., 2014). According to the study conducted by Tang et al. (2014), in Lake Stechlin (northeast Germany) the peak of methane concentration found in the thermocline was due to methane production in the oxygenated water related to photosynthesis, nitrogen fixation, and reduction of methane photo–oxidation, which contributed to accumulation of dissolved methane in this water layer.

After formed, methane can be either accumulated in sediment or dissolved in the water column or be transferred to the atmosphere. There are three main paths from which methane can reach the atmosphere: diffusion flux, ebullition flux and through rooted plants (JOYCE; JEWELL, 2003). While the diffusion flux is driven mainly by methane concentration gradients between water and atmosphere (BASTVIKEN et al., 2004), ebullition flux is not continuous and is influenced by several factors, which will be better discussed in this document. Rooted plants can either be favorable to methane production or suppress methane production and it must be taken into account in wetlands and rice paddies (SEGERS, 1998).

Besides ebullition, diffusion, and flux through rooted plants, degassing also contributes to methane emissions. Degassing occurs after water passes through turbines and spillways. A representation of the methane transference pathways is shown in figure 2.

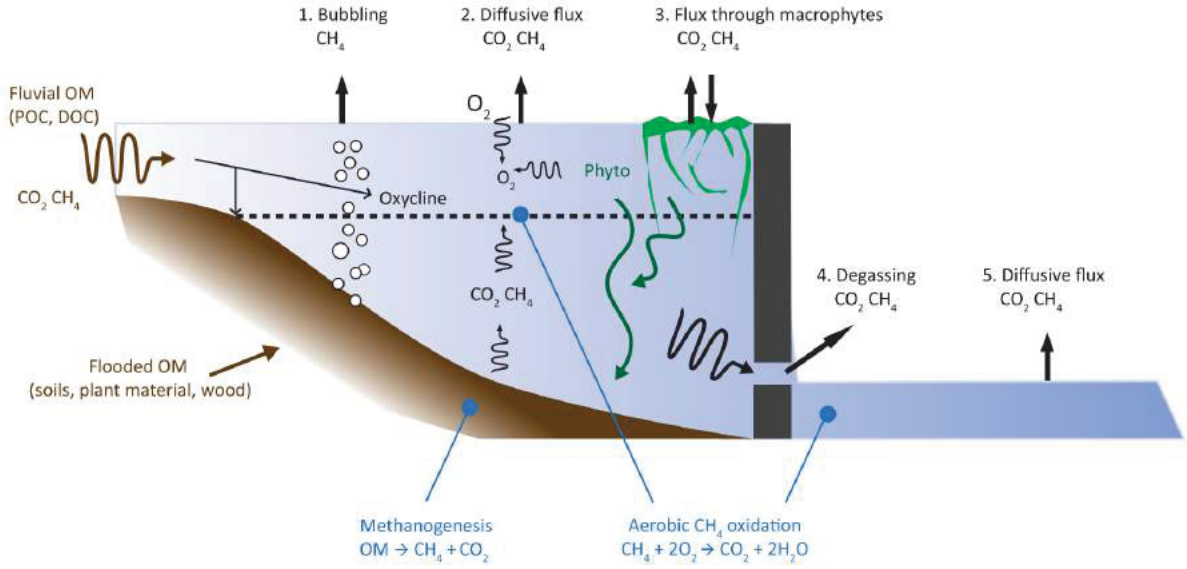


Figure 2: Pathways of carbon dioxide and methane in a freshwater reservoir. Source: International Hydropower Association (IHA) (2010).

In addition to the mechanisms of gas transference mentioned, Bastviken et al. (2004) point storage flux as another important pathway. According to the author in stratified lakes methane can be stored in the anoxic layer until water turnover when then is easier for methane to diffuse to the atmosphere without being oxidized. Methane oxidation occurs in the presence of oxygen through bacterial activity known as methylotrophic bacteria, which occurs mostly in the transition zone between anoxic and oxic regions (LAMPERT; SOMMER, 2007).

Another way of reducing the amount of methane in the water is through anaerobic oxidation. However, Segers (1998) noted that the amount of methane oxidized by anaerobic processes is smaller than the amount of methane emitted. Furthermore, Lampert and Sommer (2007) stated that in freshwater this process does not play an important role since the sediments are often poor in sulfate and this oxidation occurs by the electron transference between archea and sulfate-reducing bacteria and therefore, it is reasonable to neglect anaerobic oxidation in reservoirs.

In a study conducted by Bastviken et al. (2004), they estimated what would be the contribution of each pathway (ebullition, diffusion and storage flux) to the total methane emission to the atmosphere, Figure 3. The main observations were that emissions from ebullition can be between 40–60% of the total methane emitted; Diffusion can represent up to 50% in lakes with a large area and on the other hand storage flux is higher in lakes with a small area where it can contribute up to 45% of total emissions (BASTVIKEN et al., 2004). Although Figure 3 illustrates the relative contribution of different pathways to methane emissions, the authors pointed that besides lake area ebullition depends upon several other parameters, which are mentioned in the following paragraphs, and thus, considering just lake or reservoir area may not be enough to quantify and to represent the heterogeneities of emissions among different water bodies.

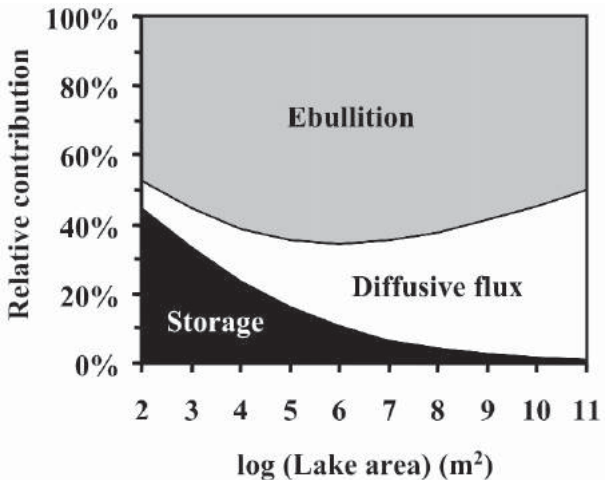


Figure 3: Contribution of ebullition, diffusive flux and storage flux related to lake area. Source: Bastviken et al. (2004).

Bastviken, Ejlertsson and Tranvik (2002) carried out a study on methane oxidation in lakes and observed that the percentage of methane oxidized before reaching the atmosphere varies from 57–100%, which indicates that diffusion is not the most efficient way of transporting methane through the water column. A similar observation was made by Deemer et al. (2016). The authors compiled results from measurements of different reservoir worldwide and mean methane emission from total diffusion and ebullition fluxes were estimated to be more than twofold the mean emissions from diffusive flux only. Nevertheless, the contribution of ebullition is reported to vary from 0 to 99% which indicates that it is important to know the peculiarities of each water body and to measure both fluxes when total emissions are to be considered (DEEMER et al., 2016).

In contrast to diffusion which is a slow process, bubbles rapidly transport gas through the water column and as a consequence, the losses due to oxidation are smaller (JOYCE; JEWELL, 2003; LAMPERT; SOMMER, 2007). Nevertheless, the amount of methane released into the atmosphere depends on the methane concentration in gas bubbles which in turn, rely on the organic matter characteristics and the ambient conditions. For Saar River in Germany Maeck, Hofmann and Lorke (2014) determined

methane concentration in bubbles through gas chromatography and found concentrations varying from 48.6% to 92.1%. For hydroelectric reservoirs in Brazil Santos et al. (2006) found methane concentration in bubbles as high as 97%.

## 1.3 Ebullition processes

Ebullition is normally associated with methane bubbles, as they are formed in the bottom sediment of water bodies from the decomposition of organic matter in anoxic conditions which results in methane production. In addition, this gas is less soluble in water in contrast with other gases as carbon dioxide and nitrous oxide (DEEMER et al., 2016), as a consequence, the concentration of methane present in the bubbles tend to be greater than the portion of other substances.

Bubble formation occurs when water in the sediment became supersaturated and the dissolved gas molecules might merge forming bubbles, which is also denominated as free gas (ANDERSON et al., 1998). Joyce and Jewell (2003) observed that a large portion of methane ebullition comes from the top sediment layer from 10 cm to 20 cm. Bubbles contained in the sediment might be divided into three types (ANDERSON et al., 1998), Figure 4.

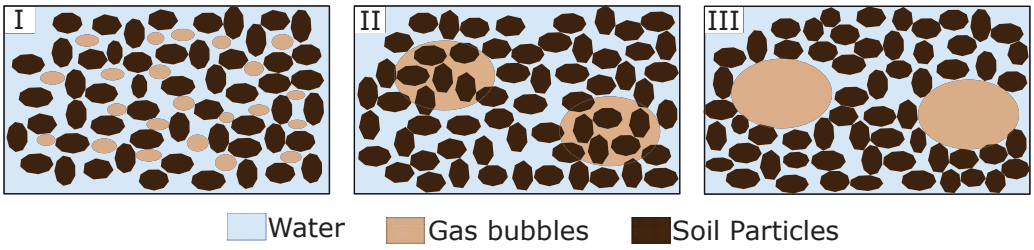


Figure 4: Type of bubbles in the sediment. Modified from Anderson et al. (1998).

According to Anderson et al. (1998) type I bubbles are small and can float within the interstitial pore water. In the case II some of the soil voids are fulfilled by gas which leaves "dry" spaces, and in the third configuration (case III), bubble displaces the soil particles. By analyzing seafloor samples from Eckernförde Bay Anderson et al. (1998) noticed the presence of methane bubbles prevailing type III configuration with a size range of 0.42 mm to 5 mm equivalent radius.

The growth of gas bubbles in sediment depends on the sediment characteristics. In fine-grained cohesive sediments, Algar, Boudreau and Barry (2011a) suggest that bubbles grow by elastic expansion and fracture. According to the author, pressure caused in the bubble walls due to the inside gas opens fracture in the sediment, and results in stress forces in the surroundings; the fracture propagates if the stress caused by bubble pressure exceeds the intensity that the material can endure.

Bubble growth can be divided into two parts: In the first case, which stress intensity around the fracture provoked by the gas is smaller than the intensity that the material can support, bubble increases its width by elastic expansion; and for the second case the stress intensity due to gas is greater than the intensity that the material can support provoking a propagation of the fracture and as a result, bubbles expand by fracture alternating with elastic expansion (ALGAR; BOUDREAU, 2009).

On the other hand for sandy sediments, gas can percolate through sediment pores and leave regions free of water (ALGAR; BOUDREAU; BARRY, 2011a), Figure 4.II. Jain and Juanes (2009) studied gas migration in seafloor at grain scale. The authors suggested that while in fine-grain sediment fracturing processes prevail in gas transport, in coarse-grain sediment capillary invasion dominates. According to

the researchers, the gas occupies the soil pores when the capillary pressure is greater than the capillary entry pressure.

In sediment, bubbles rise due to a buoyant force which arises from the pressure difference between the top and the bottom portion of the bubble and the density differences of the bubble and the ambient (ALGAR; BOUDREAU; BARRY, 2011a). The increase in bubble size leads to an increase of the buoyant force as well, which might cause the bubble to rise through the sediment (ALGAR; BOUDREAU; BARRY, 2011a). This rise of the bubble creates paths in the sediments that tend to be a preferred way for other bubbles to follow since the bubble will face less force resisting movement than it would face in an undisturbed sediment (ALGAR; BOUDREAU; BARRY, 2011b).

Del SONTRO et al. (2015) evaluated by a hydroacoustic method in the Wohlen Lake the contribution of bubble size to the volume of gas emitted. It is pointed in the study for the region observed that the 10% largest bubbles carry around 65% of the total gas, which supported the researchers to affirm that bubble size is more important than the number of bubbles for quantifying overall ebullition flux.

Nonetheless, not all bubbles make their way up to the surface. McGinnis et al. (2006) conducted a study to observe methane transport in the water column using modeling and comparing with acoustic data. According to the authors' findings, just methane released from shallow regions will reach the atmosphere, for depths greater than 100 m bubbles are dissolved in the water column and even if they reach the surface, bubble methane content is either dissolved or replaced by other gases such as $O_2$ and $N_2$. Once methane is dissolved in the water, it will become available for transport through diffusive processes. Initial bubble size and release depth are mentioned to have great influence in the volume of methane reaching the atmosphere through ebullition (MCGINNIS et al., 2006).

For water bodies with depths less than 100 m, which is the case of most inland water bodies, a large amount of methane can be released to the atmosphere. Maeck et al. (2013), for instance, analyzed methane flux through ebullition, diffusion and degassing in a region near the dam of an impounded river and upstream the dam in the river considered. The greater emissions were recorded in the deeper region near the dam where the highest sedimentation rate occurred. The researchers concluded that 90% of the methane emitted came from the reservoir portion which represents 16% of the total area analyzed.

By relating ebullition flux with depth Del SONTRO et al. (2015) noticed that the ebullition flux does not necessarily increase with a reduction in depth, it was recorded the highest flux from the middles depths instead. A similar observation was made by Wik et al. (2013) for a fall period of three subarctic lakes. During early fall the ebullition fluxes seemed higher from intermediate and deep zones in the lakes. The main reason mentioned was the water and sediment temperatures which are warmer in deeper zones than in the shallow regions and thus, favorable for bacterial activity and additionally reduces gas solubility.

On the other hand, considering enough methane available in sediment ebullition from a shallow location would be greater if compared with a deeper location, due to the lower hydrostatic pressure that the bubble would have to overcome and less dissolution of methane since the bubble would go through a shorter water column. This was verified by Del SONTRO et al. (2011) studying Lake Kariba. The researchers' findings were that in river delta regions ebullition flux is larger than in non-river bay regions in at least one order of magnitude.

Atmospheric conditions directly affect temperature and pressure over water bodies and thus, have an effect on ebullition flux. On a daily scale in a subtropical hydropower reservoir in Southeast Asia, Deshmukh et al. (2014) observed a twofold increase in ebullition at daytime comparing with the ebullition that occurred during the night when atmospheric pressure was recorded to be larger. Other studies such as Casper et al. (2000), Wik et al. (2013), Natchimuthu et al. (2016) reported an increase

in ebullition with a decrease in the atmospheric pressure. Casper et al. (2000), for instance, recorded for Priest Pot lake in the United Kingdom that a reduction of 2% in the barometric pressure caused a pulse in ebullition rate which was tenfold the mean recorded.

A reduction in air pressure might be related to systems of low pressure that results in precipitation events. Precipitation can increase the load of organic matter entering the system due to runoff and enhance methane production, but can also augment water level which would represent a limitation for ebullition to occur due to increase in hydrostatic pressure. Natchimuthu et al. (2016) noticed only for few events in the studied area in Sweden a relation between precipitation and ebullition. The authors assign the poor relation to the aforementioned aspects of rainfall.

Considering seasonal variations Deshmukh et al. (2014) concluded that for the lake studied from the total yearly ebullition 50% was recorded during the four months of warm and dry weather. A similar result is pointed by Wilkinson et al. (2015) whose research analyzed methane ebullition in Saar River in Germany. The authors concluded that during summer time the ebullition peaks were from 4 to 10 times the minimum ebullition recorded during winter, and the temperature was the major parameter that influenced this seasonality.

Factors such as wind incidence and boat traffic that results in pressure changes in the water–sediment interface by generating internal waves, bottom currents, surges, and so on, also will have effects on ebullition flux. The total pressure acting in the water–sediment interface is represented by the sum of atmospheric pressure and the pressure due to the water column (MAECK; HOFMANN; LORKE, 2014). Maeck, Hofmann and Lorke (2014) mention that hydrostatic conditions cause 74% of the total pressure variation at sediment-water interface and the others 24% variation is due to changes in atmospheric pressure.

In a study, Keller and Stallard (1994) reported high fluxes of bubbling events associated with strong winds. Winds acting on water surface transfers momentum to water and generate oscillations, such as waves and currents, and mixing depending on the wind and the lake/reservoir characteristics (FISCHER et al., 1979).

A direct effect of bottom currents on ebullition is to release bubbles through shear stress, that wouldn't have enough buoyancy to rise from the sediment otherwise (JOYCE; JEWELL, 2003). Joyce and Jewell (2003) calculated a correlation of r=0.63 between wind velocity and methane flux while considering methane flux and current velocity a stronger correlation (r=0.84) was obtained, which indicated that bottom currents have a larger influence on methane flux than the wind itself.

Besides the wind, water inflow and ship activities also provoke oscillations in the water. Maeck, Hofmann and Lorke (2014) pointed that for Saar River in Germany ship induced waves were responsible for changes in the hydrostatic pressure for 46% of the sample time. In addition, by relating ebullition events with surges it was verified that around 59% of the ebullition rates coincided with the passage of negative surges from ship activities, and as a result, the ebullition flux recorded during daytime were greater than overnight.

An important aspect to be considered for the analysis of methane ebullition flux is the time scale in which the mechanisms affect ebullition. And this is because while variations in atmospheric pressure can be the order of days to weeks induced waves can occur on time scales in the order of seconds to minutes (MAECK, 2014). Thus, not taking into account the temporal variations in the measurements might results in underestimated ebullition rates up to 50% (MAECK; HOFMANN; LORKE, 2014).

It seems from literature overview that effects from some forcings act differently in various regions of the reservoir. While low air pressure triggered events mainly from deep regions, temperature appeared

strongly correlated with ebullition in shallow waters. This could give a clue of why ebullition presents such high spatial variability. Natchimuthu et al. (2016) point that the degree in which forcings affect emissions variability is not known, neither how forcings interact with each other and which would be the influences on emissions from the entire system.

## 1.4 Methane measurement techniques

Different methods have been used for estimating methane emissions from water bodies. According to the report published by International Hydropower Association (IHA) (2010) when choosing the method and defining measurements locations, it must be taking into account different regions from the water body in order to include many of the distinct regions as possible. Aspects as cost, logistics, and available people will have an impact over the planning survey. Considering that a reservoir is a dynamic system in terms of the carbon cycle, Tremblay et al. (2005) state that it is preferable to work with long term measurement in order to have a better understanding of how emissions behave.

When point measurements will be performed the points may be set in an arbitrary way or supported by statistical tools. The latest may be divided into three categories: systematic sampling, stratified random sampling, and cluster sampling (International Hydropower Association (IHA), 2010). Basically, in the first case, systematic sampling, samples are uniformly distributed and therefore, it is recommended for a homogeneous population. In the stratified random sampling, the area is subdivided into subgroups and can be applied for the cases where variability is larger among groups than within a group itself. In cluster, the area is also divided into subgroups, however, in this case, it is not required that the variables in each cluster are more homogeneous than the entire population (International Hydropower Association (IHA), 2010).

Beaulieu, McManus and Nietch (2016) applied a generalized random tessellation survey design (GRTS) which contributed to defining the measurement locations considering two regions classified as tributary and open water for the reservoir-like regions. From the results measured the authors calculated a spatial-balanced mean emission rate for each region. Such method allowed the authors to identify regions with no ebullition recorded from areas that occurred emissions and in this way the mean could be estimated considering spatial variabilities. However, no temporal variability was considered, since the strategy was to maximize area coverage.

Gas emissions from water bodies can be obtained by direct volume measurement of the gas emitted or through methods that require a mathematical approach. The eddy covariance method is developed considering turbulent motions in which the flux is a function of wind speed and gas concentration (PELTOLA, 2011). This method has the potential to provide information on spatial and temporal gas fluxes variability (DESHMUKH et al., 2014), on the other hand, has limitations due to assumptions made in the mathematical formulation and requires equipment capable of measuring wind and gas concentration in high frequency (PELTOLA, 2011). Although few studies have applied this method for methane emissions from water bodies, it might contribute for long-term measurements.

In the so called thin boundary layer method (TBL) gas flux is calculated through empirical equations (Boundary Layer Equation) in which flux depends upon the gas concentration gradient of water and air, and the gas exchange coefficient for a given temperature (DUCHEMIN et al., 1999). However, this method does not predict fluxes well during low and high wind periods. In addition, uncertainties might arise also due to lack of knowledge on the factors that have influence over the process (International Hydropower Association (IHA), 2010).

A recently adopted method for flux estimation is based on acoustic methods. Essentially, sound

waves are generated and bubbles contained in the water column and in the sediment are identified by the backscatter of acoustic energy and the volume of gas is obtained through a relation between backscattering and bubble volume (OSTROVSKY et al., 2008). The main difficulties of the method rely on costs, the requirement of some effort to calibrate the equipment considering characteristics of the water body, and to filter the signal to remove noise and fish (OSTROVSKY et al., 2008). Although this method does not account for temporal measurements, Hilgert (2014) showed its potential to identify bottom sediment properties and its correlation to methane production which would contribute to planning measurements.

Floating chambers is a commonly used method for determining diffusion and ebullition fluxes. The chambers might be installed in a way to remain in a fix location or drifting on the water surface. A comparison and discussion on both ways can be found at Lorke et al. (2015). Mannich, Fernandes and Bleninger (2017) investigated the errors in flux estimation due to chamber's geometry characteristics and measuring time. The authors suggest for better results to calibrate the chamber, to include the effects of chamber-induced turbulence, and to evaluate measuring time and its impact in gas concentration changes inside the chamber.

Except for the acoustic approach, all the aforementioned methods are applied to quantify either diffusion flux or the sum of diffusion and ebullition flux. In contrast, funnels are used to assess ebulliton fluxes alone. These equipments are conical structures constructed in PVC canvas or polypropylene that remain submerged in the water column and capture ascending gas bubbles from which the gas volume is determined (SANTOS; ROSA; SANTOS, 2002). The International Hydropower Association (IHA) (2010) report gives instructions on funnel configuration and suggests the use of one-meter base diameter.

Even though diffusion chambers and funnels are the commonly used method, their biggest disadvantage is the short deployment time (for chambers of the order of minutes and for funnels up to a few days) providing data with a very low temporal resolution. As a consequence, flux extrapolation may show huge uncertainties compared to continuous measurements which are scarce currently.

Funnels might be separated into conventional funnels and automatic funnels referred from now on as Automated Bubble Traps (ABT). The main difference between both is that while in the conventional funnel the volume of accumulated gas is manually measured, in the automatic version the volume is determined by the equipment which allows for more detailed data acquisition. In this study, both funnels were used, however with a focus on the ABT.

Automated bubble traps have already been applied for methane ebullition flux measurement in previous studies. Varadharajan, Hermosillo and Hemond (2010) developed an automated bubble trap and measured data for around six months with the aim to analyze circuit performance in a field survey. Maeck (2014) developed a similar version of the equipment and evaluated forcing mechanisms on ebullition flux by comparing data collected from ABT with ambient parameters. Wilkinson et al. (2015) also obtained long-term ebullition flux measurement from Saar River in Germany using ABTs and evaluated seasonal variations on fluxes. The most relevant aspect of this method is to obtain ebullition measurements with high temporal resolution, which might not be easily achieved by other methods, nonetheless, it still has limitations regarding spatial variability that could be investigated through hydroacoustic methods (Del SONTRO, 2011; Del SONTRO et al., 2011).

Each of the presented methods has its advantages and restrictions, a brief summary is given in Table 1. Some studies from literature compared fluxes obtained from different methods. Deshmukh et al. (2014) found that for the Nam Theun 2 reservoir in Lao People's Democratic Republic the emissions flux determined by eddy covariance were consistent with the fluxes obtained through floating chamber and funnels, for the specific case when ebullition and diffusion from funnels and floating chambers were separately added up. Deemer et al. (2016) compared data flux from reservoirs worldwide and mention

that the mean emissions from eddy covariance and acoustic methods are much higher than other methods.

Table 1: Overview of methods applied for estimating gas emission from water bodies.

| Methods | Main aspects | Advantages/drawbacks | Reference |
|---|---|---|---|
| Eddy covariance | Sensors installed in a tower records data of wind velocity and gas concentration. | It can be obtained continue information in short time steps/ High costs and extensive mathematical manipulation. | Deshmukh et al. (2014), Peltola (2011) |
| Thin Boundary Layer | The emission flux is calculated through empirical equations and is proportional to the gas concentration at air-water interface. | Gas concentration is easy to measure; however, the method has a high variability in the results. | Duchemin et al. (1999), International Hydropower Association (IHA) (2010) |
| Floating chamber | A closed chamber is used to measure gas flux at the air-water interface. Gas is collected for further analysis in the laboratory. | Gas has to be collected to be analysed in the laboratory/Chamber itself might cause disturbances in the environment leading to uncertainties in fluxes estimation. | Lorke et al. (2015), Mannich, Fernandes and Bleninger (2017) |
| Eco sound | Acoustic method based on backscatters of sound wave.s | High spatial resolution; avoid disturbances in sediment and water column./ Requires adjustments in order to identify a specific target; high cost. | Ostrovsky et al. (2008) |
| Conventional Funnel | Upside down funnel which captures gas bubbles that rise in the water column. | Low cost; easy installation / Point measurement, volume of gas is determined manually. | Santos, Rosa and Santos (2002), International Hydropower Association (IHA) (2010) |
| Automated Bubble Trap | Upside down funnel which captures gas bubbles that rise in the water column. | High temporal resolution; long term measuremnents, gas volume calculated automatically by the equipment/ Point measurement. | Varadharajan, Hermosillo and Hemond (2010), Maeck (2014) |

Most of the methods are not able to provide data with both spatial and temporal resolution at the same time. A solution would be to combine information from different techniques that are capable of solving both variabilities, meaning measurements over large areas for long periods of time. However such measurements have constraints such as high costs, time demanding and requirement of qualified people for operating the technology.

Several studies have been conducted in the attempt to estimate methane ebullition flux from aquatic environments and to have a better understanding of the underlying processes. A summary of some selected studies is presented in Table 2. It is perceived that most of the measurements were not continuous but conducted during few days only. Another point to be observed is that even if the same method is applied, the geometric characteristics differs from one study to another, for instance, the diameter of conventional funnels varied from 0.26 m to 1 m. The unit used to represent fluxes also alters from one study to another which makes it difficult to directly compare results.

In the case of studies carried out in Brazil, data were mostly collected in periods of 24–48 hr in different seasons. For some cases a large number of sampling points improved the spatial resolution, nevertheless the temporal resolution wasn't achieved. The implications of missing temporal patterns were already reported in studies as being a under-over estimation of emissions and make the identification of predominant forcings difficult.

The International Hydropower Association (2010) proposed a range of methane and carbon dioxide emissions from different pathways for boreal/temperate and tropical regions, Table 3. Although the range of ebullition flux is larger in the tropical region than the one for the boreal/temperate region, Deemer et al. (2016) showed that according to their analyses methane fluxes from tropical regions such as Amazonian reservoirs are statistically similar to the fluxes from reservoirs located in subtropical regions.

Table 2: Summary of some studies conducted in which gas emissions through bubbles from water bodies was addressed.

| Reference | Study site | Method | Period of measurements | Methane ebullition flux |
|---|---|---|---|---|
| **Wordlwide** | | | | |
| Keller and Stallard (1994) | Gatun Lake - Panama | Conv. funnel (D=0.26 m) | Feb.– Oct. 1988.<br>Deployed: 12–60 hr<br>24 hr sampling interval | site depth > 7 m: 10–200 $mgCH_4\,m^{-2}\,d^{-1}$<br>site depth < 2 m : 300–2000 $mgCH_4\,m^{-2}\,d^{-1}$ |
| Casper et al. (2000) | Lake Priest Pot - UK | Conv. funnels (D=0.29 m) | Jun.– Oct. 1997<br>Weekly measurements<br>24 hr sampling interval | mean 162 $ml\,m^{-2}\,d^{-1}$ |
| Eugster, Delsontro and Sobek (2011) | Lake Wohlen - Switzerland | Eddy covariance (EC)<br>Floating chamber (FC) | EC: 26 days in Jun/08; 21 Jul.–12 Aug. 2008<br>FC : 4 days in Jul/08.<br>Deployed: 0.3–1.75 hr | Average flux<br>EC: 3.8 $\mu gC\,m^{-2}\,s^{-1}$<br>FC (Ebullition + diffusion): 7.4 $\mu gC\,m^{-2}\,s^{-1}$ |
| Wik et al. (2013) | Subarctic lakes - Sweden | Conv. funnels (D=0.5 m) | Summers (Jun.-–Sep./2009-–2012)<br>24-–72 hr sampling interval | mean 13.4 $mgCH_4\,m^{-2}\,d^{-1}$ |
| Deshmukh et al. (2014) | Nam Theun 2 Reservoir - Laos | Conv. funnels (D=0.26 m) | Seasonal: May/09 to Jun./11<br>Weekly: Mar./12 to Aug./13<br>24–48 hr sampling interval | 0–201.7 $mmol\,m^{-2}\,d^{-1}$ |
| Maeck, Hofmann and Lorke (2014) | Saar river - Germany | ABT (D=1 m) | Continuous measurements from Oct. 2012 to Mar. 2013 | mean 11.67 $mmol\,m^{-2}\,d^{-1}$ |
| Beaulieu, McManus and Nietch (2016) | William Harsha Lake - US | Floating chambers | Aug. 2014<br>5 minutes deployment | mean 7.66 $mgCH_4\,m^{-2}\,hr^{-1}$ |
| **Brazil** | | | | |
| Rosa et al. (2006) | Reservoirs: Miranda<br>Três Marias<br>Barra Bonita<br>Segredo<br>Xingó<br>Samuel<br>Tucuruí | Conv. funnels (D=0.75 m) | 2 campaigns (1998–1999)<br>24 hr sampling | mean for the entire reservoir campaign 1 / campaign 2 [$mgCH_4\,m^{-2}\,d^{-1}$]<br>Miranda: 29.16 / 18.48<br>Três Marias: 273.09 / 55.92<br>Barra Bonita: 4.81 / 3.06<br>Segredo: 1.71 / 1.86<br>Xingó: 1.95 / 19.56<br>Samuel: 19.33 / 13.61<br>Tucuruí: 13.15 / 2.47 |
| Carvalho and Carvalho (2015) | Sinhá Mariana pond | Conv. funnels (D=0.7 m) | Sept. 2012 and Mar. 2013<br>24 hr sampling | 0–16.85 $mmol\,m^{-2}\,d^{-1}$ |

In this way, the authors raised the possibility that reservoir's location may not be the only aspect to be considered to quantify gas emissions, but reservoir characteristics may be equally or more important than the location itself.

Table 3: Estimated range of carbon dioxide and methane emissions from freshwater reservoir. Source: International Hydropower Association (IHA) (2010)

| Pathway | Boreal and temperate | | Tropical | |
|---|---|---|---|---|
| | $CO_2$ $mmol\,m^{-2}\,d^{-1}$ | $CH_4$ $mmol\,m^{-2}\,d^{-1}$ | $CO_2$ $mmol\,m^{-2}\,d^{-1}$ | $CH_4$ $mmol\,m^{-2}\,d^{-1}$ |
| Diffusion | −23 to 145 | −0.3 to 8 | −19 to 432 | 0.3 to 51 |
| Ebullition | 0 | 0 to 18 | 0 | 0 to 88 |

## 1.5 Summary

In this chapter was showed that decomposition of organic matter in a reservoir results in the production of gases as carbon dioxide and methane, thus making reservoirs sources of GHG to the atmosphere. Although ebullition is reported to be an efficient pathway of gas transfer from the sediment to the atmosphere, the process is a result of an interplay of several parameters, which leads to high spatial and temporal variability of gas ebullition from a water body. Environmental conditions, such as temperature, sedimentation rate, atmospheric pressure changes, wind conditions, and so forth were mentioned in the literature to have an effect over ebullition.

Considering the studies consulted and mentioned throughout this chapter, a simplified representation of some parameters that have an influence on ebullition process (from bubble formation to its potential release to the atmosphere) is presented in Figure 5. In summary, the amount of organic matter entering the system supplies the methane production in the ambient by bacterial activity which is influenced by ambient temperature; In turn the amount of methane available and sediment characteristics impact bubble formation and its movement in the sediment; Finally, ambient conditions will determine whether or not bubbles will reach atmosphere and the amount of gas to be released.

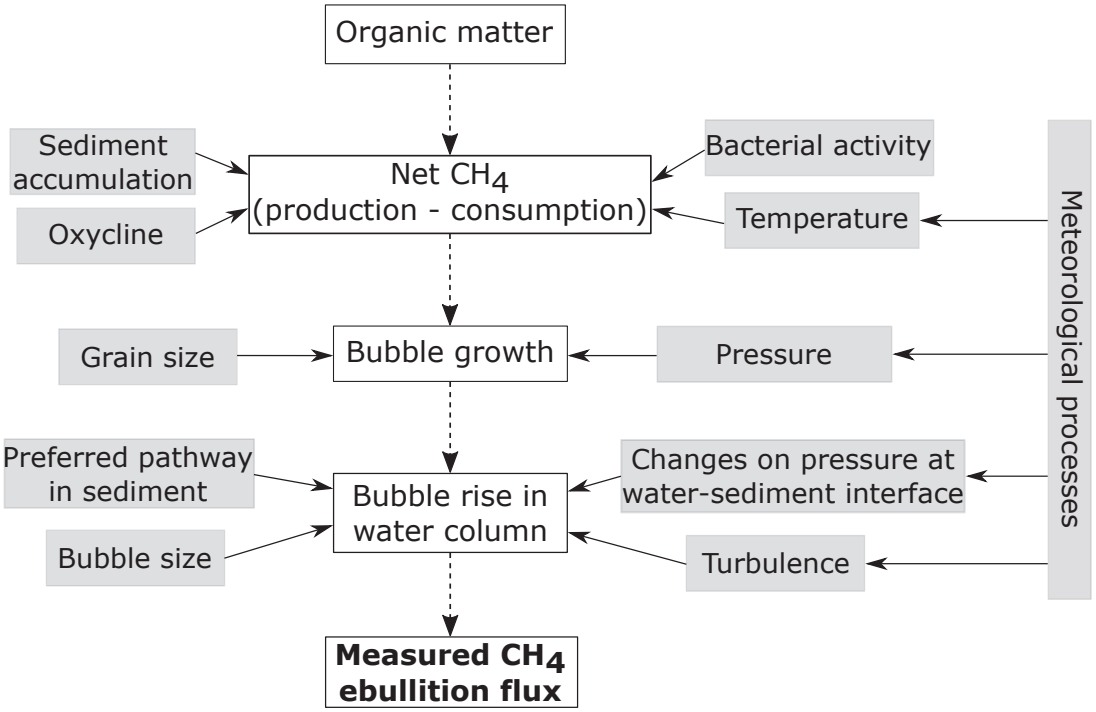


Figure 5: Simplified representation of the parameters influencing ebullition events.

Nonetheless, the exact effect of each parameter over ebullition and the interaction among the parameters are not totally understood. In addition, they may or may not be linearly correlated. The gas flux emissions vary from one reservoir to another, as presented in Table 2. The methods applied to estimate the emissions also varies among the studies and in Brazil no study before, measured ebullition with high temporal resolution and for long periods of time. Therefore, this study aims to contribute with information of gas ebullition measured with high temporal resolution in a water supply reservoir located in Brazil.

# 2 Materials

In this chapter is presented information about the study area, which is Passaúna reservoir, regarding hydrography, prevailing weather conditions, and some characteristics of the reservoir itself. It is also showed details about the equipment that is being used for gas flux measurements and for obtaining auxiliary data.

This master's thesis project has been embedded in the SeWaMa Project (Innovative approaches for future **Se**diment and **Wa**ter **Ma**nagement in Brazil) within the NoPa call (**No**vas **Pa**rcerias, funded by CAPES and DAAD, 2015 - 2018) and within a consortium between Germany – Brazil integrating Universities, municipal sanitation company and companies from the private sector. The project involved researchers from different areas studying sedimentation in reservoirs, water quality aspects, land use, and GHG production and emission in a water supply reservoir in Brazil – Passaúna reservoir, located near Curitiba city in the southern region of Brazil. The present study contributes with information on the subject of greenhouse gas emissions.

## 2.1 Study area

Passaúna reservoir is located near to Curitiba city in Paraná state, Brazil and was formed by a dam built in 1989 in Passaúna river. Passaúna sub-basin (Figure 6) has a drainage area of 217 $km^2$, the reservoir which is used for public water supply has a live volume of $48 \times 10^6\,m^3$ and capacity to deliver a freshwater flow rate of $2\,m^3\,s^{-1}$ to the Curitiba's municipal water supply company, Sanepar (Empresa de Saneamento do Paraná) (SUDERHSA; RDR, 2007). The residence time of the reservoir is 292 days (CARNEIRO; KELDERMAN; IRVINE, 2016), the main water inflow is from Passaúna river with a mean flow rate of $1\,m^3\,s^{-1}$. Other small rivers also contribute to water inflow such as Ferraria river with a flow rate of $0.14\,m^3\,s^{-1}$ (XAVIER, 2005) and approximately 69.7% of the sub-basin area contributes for runoff to the reservoir.

According to results of water quality monitoring in Passaúna from 1999 to 2008, the reservoir has mesotrophic characteristics and was classified as moderately degraded (XAVIER et al., 2009). This class (Class III) is characterized by the possible occurrence of anoxic conditions at the bottom portion of the deepest area of the reservoir, receive a medium load of nutrients and of organic matter, it has large algae density, moderated tendency for eutrophication and has regular water quality which means that the water meets the parameters required for public supply (XAVIER et al., 2009).

Xavier (2005) point out that reduced percentage of sewage treatment, industrial and agriculture activities that are developed in the watershed of Passaúna are the major threats to the reservoir water quality. These activities, in addition to city growth, increases the point-source and diffuse sources of material to the reservoir (SAUNITI; FERNANDES; BITTENCOURT, 2002). According to Xavier (2005) around 40% of the sub-basin area is used for agricultural activities for corn, potato and bean farming. It is largely adopted the practice of crop rotation and the elevated usage of fertilizers and agrochemicals which might be carried to the reservoir during rain events represent a load of nutrients to the water (XAVIER, 2005).

The increment of sediment entering into the reservoir is also a consequence of land use in the sub-basin. By analyzing sediment samples from Passauna reservoir Sauniti, Fernandes and Bittencourt

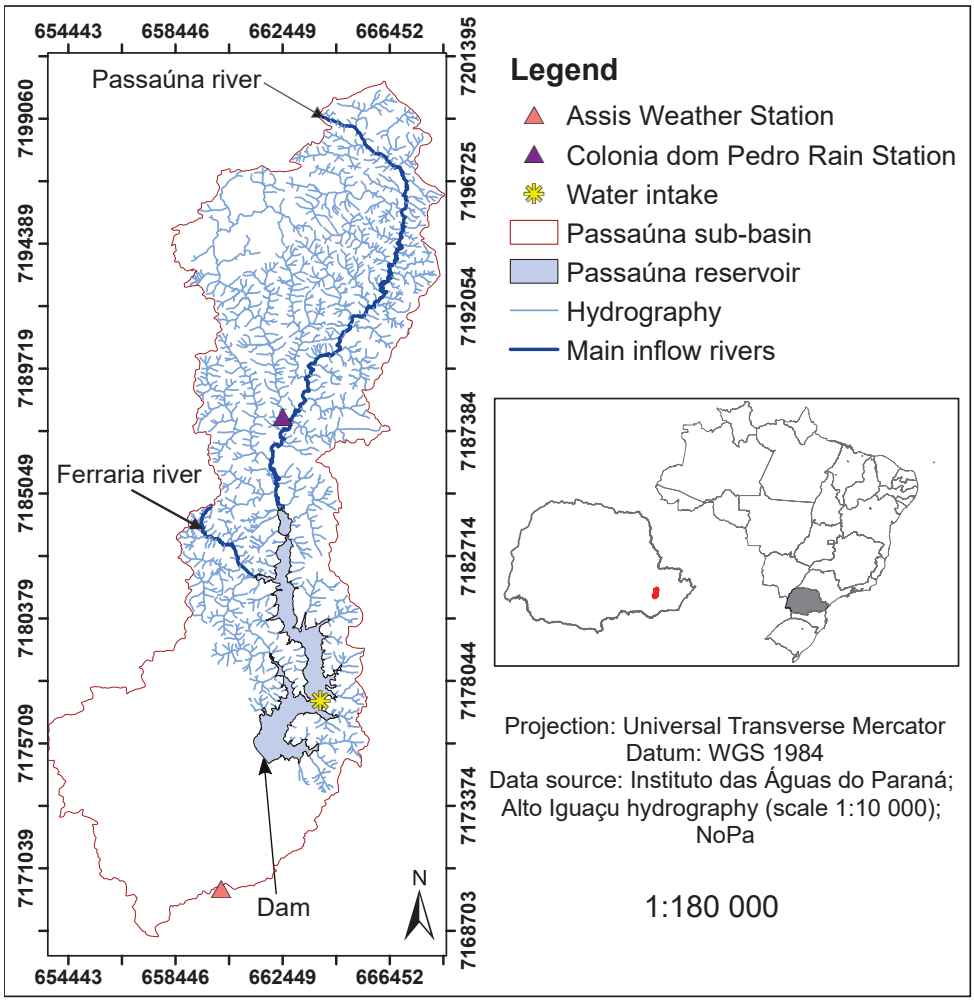


Figure 6: Location of Passaúna Reservoir in the sub-basin with the rivers that most contribute to water inlet in the reservoir.

(2002) verified layers of sedimentation in different regions within the reservoir. According to the results, the thickness of the sedimentation layers varied from 8.0 cm to 36.5 cm which represented a sedimentation rate between 0.66–3.04 cm per year for the period analyzed.

A more recent study performed by Sotiri (2016) mapped Passaúna bathymetry and sediment thickness. According to author's results, the reservoir has a mild slope with depths varying from 0 m to 16 m and the sediment thickness is greater in the deepest part of the reservoir near the dam where it can reach up to 1.3 m. By analyzing bottom sediment samples the author verified that it is composed mainly of fine grain.

### 2.1.1 Precipitation and water level

Meteorological data such as precipitation, wind conditions, atmospheric pressure, and temperature can be obtained from different stations that are installed in the reservoir vicinity. In Table 4 and in Figure 7 are showed some identified stations with measured variables and distances from Passaúna reservoir.

According to the Koppen climate classification map produced by Agronomic Institute of Parana (IAPAR) the region of Passaúna sub-basin is classified as Cfb which is a temperate climate with a mean

Table 4: Stations located nearby Passaúna reservoir, measured variables, and period of data available.

| Type | Measured variables | Station | Time interval between measurements | Coordinates | Distance from reservoir | Period of available data | Data base |
|---|---|---|---|---|---|---|---|
| Weather station | Temperature, relative humidity, pressure, wind velocity and direction, and radiation | Verde river dam | 10 minutes | 25°31′36.8″S 49°31′39.1″W | 13.8 km from the dam | 15/12/16 – 07/03/17 | – |
| | | Assis – Fazenda velha | 1 hour | 25°34′35.3″S 49°24′20.1″W | 5.2 km from the dam | 01/01/06 – 28/02/17 | – |
| Rain station | Precipitation (mm) | Dam Sanepar 02549081 | 12 hours | 25°32′0″S 49°23′11″W | Nearby the dam | Since installation | Águas Paraná |
| | | Colônia dom Pedro 02549080 | 12 hours | 25°25′1″S 49°23′5″W | 4.7 km from upstream reservoir | Since installation | Águas Paraná |
| Solarimetric station | Temperature, relative humidity, pressure, wind velocity and direction, and radiation | CTB–60 | 1 minute | 25°29′43.6″S 49°19′52.4″W | 4 km from water withdrawal | Since 2015 | Smart Energy-TecPar |

temperature of 22 °C for the warmest month and the dry season is not defined, in addition, mean annual precipitation ranges from 1400 mm to 1600 mm (CAVIGLIONE et al., 2010). Xavier (2005) analyzed precipitation data of Colônia dom Pedro station from 1993 to 2003 and observed that January and February are the rainier months while April and May are the drier months. It is observed from data of the last 3 years, Table 5, that precipitation tend to follow the pattern of being higher during the hotter months.

Table 5: Monthly accumulated precipitation [mm] measured at rain station Colônia dom Pedro - Campo Largo, Paraná. Source: Instituto das Águas do Paraná.

| year | Jan | Feb | Mar | Apr | May | Jun | Jul | Aug | Sep | Oct | Nov | Dec |
|---|---|---|---|---|---|---|---|---|---|---|---|---|
| **2015** | 162.5 | 253.3 | 220.8 | 71.3 | 142.7 | 86.6 | 224 | 37.7 | 143.2 | 290.6 | 267.3 | 331.4 |
| **2016** | 207.7 | 223.6 | 139 | 71.7 | 187 | 107.9 | 119.3 | 214.1 | 97.6 | 251.4 | 156.1 | 197.8 |
| **2017** | 319.8 | 223.9 | 89.3 | 88.0 | 104.3 | 160.2 | 5.1 | 101.9 | 49.0 | 284.4 | – | – |

During rain events, organic matter, soil, and nutrients can be carried to the reservoir by runoff and subsurface flow. Another effect of precipitation occurring in the sub-basin is an increase in reservoir water level. The main influence of water level in ebullition is observed when the water level decreases and as a consequence, there is a reduction in hydrostatic pressure at the sediment-water interface which could trigger ebullition events if there is enough accumulated gas in the sediment. Reservoir water level is daily measured by the reservoir operator company (Sanepar). According to data from 2016, Figure 8, the greatest changes in water elevation occurred between the period of January/February and March/April/May when the difference calculated was 0.14 m. In 2017 the reservoir water level was smaller than the year before. The highest and lowest water levels were recorded during the months of most and lowest rainfall respectively.

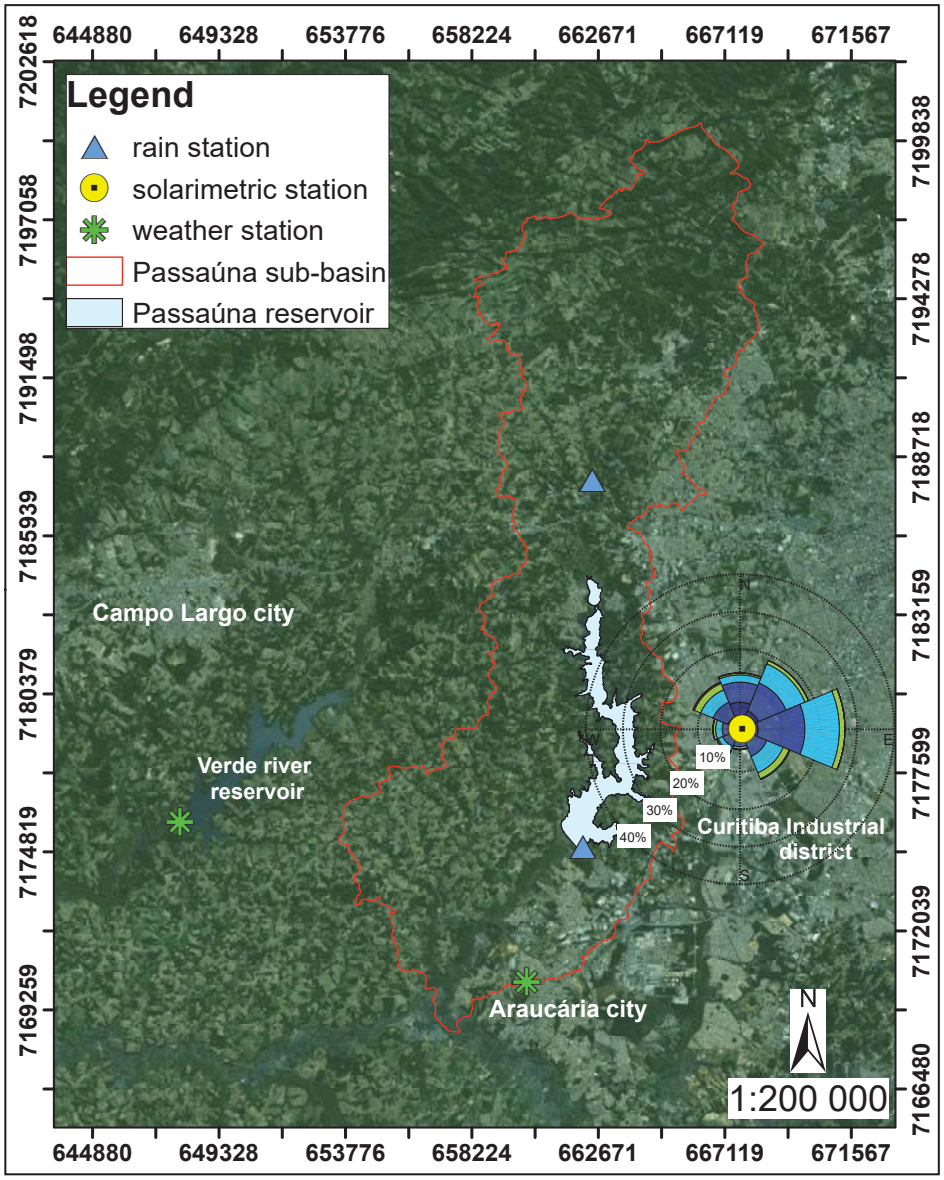


Figure 7: Weather stations, rain stations, and solarimetric station location. Wind frequency distribution from solarimetric station (Smart Energy-Tecpar) data from January 2017 to September 2017.

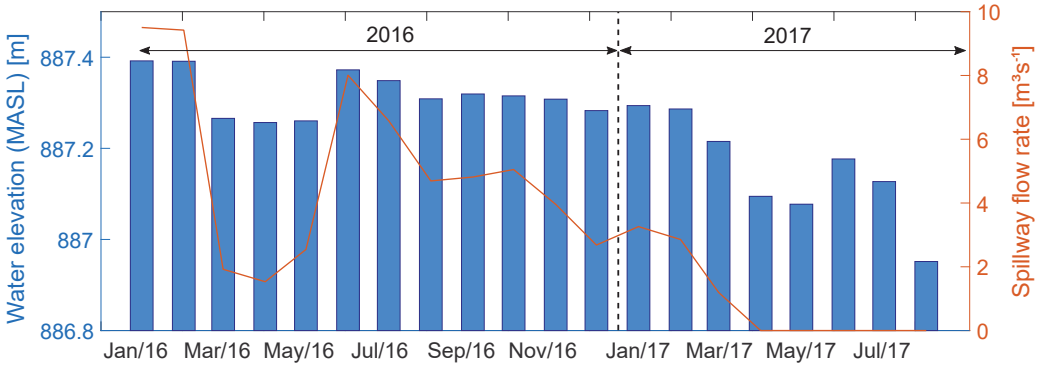


Figure 8: Mean upstream water elevation and spillway flow rate at Passaúna reservoir.

### 2.1.2 Wind, air temperature, and atmospheric pressure

Wind incidence at reservoir water surface can potentially provoke water mixing, form internal currents and lead to disturbances at bottom sediment, such disturbances can favor gas bubbling. Maack (1981) *apud* Xavier (2005) states that the South Atlantic Anticyclone (SAA) acts over the region, as a results prevail northeast and southwest winds. The solarimetric station located at Paraná Institute of Technology (TECPAR) in Curitiba is managed by the Smart Energy project. The station records data at one-minute time step. From the data of the last two years, Table 6, is verified that prevailed east and northeast winds with a percentage of occurrence of 23.33% and 18.59% respectively. The highest average wind speed was from northwest winds that occurred in 14.46% of the time and wind speeds in the range of 1.1–2.2 $\mathrm{m\,s^{-1}}$ were the most frequent.

Table 6: Wind measured in one-minute time interval at Smart Energy-TecPar solarimetric station from 2015 to 2016

| **Speed [m/s]** | Percentage of occurence [%] | | | | | | | | **Total** [%] |
|---|---|---|---|---|---|---|---|---|---|
| | **N** | **NE** | **E** | **SE** | **S** | **SW** | **W** | **NW** | |
| 0.1–1.0 | 5.93 | 4.16 | 3.24 | 1.48 | 1.41 | 1.76 | 1.62 | 2.36 | 21.96 |
| 1.1–2.2 | 5.96 | 8.28 | 10.83 | 3.81 | 1.60 | 2.39 | 2.55 | 4.45 | 39.88 |
| 2.3–3.6 | 2.51 | 5.33 | 7.74 | 3.77 | 0.70 | 1.78 | 1.87 | 4.26 | 27.96 |
| 3.7–5.2 | 0.66 | 0.79 | 1.46 | 1.48 | 0.19 | 0.58 | 0.65 | 2.47 | 8.28 |
| 5.3–7.0 | 0.11 | 0.03 | 0.05 | 0.18 | 0.04 | 0.08 | 0.10 | 0.79 | 1.38 |
| $> 7.0$ | 0.03 | 0.00 | 0.00 | 0.00 | 0.01 | 0.01 | 0.01 | 0.13 | 0.19 |
| **Total** | 15.19 | 18.59 | 23.33 | 10.74 | 3.94 | 6.61 | 6.79 | 14.46 | 99.65 |
| Average speed [m/s] | 1.49 | 1.82 | 2.03 | 2.34 | 1.59 | 1.93 | 2.00 | 2.55 | |

It was verified gaps in the wind data set from 2015 to 2016. A total of 32.8 days (4.82%) had no data recorded, the longest period without data was 23.2 days in February of 2016. Additionally, a few inconsistencies were found in this period. Nine out of 932740 data points had not a number values or values out of the expected range and were not considered. For 2017 it was analysed data from January to September. In this period 4 values out of 272464 data points were inconsistent; 64.5 days (25.44%) without data recorded. Three long period without data were identified: 23.9 days at end of January begin of February, 22.1 day in May – June, and 18.3 days in July. The available wind data recorded in 2017 were used to correlate with ebullition time series at section 4.7.

According to the monthly frequency distribution of winds of 2017, Figure 9, prevailed East winds in all months occurring also with higher frequency winds of Southeast (January and March), North (mainly in June, July, and September), and Northeast after April.

Temperature can range from values just below zero up to 35 °C. The mean annual temperature for 2016 was 17 °C with a maximum temperature of 32.6 °C recorded in December and minimum of −2.8 °C recorded in June, Figure 10. From Figure 10 is possible to identify the occurrence of lower temperature during fall and winter months. The mean annual pressure was 903.8 mbar in 2016. The difference between highest pressure and lowest pressure value was 18.8 mbar and the drop in air pressure was in most of the time associated with rain events.

### 2.1.3 Water temperature and dissolved oxygen profiles

Within the SeWaMa research project water quality data has been measured. Profile data of water temperature and dissolved oxygen were directly measured in the reservoir. During ABT maintenance a CTD Sontek CastAway, which stands for Conductivity-Temperature-Depth, was used by the author for

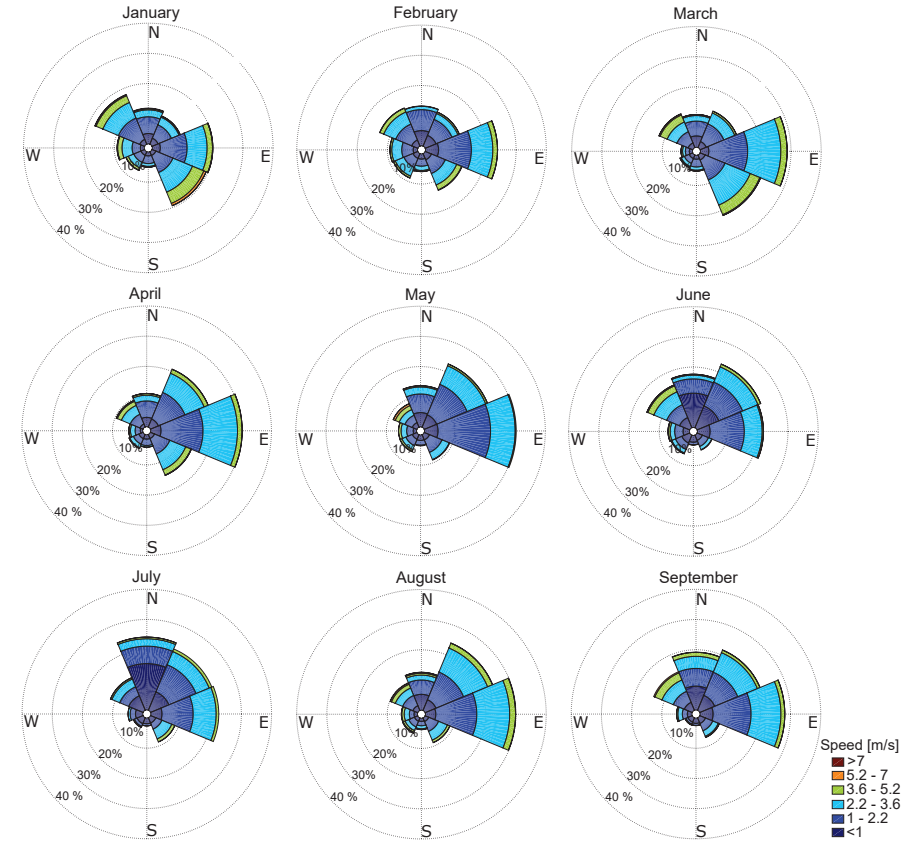


Figure 9: Monthly frequency distribution of winds. Smart Energy-Tecpar data from January 2017 to September 2017.

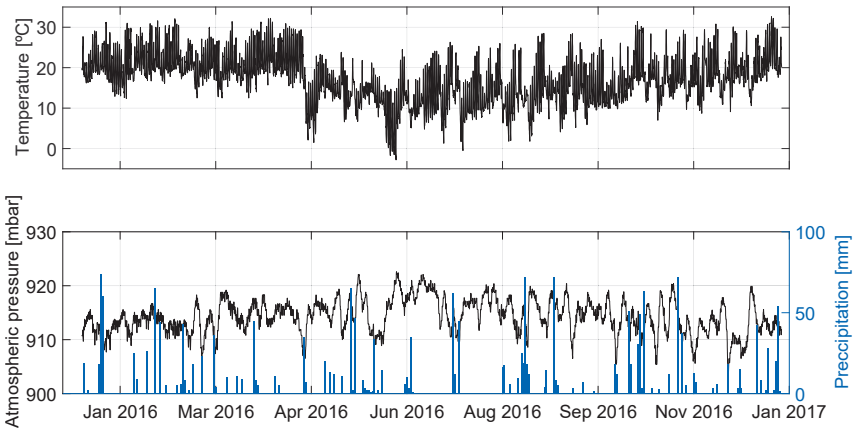


Figure 10: Air pressure and air temperature of 2016 from Assis weather station and daily accumulated precipitation from Colônia dom Pedro rain station.

water temperature measurements. The equipment has an integrated GPS and allows for point or cast measurements. For conductivity the equipment has six electrodes, 2 of which generate electrical current and the others measure water resistivity. The temperature is determined by a thermistor and the depth is derived from pressure measurements (SONTEK, 2012).

A multi-parameter water quality probe, Horiba U-53, was used to obtain dissolved oxygen (DO) profiles. In addition to the DO, the equipment measures several other parameters such as pH, turbidity, temperature, depth, conductivity, total dissolved solids (TDS), and oxidation-reduction potential (ORP).

For the case of the DO, its concentration in water is determined by a membrane electrode method (HORIBA Ltd, 2009). The multi-parameter water quality probe was regularly calibrated in the laboratory before each field campaign.

### 2.1.4 Water quality measurements

As a part of the NoPa-SeWaMa project, several measurements regarding water quality parameters were done at Passaúna reservoir. These data were collected, processed and the preliminary results are found at Knapik et al. (2017) while the complete data analysis will be presented as a master's thesis at Godoy (2017). Data were collected in different field campaigns, during 2017 the campaigns occurred on February $14^{th}$ and May $07^{th}$, and in five different locations along the reservoir two of which are near ABT-P1 and ABT-P2 location, and another one in the deepest region of the reservoir in 800 m downstream ABT-P3.

Several parameters were analyzed from water samples collected from the surface and from the bottom portion of the water column, and from measurements using a multi-parameter water quality probe (Horiba U-53). The parameters included were biochemical oxygen demand (BOD), chemical oxygen demand (COD), phosphorus, nitrogen, pH, oxidation-reduction potential, dissolved oxygen, and others.

Additionally to the study on reservoir water quality, is being conducted an apart research on dissolved methane concentration. The first measurement campaign was in February of 2017 when methane concentration profile was obtained for three locations transversally distributed in the deepest region of the reservoir near ABT-P3 location. The equipment used was a TDLS Franatech probe and the results can be found at Schumack and Mannich (2017).

### 2.1.5 Sediment characteristics

Regarding reservoir sediment characteristics two recent studies were performed in the reservoir in 2016. Sotiri (2016) conducted echo-sounding measurements resulting in a reservoir's bathymetric and sediment thickness map. In addition core and grab sediment samples were collected during the study to be used for seabed classification.

Together with this study Zarebska (2016) analysed some parameters of the reservoir's sediment. In field campaign, which also occurred in February of 2016, 14 sediment cores and 7 grab samples were collected. The parameters analysed were sediment granulometry, loss of ignition (LOI) for estimating organic matter and carbonate content in the sediment, total phosphorus, and manganese. The ABTs were placed considering the locations where sediment was analysed, thus the ABT-P1 corresponds to point core 5 (C5) and grab 4 (G4), ABT-P2 to the core 11 (C11), and ABT-P3 to core 2 (C2).

## 2.2 Funnels for ebullition measurement

### 2.2.1 Automated Bubble Trap (ABT)

The Automated Bubble Traps (ABT) used in this research were developed by the German company Senect, provided by the Karlsruhe Institute of Technology (KIT) within the NoPa–SeWaMa project. The equipment consists of a rigid structure with an upside down polypropylene funnel attached, which conducts gas bubbles that leave the sediment through ebullition and rise towards the water surface to an inner tube. The equipment stays entirely submerged in the ambient water and remains suspended

in the water column by buoys that are connected to the ABT through ropes. Two anchor weights are used to prevent ABT moving.

Initially, the ABT's inner tube is filled with ambient water. As gas enters in the funnel, it displaces water and occupies the volume of the inner tube, Figure 11. When the maximum volume is reached a solenoid valve flushes the gas out and a new measurement cycle will initiate (SENECT, 2016).

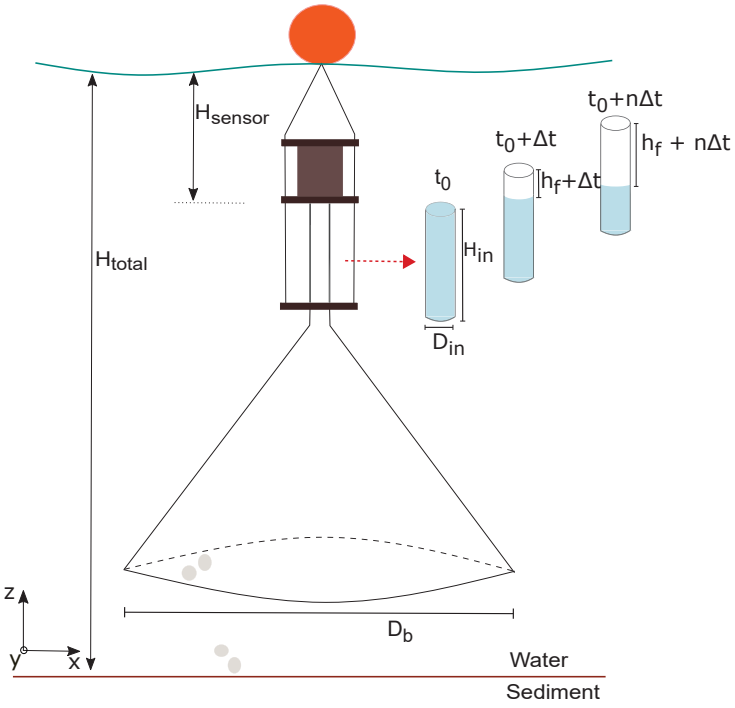


Figure 11: ABT's representation in the water column and measurement cycle with increase of gas stored in the inner tube in different time steps.

The parameters from Figure 11 are: total water depth ($H_{total}$ ); water column above pressure sensor ($H_{sensor}$); diameter of the inner tube ($D_{in} = 27.2\,\text{mm}$ ); total height of the inner tube ($H_{in}$); gas fill height ($h_f$); and funnel base diameter ($D_b = 1\,\text{m}$). In addition to the gas fill height, the ABT also measures temperature and absolute pressure.

The equipment is powered by four size C batteries. The recording time interval can be set by the user and range from 5 seconds up to 60 seconds. The volume of gas is calculated from the differential pressure measured which compares pressure in the inner tube and outside ambient pressure at the same level. After having the differential pressure, the height of gas ($h_f$) in the inner tube is determined and so, as the diameter of the inner tube is known, the volume of gas ($Vol$) contained in the tube can be calculated through

$$Vol = h_f \pi \frac{D_{in}^2}{4}. \tag{2.1}$$

The gas volume flux ($Vol_f$) can be calculated taking into account the time interval ($\Delta$t) and the funnel area,

$$Vol_f = \frac{Vol}{\Delta t A_b}, \tag{2.2}$$

where the funnel base area ($A_b$) is calculated as $A_b = \frac{\pi D_b^2}{4}$.

As proposed by Maeck, Hofmann and Lorke (2014) methane ebullition rate can be calculated by applying the Ideal Gas Law and considering the methane partial pressure ($p_i$) within the gas bubbles the number of moles can be estimated with equation

$$n = \frac{p_i Vol_f}{RT}, \tag{2.3}$$

where $R$ is the gas constant ($8.314\,\mathrm{J\,mol^{-1}\,K^{-1}}$) and $T$ is the temperature. By letting the number of moles be equal to $n = \frac{m_1}{M_1}$ , where $m_1$ is methane mass and $M_1$ is methane molar mass ($16\,\mathrm{g\,mol^{-1}}$), the Equation 2.3 for the methane ebullition rate ($ER$) can be rewritten as

$$ER = \frac{p_i Vol_f M_1}{RT}, \tag{2.4}$$

where the unit will be given in $\mathrm{mgCH_4\,m^{-2}\,d^{-1}}$.

Internally the ABT's software calculates ebullition rates, these values as well as temperature, pressure, and fill height are saved in discrete time steps, which is saved in a '.csv' format file in the ABT's internal memory. In addition to the internal memory, the equipment contains an SD card installed in which a second data file is supposed to be saved. The data file recorded can be downloaded from the funnel either by a USB cable or by copying the file from the SD card. After downloaded to a computer data can be easily accessed using computational tools as Excel or MatLab.

The ABTs have been calibrated by the manufacturer for pressure, temperature and fill height. The calibration coefficients were obtained from linear regression from laboratory tests and the goodness-of-fit ($R^2$) values are greater than 0.9. More details on equipment calibration can be found at Maeck, Hofmann and Lorke (2014). A summary of measurements' precision is presented in Table 7.

Table 7: Precision on measurements provided by the manufacturer. Source: SENECT (2016).

| Measurement | Precision |
|---|---|
| Pressure | ±5% of full scale (FS) |
| Temperature | ±0.3 °C |
| Fill height (scale bar) | < ±2 mm |

## 2.2.2 Conventional funnel and large volume measurement

Conventional funnels have a similar structure as the ABTs, however, they don't have electronic components and therefore, the stored gas volume must be determined manually. The funnels stay also submerged in the water column and plastic bottles are used as buoys while an attached weight provides equipment stability in the water column. On the top of the funnel neck, there is a syringe with a 3-way polypropylene stopcock attached which is used to connect a second syringe to remove the trapped gas and to determine its volume.

Two important publications regarding approaches for GHGs measurements and quantification from water bodies are the guideline published by the International Hydropower Association (IHA) (2010) and the publications of the International Energy Agency (IEA). The IHA's guideline includes geometric aspects of the funnels used for measurements, reservoir's regions that are important to be considered, and procedures to be followed. The three volume publications of the IEA address aspects of GHG measurements in different stages of the reservoir (pre and post-impoudment conditions), modelling related issues, and management/mitigation actions.

In a more general way when considering inverted conventional funnel for gas measurement the volume of gas should be measured in a time interval of 24–48 hours to avoid gas dissolution (International Hydropower Association (IHA), 2010) and field campaigns distributed along the year to account for seasonal variations (International Energy Agency (IEA), 2012).

The conventional funnels were deployed in the water, and the gas volume was measured using a 60 ml syringe which was connected to the 3-way valve contained in the funnel. For measurement of a large volume of gas, a 1000 ml graduated cylinder was used. The cylinder was initially full of water and was held upside down in the water in a way that the gas was transferred to the cylinder and displaced the water in the cylinder, Figure 12. Then, the volume of gas contained in the cylinder was verified keeping the gas level at the water level for the reading. The uncertainty in the gas volume measurement was considered to be due to the reading in the scale bar of the graduated cylinder. The cylinder has a volume capacity of 1000 ml, its minor scale is 10 ml which results in an error of ±5 ml. The gas volume flux can be calculated with Equation 2.2 considering the volume of gas measured and the time interval as the total amount of time that the funnel was deployed.

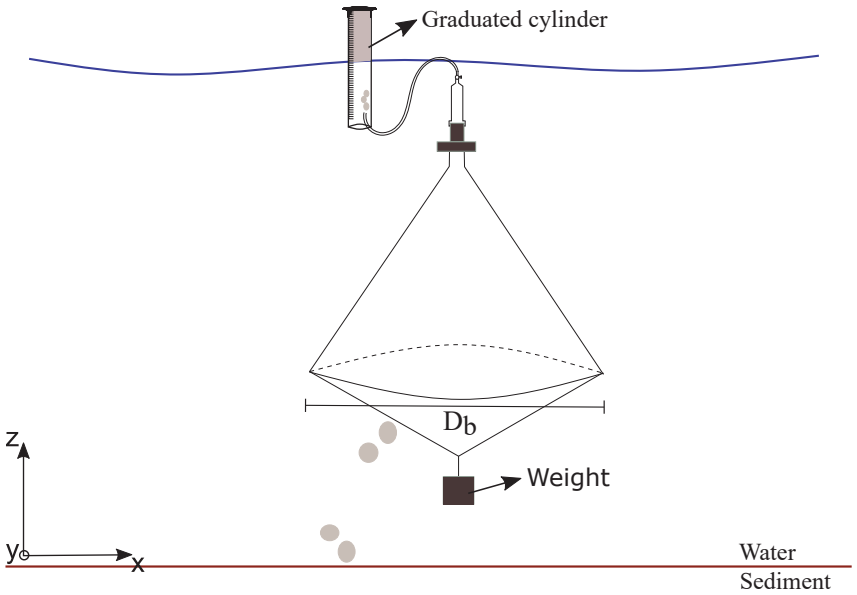


Figure 12: Conventional funnel and graduated cylinder for measuring the volume of gas.

# 3 Methods

In the following chapter it is described previous ABTs tests performed in the laboratory and how field data was obtained, including measurement locations in the reservoir and the auxiliary data used for ebullition analysis. The steps followed in data processing and flux calculation is also pointed and lastly is summarized some statistical tests applied for data analysis.

## 3.1 Automated bubble trap calibration and data acquisition

### 3.1.1 Laboratory tests

Three ABTs were installed in different locations in Passaúna reservoir in the beginning of 2016, but no data was recorded. As the equipment is a prototype it was opted to perform some tests in the laboratory in order to have a better understanding of its operation and to evaluate its measurements. A water tank in the laboratory of the Federal University of Paraná with dimensions of 70 cm width, 60 cm height and 100 cm length, Figure 13, was used for the test. The ABTs were fixed in the water tank and the water level kept above the pressure sensor. Bubbles were generated with an aquarium pump of $250\,\mathrm{L\,hr^{-1}}$ capacity.


Figure 13: Laboratory test setup and live reading data from ABT's software.

Water tank temperature was also measured for posterior comparison with ABTs measurements. The conducted tests are shown in Table 8.

Real-time measurements can be monitored at ABT's software when it is connected to the computer. It could be observed if the variables measured agreed with actual conditions, such as water temperature and fill height. The equipment software allows setting ABT's configurations such as time interval, gas fill height limit that is used by the software to activate the solenoid valve for gas flushing, geometric characteristics of the equipment, and start/end measurement date. Additionally, the software is used for downloading and erasing ABT's internal memory data.

The solenoid valve operation was tested by filling up the inner tube with gas bubbles when the gas level reaches the level specified for flushing the valve activate and flush out the gas contained in the

Table 8: ABT testing performed at the laboratory

| Test | Objective | Procedure |
|---|---|---|
| Data visualization | To verify live reading data and stored data in the internal memory and in the SD card. | Live reading was checked when the ABT was connected to the computer by an USB cable. Stored data could be downloaded by ABT software and the SD card was checked for the data file. |
| Valve openings | To check if the solenoid valve was working. | Bubbles were generated and released inside the inner tube and valve opening was verified if occurred when the gas level reached the pre-defined flushing level. |
| Temperature and pressure sensors | To validate pressure and temperature readings. | ABT temperature and pressure measurements were compared with temperature and pressure data from a weather station located at the university. |
| Fill height | To validate ABT fill height measures. | Gas was added in the funnel's inner tube and the fill height was read from scale bar to further compare with the fill heigh recorded by the equipment. |
| Baterry consumption | To estimate the consumption of battery by the equipment. | A multimeter was used to measure battery voltage over time. |

tube. Even if the gas level does not reach its limit for flushing the valve is activated each 12 hours to avoid blockage. It was observed from the tests that the solenoid valve has a delay from 1–3 seconds when the battery is running low and it did not activate if battery package voltage was lower than 5.0 V.

The temperature measured by the ABT's sensor when the inner tube was filled with water was compared with water tank temperature measured by a thermometer. No significant variations were observed between the two. The absolute pressure from ABT's measurement ($P_{absolute} = P_{atm} + P_{water}$) was compared with air pressure measured by a weather station that is installed in the university. It was noticed that the behavior of pressure from the ABT is very similar to the pressure behavior from the weather station.

In order to verify fill height readings, each time that air was added to the tube the fill height was verified in the scale bar and was later compared with fill height from ABT's data file. For the case that the fill height differed from reading values, a new calibration of the fill height was done. Fill height calibration was made using the ABT's software following procedures specified in the equipment user's manual. The new calibration was accepted when the goodness-of-fit value was greater than 0.98 when new measurements were conducted to double-check the fill height reading.

Battery consumption was verified for planning future field campaigns. The larger amount of battery consumption is due to solenoid valve opening. ABT's autonomy was estimated as 14 days, after this period the equipment might record pressure, temperature and fill height data, however, it may not have enough energy to open the solenoid valve.

The overall tests of the equipment showed the following general results:

- Careful preparation and connection to batteries and checking of contacts allows for proper equipment operation;

- Data storage on internal memory and SD-card has been corrected and improved by updating the firmware, nonetheless, not all versions of the ABTs save data file in the SD-card; and

- Data extraction can be time-consuming, due to large manual works to open the sensor, but also due to low data-transfer rates.

### 3.1.2 Field measurements

A total of three ABTs are installed along Passaúna reservoir recording continuous gas ebullition. ABTs' deployment locations were defined taking into account previous studies (SOTIRI, 2016; ZAREBSKA, 2016) of bathymetry and bottom sediment characteristics. As at both studies sediment and water samples were taken from defined locations, the ABTs were installed considering three of the locations previous defined in the mentioned studies to facilitate the comparison of results. The location P1 is approximately 500 m away from Passaúna park and is the shallowest point. The P2 was placed right in front of the water intake facility and the P3 is at the deepest region of the reservoir at 1 km far away from the spillway, Figure 14.

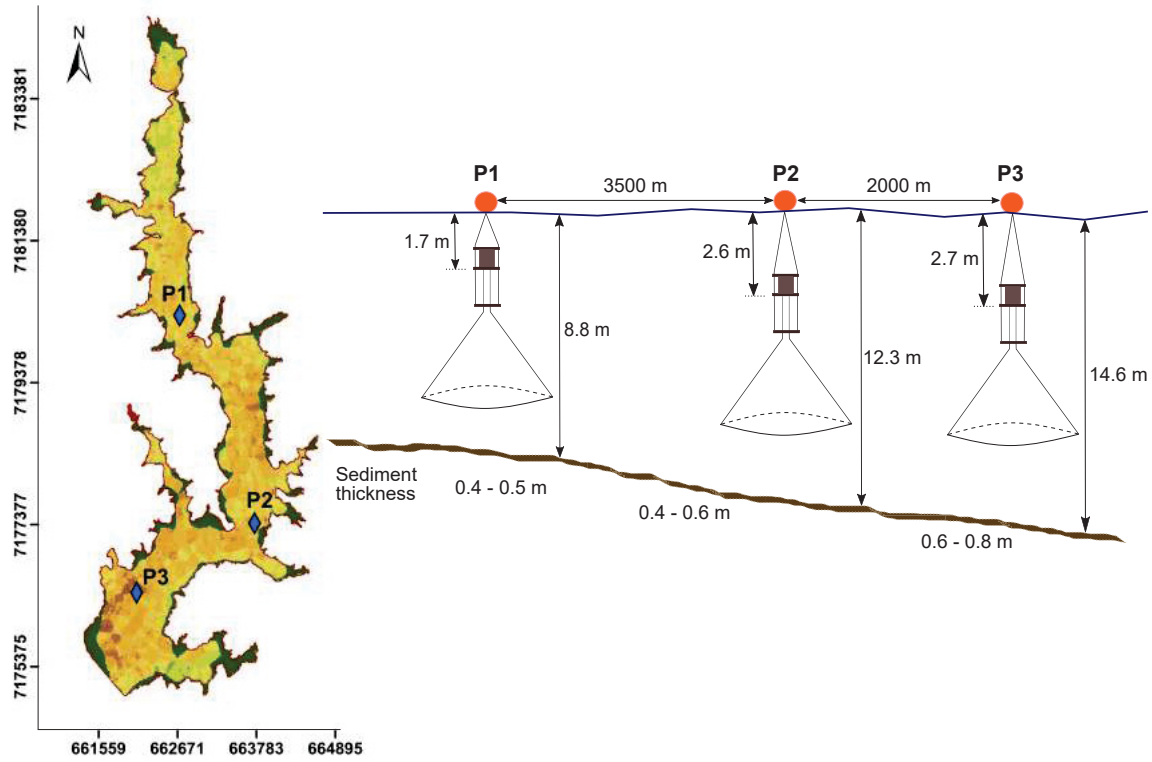


Figure 14: Sediment thickness map of Passaúna reservoir from Sotiri (2016) with ABTs' locations. On the right hand side is a representation of each equipment placement in the water column.

The installation of the ABTs and the later ebullition data acquisition followed some steps, Figure 15. The first step begins at the reservoir bank where ropes, buoys, and weights are prepared. The ropes are cut according to each location depth; buoys and the weights are then attached to it. Each one of the location is accessed by a boat. After arriving at the location the ABT configuration is set to start measurement, the equipment is carefully placed in the water while it is checked if the equipment releases the air contained inside. After the ABT is submerged the two weights are placed in opposite directions and away from the equipment. Both weights work as anchor to avoid that the equipment moves from the location.

With a frequency of twice a month the ABTs were verified. The procedure followed was to remove the equipment from the water, clean the funnel and the inner tube to remove algae that had accumulated over it. The ABT is then opened in order to change battery and to download the data from its internal memory by an USB cable connected to a computer. Finally, after downloading the data, the memory is erased, the ABT's configurations are set, and the equipment is placed back into the water.

The ABTs remain constantly installed in the reservoir unless the equipment requires repair that can not be performed in the field.

All the field campaigns activities were time demanding. Not only in the field itself but also preparing the material and tools needed. The reservoir is located 27 km from the university campus which required at least 40 minutes drive by car to arrive at the study site. Once in the reservoir, the boat was placed in the water. The farthest monitoring location was P1 which took 30 min by boat to access the ABT. The time required for downloading the data depended on the amount of data to be transferred, but on average was 30 minutes for each ABT. In addition to time, the campaigns had costs involved and a detailed discussion is presented in section 4.8.

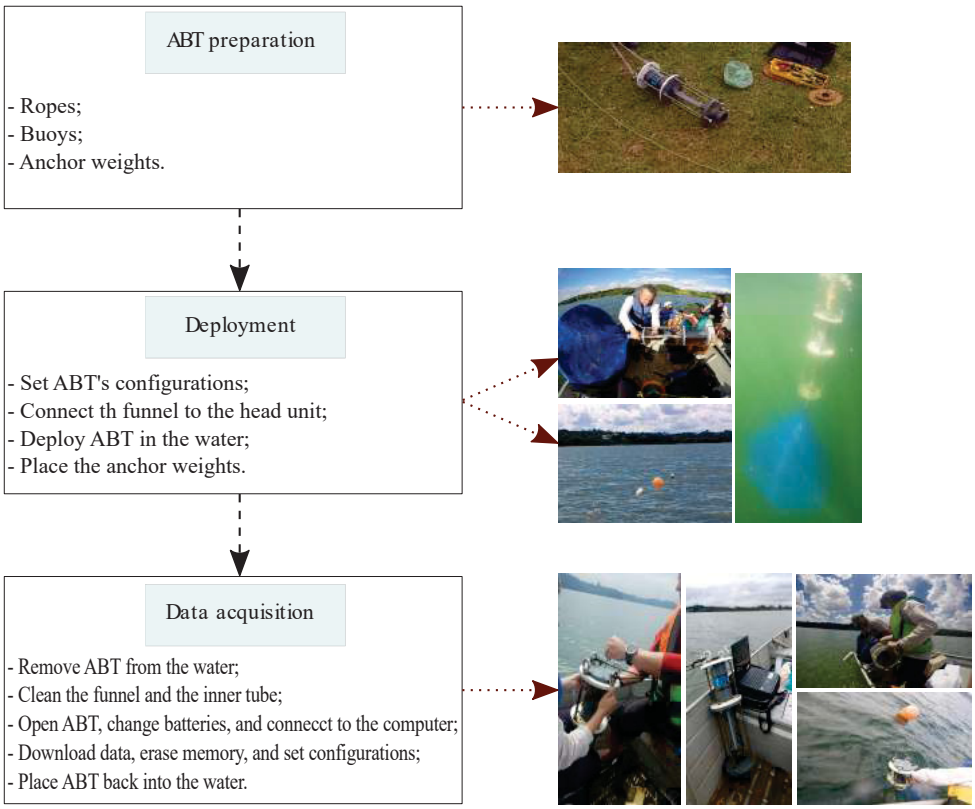


Figure 15: Representation of procedures followed during field campaigns for ABT‘s deployment in the water and later for data download.

### 3.1.3 Conventional funnels

In each measurement location, three conventional funnels were installed in order to obtain a coarse volume comparison with the automated bubble trap measurements.

Two distinct measurements were performed using the conventional funnels. The first one was a 24 hours sampling interval measurement when the funnel remained deployed for 2 days and the second one was a long term measurement when the gas volume was verified after several days. Although it is recommend sampling in 24–48 hours interval, the conventional funnels were left in the reservoir for long-period of time in order to have a gross comparison in terms of total gas volume with ABTs measurements. For long time deployment is expected that a portion of methane from the accumulated gas dissolves into ambient water, nonetheless, gases tend to expand and occupy all available volume, therefore in terms of volume we assumed that methane dissolution into the ambient water didn’t have a significant effect on the total volume of gas.

## 3.2 Secondary data of water and sediment

In this section is given an brief overview and some of the results observed from auxiliary data. Some of the parameters here presented are results from other studies that are being conducted in parallel in the reservoir.

### 3.2.1 Temperature and dissolved oxygen profiles

Auxiliary measurements were performed during field campaigns. CTD (Conductivity–Temperature–Depth) profiles for water temperature at ABTs' locations in different months is presented in Figure 16. It can be observed that temperature stratification is stronger in February and March with the largest temperature gradient. In May temperature is uniform indicating that mixing occurred. The water stratification is observed again in the end of August when a well defined thermocline is observed at 5 m. The depth of the thermocline also varies, as can be observed in the temperature profiles measured at March $06^{th}$ with termocline at 6 m and in March $22^{nd}$ when the termocline is at 10 m deep. It can be caused by a combination of mixing of the top layer of water due to wind incidence and surface cooling due to a reduction of air temperature. The warmest bottom temperature was recorded in March $22^{nd}$ while the coldest temperature was verified in August $10^{th}$.

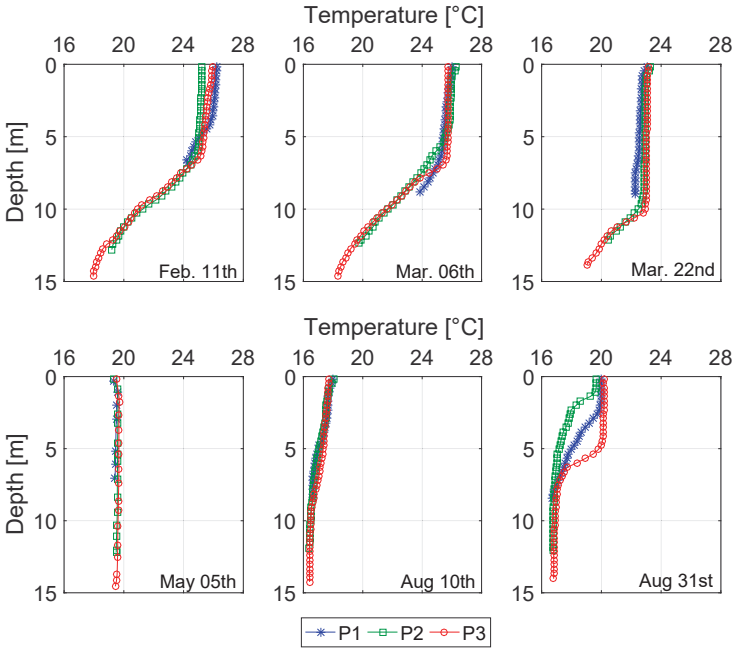


Figure 16: Temperature profiles measured at ABTs location from February of 2017 to August of 2017. The measurements of February, March, and August were done with a CTD while the temperature profile in May was obtained with a Horiba (NoPa-SeWaMa project data). In this case the P3 temperature was measured approximately 800 m downstream the actual ABT position.

The temperature profile may give a hint on the oxygen profile in the water column. Dissolved oxygen (DO) profiles measured with a Horiba U-53 in February $14^{th}$ and in May $05^{th}$ is shown in Figure 17. In February $14^{th}$ the DO profile wasn't obtained for P3 location and the values measured in May $05^{th}$ for P3 was in fact measured 800 m downstream the ABT-P3. It is observed that the dissolved oxygen concentration raged from 0.86 mg $L^{-1}$ to 8.9 mg $L^{-1}$ with the lower concentrations near to the bottom sediment. While the water temperature decrease from February to May mainly in the surface the DO

concentration increased essentially in the bottom layer of the water column resulting in a smaller DO vertical gradient.

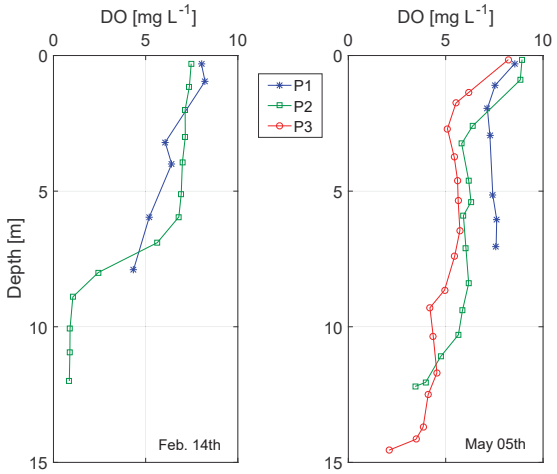


Figure 17: Dissolved oxygen profiles measured with a Horiba U-53 at the ABTs' location in February $14^{th}$ and May $05^{th}$. The DO profile measured for the P3 in May $05^{th}$ was obtained 800 m downstream the ABT placement.

### 3.2.2 Water quality and sediment characteristics

In this sub-section is briefly presented some of the results regarding water quality parameters and sediment characteristics obtained by studies conducted at Passaúna reservoir. Figures 18, 19, and 20 are unpublished data of dissolved organic carbon, chemistry oxygen demand, and total nitrogen obtained from Godoy (2017). The three locations have a different pattern and concentration of the component considered. The concentration also varied from one month to another and this was attributed to meteorological conditions as in February had a 10-days accumulated precipitation of 118.7 mm while in May the 10-days accumulated precipitation was 10.6 mm.

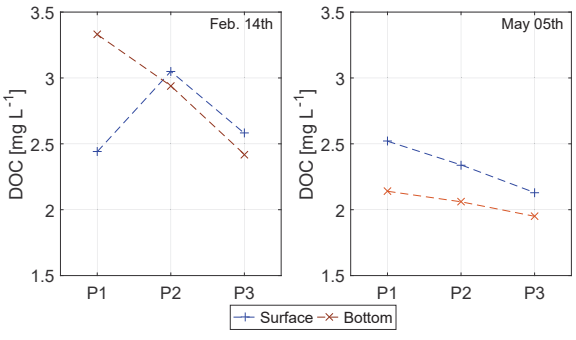


Figure 18: Dissolved organic carbon (DOC) concentration for water samples collected at each location in February $14^{th}$ and May $05^{th}$ of 2017. The P3 is located 800 m downstream the ABT placement.

Zarebska (2016) analysed the bottom sediment of Passaúna reservoir in several locations. The locations denominated by the author as C5, C11 and C2 correspond with P1, P2, and P3 locations respectively. Considering the author's result from core samples the bottom sediment in all measurement points is composed mainly of silt and clay being the corresponding percentage of 99.21%, 96.94% and 95.77% for locations P1, P2 and P3 respectively. It is pointed in the study that the total carbon and total phosphorus were higher in these points, mainly in P2 and P3 (C11 and C2 at Zarebska's (2016) study)

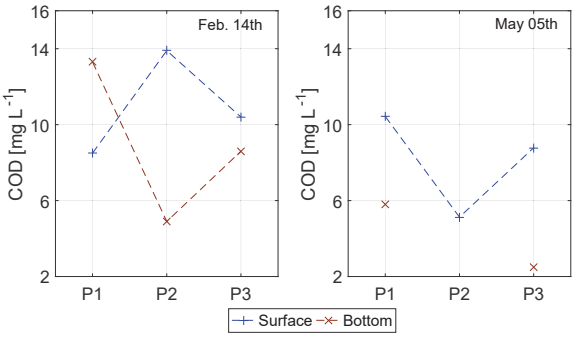


Figure 19: Chemistry oxygen demand (COD) concentration for water samples collected at each location in February $14^{th}$ and May $05^{th}$ of 2017. The P3 is located 800 m downstream the ABT placement.

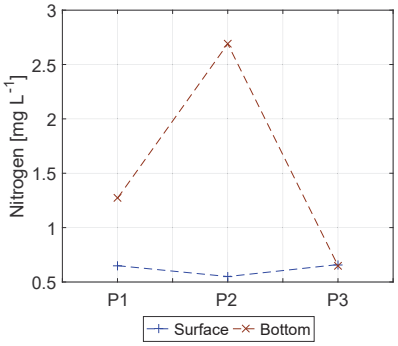


Figure 20: Total nitrogen concentration for water samples collected at each location in February $14^{th}$ of 2017. The P3 is located 800 m downstream the ABT placement.

than in the others points due to elevated organic matter content, which led the author to suggest that both locations, P2 and P3, are possible hot spots of methane production. In addition, it is reported the occurrence of bubbling when sediment was disturbed to obtain the core samples (ZAREBSKA, 2016).

## 3.3 Data analysis

An overview of environmental data that will be considered in this research is presented in Figure 21. Data from CTD and Horiba were measured, when possible, during the campaigns to the reservoir for ABTs' maintenance. Reservoir water stage is daily measured in a staff gage, precipitation at the rain station is read twice a day and weather stations record hourly data. ABTs are set to record data with high temporal resolution with time steps of seconds.

Ebullition data has been obtained in discrete time steps interval initially of 5 seconds and later set to 15 seconds due to the elevated time required to download data from the equipment. Field measurements started in February 2017. ABTs installed at locations P1 and P2 operate with high power battery type which lasts more than the rechargeable batteries that are used in ABT-P3. The periods without recorded data from P1 were due to ABT malfunctioning and the equipment had to be removed from the water. The same happened to ABT-P2 which was removed from water in the end of June of 2017. The multi-parameter probe (Horiba U-53) was used just in February and May during the water quality campaigns while the CTD (Castway SonTek) was used during field expeditions

Gas volume with conventional funnel was measured for two days in 24 hour time steps in February while long term measurement of 23 and 30 days was performed in April and May respectively. After this

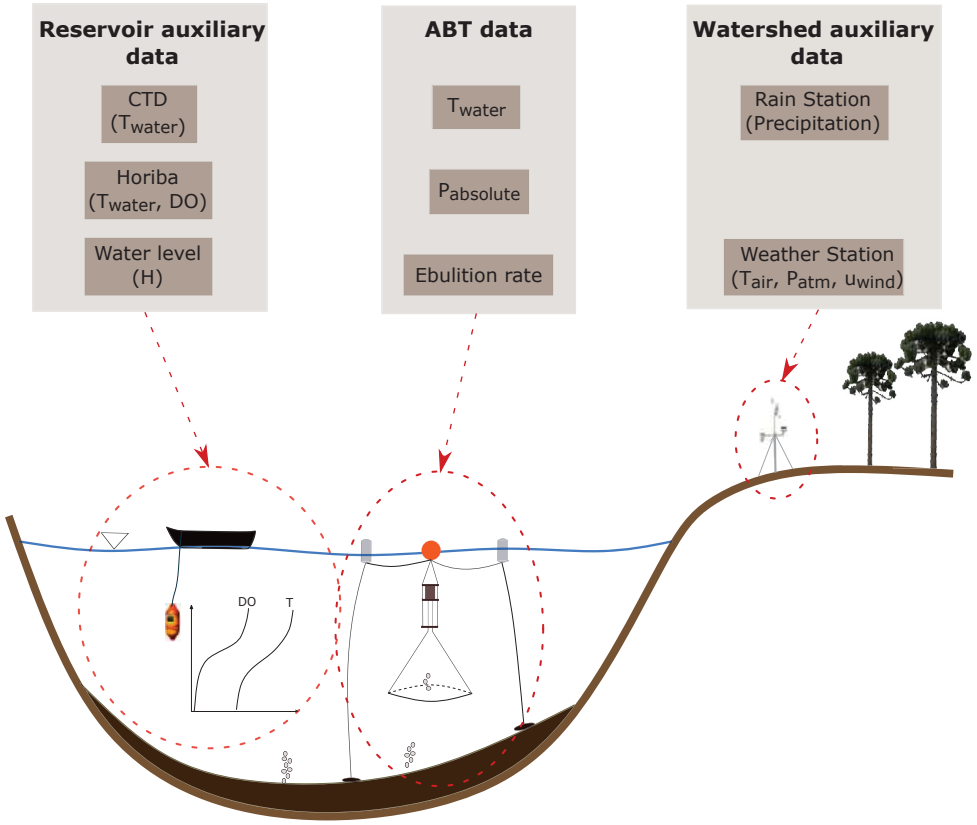


Figure 21: Scheme with the overall data

period, the conventional funnels were removed from the monitoring locations as te equipment material was damaged after being deployed for long period (more than 4 months). A summary containing the period of data available is shown in Table 9.

Table 9: Acquired data with measured variables and period of data

| | **Measured parameters** | **P1** | **P2** | **P3** |
|---|---|---|---|---|
| **ABT** | Water temperature [°C]<br>Absolute pressure [mbar]<br>Gas fill height [mm] | 10/02-15/02 | 14/02-06/03 | 10/02-15/02 |
| | | x | | 15/02-21/02 |
| | | 06/03-22/03 | 06/03-22/03 | 06/03-19/03 |
| | | x | 22/03-10/04 | 22/04-04/04 |
| | | 10/04-03/05 | 10/04-03/05 | 10/04-24/04 |
| | | 03/05-27/05 | 03/05-27/05 | 03/05-16/05 |
| | | x | 02/06-21/06 | 02/06-14/06 |
| | | 21/06-10/08 | x | 21/06-28/06 |
| | | 10/08-31/08 | x | 10/08-24/08 |
| | | 31/08-21/10 | x | x |
| | | 21/10-31/10 | x | x |
| **Conv. funnel** | Gas volume [ml] | 14/02 - 16/02 | | |
| | | 10/04 - 03/05 | | |
| | | 03/05 - 02/06 | | x |
| **CTD** | Water temperature [°C]<br>Conductivity [mS cm$^{-1}$]<br>Depth [m] | 11/02 | | |
| | | 06/03 | | |
| | | 22/03 | | |
| | | 10/08 | | |
| | | 31/08 | | |
| **Horiba** | Water temperature [°C];<br>pH<br>Conductivity [mS cm$^{-1}$]<br>Turbidity [NTU]<br>Dissolved oxygen [mg L$^{-1}$] | 14/02 and 05/05 | | |

### 3.3.1 Data post processing

In a general way, ebullition rate was analysed in terms of statistical parameters providing a clue in the spatial ebullition characteristics within the three locations where gas flux was measured in the reservoir, and allowed to assess temporal variability of emissions fluxes with a hint on some of the external forcings that contribute in triggering bubbling events in Passaúna reservoir.

Although methane content on gas bubbles is reported in the literature to vary in the range of 42 – 90% (MAECK; HOFMANN; LORKE, 2014) its concentration for the case of Passaúna reservoir is still unknown. Therefore, ebullition data will be analyzed in terms of the total volume of gas. The gas fill height which is measured by the ABTs is used to calculate the volume flux of gas by Equations 2.1 and 2.2. Nevertheless, in order to compare gas volume from different locations which varying temperature and pressure conditions the volume was converted to standard conditions (20 °C and 1 atm), therefore the volume flux in standard conditions ($Vol_{fstd}$) is determined by Equation 3.1,

$$Vol_{fstd} = Vol_f(\frac{T_{std}}{T_a})(\frac{P_a}{P_{std}}), \tag{3.1}$$

where $T_{std}$ and $P_{std}$ are standard temperature and pressure; $T_a$ and $P_a$ are measured temperature and absolute pressure.

The equipment gives the accumulated gas fill height which is a manner of filtering out negative gas fill height that occurs when the solenoid valve flushes the gas out. Thus, the actual gas fill height in each time step is calculated as the difference between two-time steps (accumulated fill height from actual time step minus accumulated gas fill height of the previous time step). Water temperature and absolute pressure are also measured at each time step by the equipment. In order to perform flux calculations and to identify any inconsistency in temperature and pressure data a script was written in MatLab.

The Matlab script allows the user to define the start and end date to be considered for flux calculation. The gas volume is integrated in different time scales of 5 minutes, 1 hour and 1 day which is then used to calculate the volume of gas per area per time in the mentioned time scales. An additional calculation step is used in order to determine how much of methane is emitted from the total gas volume in which ebullition rate can be calculated by Equation 2.4. A simplified scheme with input data, calculation steps, and output is presented in Figure 22.

Besides flux calculation, temperature and pressure data were checked for inconsistencies, such as values out of expected range. Few inconsistencies were identified and were corrected and replaced by the mean calculated with the adjacent values. For the file recorded at the location P2 from February $14^{th}$ to March $3^{rd}$ 10 pressure values out of the 346048 points were replaced and none modification had to be done in temperature values. Nonetheless, such alterations did not result in any alteration in the fluxes values, as both variables are used for the calculation of mean temperature and mean absolute pressure for the integrated time interval (5 minutes, 1 hour or 1 day) which is then used to obtain volume flux in standard conditions.

### 3.3.2 Statistical analysis

Statistics can be defined as a set of tools that assist in the organization, description, and analysis of data (MAGALHÃES; LIMA, 2002). Ebullition events are described as being a stochastic process (Del SONTRO et al., 2015), meaning that series of ebullition can not be represented by a deterministic model, but are formed of random variables instead which are described with probabilistic and statistical

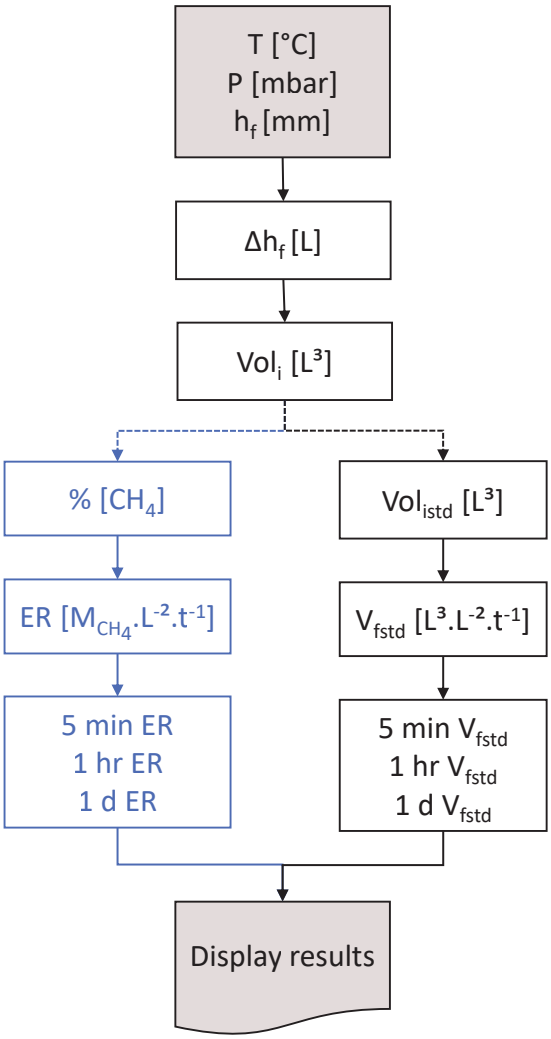


Figure 22: General procedure followed in MatLab for flux calculation

concepts. In this study, basic parameters such as mean, standard deviation, percentiles, and histograms will be calculated.

Data was analyzed by comparing results among the three locations and by comparing data of each location with another parameter (secondary data). For the first case, it can be obtained an idea of ebullition's spatial distribution which allowed a qualitative description of the ebullition taking into account local water depth and sediment characteristics, for example. For the second case, it was investigated the relation of ebullition flux with environmental parameters such as temperature, air pressure, wind velocity and precipitation, and in this way it was observed which parameters had influence in triggering ebullition events in the reservoir.

Statistical tests can be classified as a parametric or a non-parametric test. The main difference between the two categories is that for parametric test it is assumed a normal data distribution (MAGALHÃES; LIMA, 2002). The mean between points can be compared by t-test which is applied for two groups or by ANOVA (Analysis of variance) which can be used for comparing more than two groups. Both are parametric tests. Mann-Whitney test and Kruskal-Wallis test are non-parametric and useful for comparing the values of two groups and more than 2 groups respectively.

The correlation of ebullition with forcings can be investigated through correlation analysis. Pearson correlation is a parametric test which evaluates the linear correlation between variables considered

while the Spearman is a non-parametric test in which the correlation between variables does not have to be linear, however, it assumes a monotonic function between variables. Table 10 shows a short overview on some statistical methods whereas in this study non-parametric tests were applied for ebullition data analysis. For the cases that data does not have a normal distribution, it can be transformed before a parametric test is applied.

Table 10: Statistical methods for data analysis

| | Parametric | non-Parametric |
|---|---|---|
| Comparison among points | t-test (2 groups)<br>ANOVA (>2 groups) | Mann-Whitney (2 groups)<br>Kruskal-Wallis (>2 groups) |
| Correlation with forcings | Pearson | Spearman |

# 4 Results and discussion

In this chapter is shown the results obtained from field measurements of gas flux. The aim is to better understand the ebullition processes by analysing its characteristics and investigating its dependence on other environmental parameters through comparison with auxiliary data and with literature information. In order to facilitate the understanding of the results and discussions, it is presented some definitions assumed in this work.

## 4.1 Concepts and definitions

Some of the terms cited throughout the discussion and result analysis are listed below and are relevant to guide the reader to a better interpretation and to follow the idea that it is intended to present.

***Ebullition***

In thermodynamics ebullition refers to a change phase process from liquid to gas with bubbles generated (KROOS; POTTER, 2015), nevertheless, in this study ebullition is considered to be the formation and release of bubbles from the sediment matrix in an aquatic environment without necessarily being related to a change of phase.

***Detection***

Gas fill height recorded due to the ascending bubbles that were trapped in the equipment.

***Time Step Detection (TSD)***

Time interval set in the equipment to record data.

***Time Step Analysis (TSA)***

Also referred as integration time, is the time interval used for volume and flux calculation which TSA $\geq$ TSD.

***Ebullition event***

The ebullition occurred defined from a set of criterion which could have been triggered by one or more overlapping causes.

## 4.2 Conventional funnels measurements

Conventional funnels were installed with the objectives of validating ABTs measurements and to obtain gas samples for the analyses of methane content in the bubbles. A campaign for intensive data acquisition in the reservoir was conducted during the third week of February of 2017. During this period gas volume was measured every 24 hours for two days. Volumes of gas captured in all funnels weren't the same in terms of total volume, but the volume among funnels installed in the same location was in the same order, Table 11.

The conventional funnels remained in the water for long-term volume measurement. The volume of gas was measured at all points in March $3^{rd}$ after 23 days deployed and measured at locations P1 and P2 in June $2^{nd}$ after 30 days submerged in the water column. The fluxes varied among locations and within funnels installed in the same region (Table 12) showing spatial variability even in small spatial scale. The

Table 11: Gas volume flux obtained from the conventional funnels in February of 2017 (volume in standard conditions of pressure and temperature).

| | | **Gas volume flux** [ml m$^{-2}$ d$^{-1}$] | |
|---|---|---|---|
| | | 14/fev–15/fev | 15/fev–16/fev |
| **P1** | Conv. 1 | 37.4 | 21.5 |
| | Conv. 2 | 23.8 | 6.8 |
| | Conv. 3 | 44.2 | 28.2 |
| | ABT | 11.4 | – |
| **P2** | Conv. 4 | 53.4 | 85.1 |
| | Conv. 5 | 59.1 | 63.5 |
| | Conv. 6 | 39.8 | 63.5 |
| | ABT | 18.5 | 7 |
| **P3** | Conv. 7 | 22.6 | 90.8 |
| | Conv. 8 | 27.1 | 57.8 |
| | Conv.9 | 30.5 | – |
| | ABT | 26.9 | – |

greatest flux during the period of April and beginning of March was observed at location P2 with the lowest values at P1 near Passaúna park. The long-term measurements data can be compared with ABT measurements at locations P1 and P2 for the period of April $10^{th}$–May $03^{rd}$, when was obtained data from both methods. From ABTs the volume flux for the period was 13.6 ml m$^{-2}$ d$^{-1}$ and 121.4 ml m$^{-2}$ d$^{-1}$ at P1 and P2 respectively, which for the case of P1 is very similar to mean value of the three conventional funnels (15.8 ml m$^{-2}$ d$^{-1}$) and for P2 the flux obtained by the ABT was greater than the mean value from the conventional method (77.5 ml m$^{-2}$ d$^{-1}$).

Table 12: Gas flux calculated from long-term measurements of conventional funnels considering gas volume in standard conditions of pressure and temperature.

| | | **Gas flux** [ml m$^{-2}$ d$^{-1}$] | |
|---|---|---|---|
| | | 10/04/17–03/05/17 | 03/05/17–02/06/17 |
| P1 | Conv. 1 | 15.3 | – |
| | Conv. 2 | 18.4 | – |
| | Conv. 3 | 13.7 | – |
| P2 | Conv. 4 | 73.7 | 37.7 |
| | Conv. 5 | 86.8 | 24.1 |
| | Conv. 6 | 71.9 | 29.8 |
| P3 | Conv. 7 | 32.6 | 69.7 |
| | Conv. 8 | 56.7 | 32.6 |
| | Conv. 9 | – | – |

Data could not be obtained from all conventional funnels, mainly during the second long-term deployment period (May $03^{rd}$–June $02^{nd}$). After being submerged in the water over a long period of time (more than 5 months) the bottom portion of the canvas which was attached to an iron arch started to disintegrate and the conventional funnels had to be removed from the water.

## 4.3 Ebullition time series overview

Although the automated funnels still remain deployed in the reservoir, in this work is presented data collected and processed from February $10^{th}$ to October $31^{st}$ of 2017 for each location. In the time series of gas ebullition obtained, Figure 23, the blue lines are the gas flux integrated over 5 minutes time interval while the orange line (values represented in the right hand-side of y-axis) shows daily gas flux. The first peak (52 715.7 ml m$^{-2}$ d$^{-1}$) on ebullition at P1 that was recorded in February $11^{th}$ is not shown in the graph to facilitate the visualization of the other values. Areas shaded in grey represent the period of no data recorded either due to problems with the equipment or due to logistic issues and the equipment battery could not be replaced.

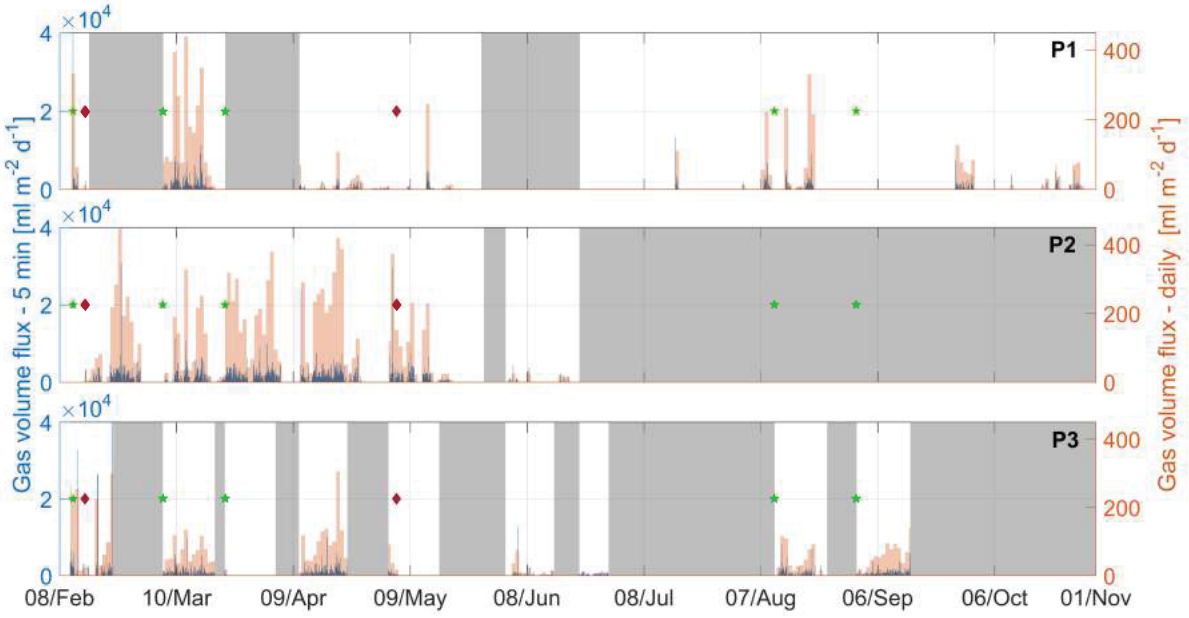


Figure 23: Time series of 5 min ebullition flux in blue line and daily gas flux in the orange bars recorded in 2017. The shaded areas represent periods without data recorded. The green stars are dates when CTD data was recorded while the red diamonds are the dates when campaigns to obtain water quality parameters occurred.

For the period showed the total amount of hours with data recorded was 4774.9, 2907.2, and 2629.8 hours at P1, P2 and P3 respectively. From February to beginning of July, the ebullition time series of P2 is the one with fewer gaps on the data recorded while after June P1 is the location with data measured continuously until the end of October. The ratio between the number of hours with ebullition recorded and the amount of time without ebullition resulted that on average ebullition occurred in less than 10% of the time only, Table 13.

Considering the 5 min ebullition time series some peaks were identified. The three largest ones verified at each location are listed in Table 13. The highest peaks were greater than 30 000 ml $m^{-2}$ $d^{-1}$ occurring in different days and in distinct periods of the day. Despite the 5 min largest ebullition peaks were verified in February, except for the P2, the days when the largest amount of gas was emitted differed. At P1 the wider daily gas flux was recorded in March $12^{th}$ and at P3 in April $15^{th}$. This suggests that the contribution of less intense emissions to the total amount of gas emitted over a day is greater than the volume of gas emitted by isolated high intense ebullition occurrences. Such characteristic is better explored in section 4.5.

Table 13: Amount of hours of data collected at all three locations, time with and without ebullition recorded and the three largest ebullition peaks observed in the 5 min gas flux time series for the entire period.

| | **P1** | **P2** | **P3** |
|---|---|---|---|
| Total hours of measurement [hr] | 4774.9 | 2907.2 | 2629.8 |
| Hours with ebullition [hr] | 232.4 | 389.2 | 268.1 |
| Hours without ebullition [hr] | 4542.5 | 2518.0 | 2361.7 |
| **Fraction of time with ebullition [%]** | **4.9** | **13.4** | **10.2** |
| Largest ebullition peak [ml $m^{-2}$ $d^{-1}$] \| date | 52715.7 \| Feb. $11^{th}$ 09:55 | 3007.6 \| Feb. $23^{rd}$ 19:35 | 42355.8 \| Feb. $21^{st}$ 10:30 |
| Second largest ebullition peak [ml $m^{-2}$ $d^{-1}$] \| date | 13288.3 \| Jul. $16^{th}$ 00:25 | 27805.4 \| May $04^{th}$ 11:30 | 32070.4 \| Feb. $12^{th}$ 17:00 |
| Third largest ebullition peak [ml $m^{-2}$ $d^{-1}$] \| date | 10703.9 \| Mar. $16^{th}$ 07:40 | 9873.3 \| Apr. $02^{nd}$ 04:20 | 304853.0 \| Feb. $21^{st}$ 10:25 |

Looking at the graphs presented, Figure 23, it is noticed that ebullition varies in space comparing all three locations and in time having days when no ebullition was recorded and on the other hand, peaks recorded sporadically. The time variation is verified in both timescales of minutes or days. When ebullition recorded over a day is observed with more detail, for instance, it can be verified that in a smaller time scale the single large ebullition flux is in fact formed by several emissions of shorter duration, Figure 24. The reason of emissions being episodic is that the formation of bubbles depends on gas production and in having enough gas accumulated in the sediment to allow bubbles to form, after that its release from the sediment depends on the bubbles capacity to overcome the pressure imposed by the ambient conditions.

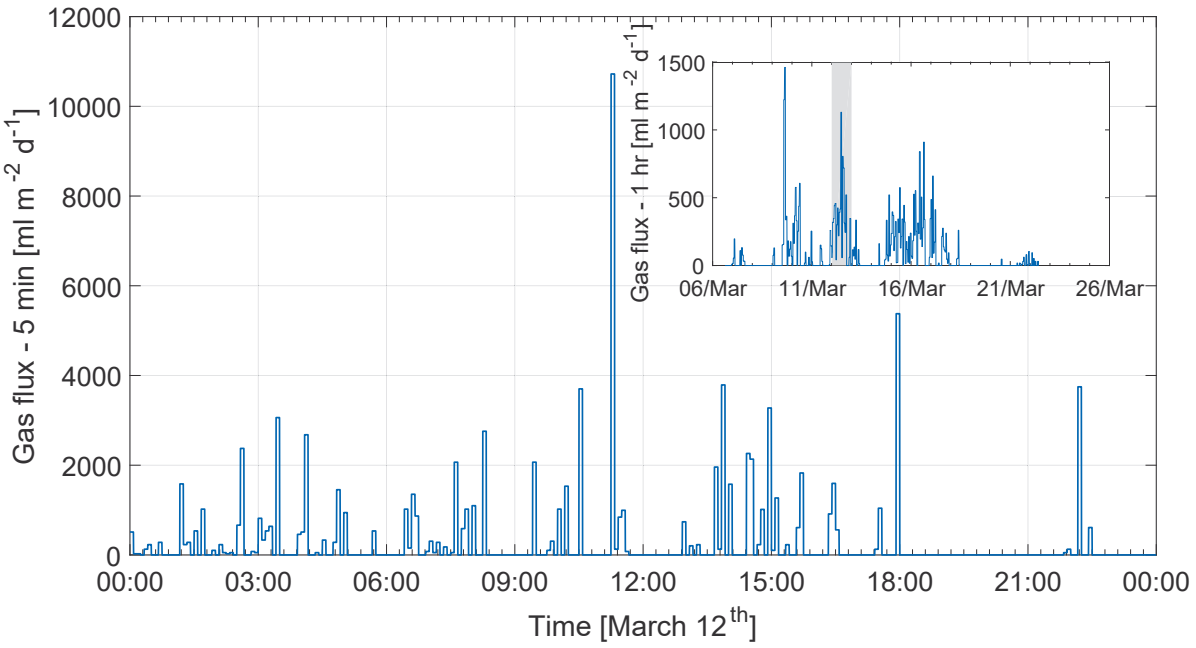


Figure 24: Five minutes ebullition flux in March $12^{th}$ of 2017 at location P2.

One of the effects of this large temporal variability is that emissions seem not to have an evident periodicity. The time interval with no ebullition recorded among the periods of emissions is not regular. On an hourly basis the time interval between any recorded event can be hours, nonetheless, on a daily basis is verified several days when little or no ebullition at all was recorded. This high temporal variability contributes to different ranges of emissions found in the literature, mainly when measurements are performed over a short period of time. The episodic characteristic of ebullition was also reported in previous studies as Baird et al. (2004), Maeck, Hofmann and Lorke (2014). Baird et al. (2004) also found by analysing ebullition from bog peats that after periods of ebullition occurs intervals of time with no or with reduced emissions, a similar pattern is perceived looking at the top graph of Figure 25. In the period showed ebullition can roughly seem as three large emissions with no ebullition in between. Besides external forcings, the type of organic matter, labile or recalcitrant, can also have an impact on the amount of gas production and the amount of time for the matter to be decomposed.

Considering the gas fluxes integrated over different time scales, Figure 25, two main aspects may be highlighted. First one is that the flux intensity is related to the duration of the emission, which is in agreement with Equation 2.2 where the volume flux is inversely related to the time step. This implies that when comparing emissions intensity from one place to another should also be considered the sampling duration. Another aspect is related to how detailed is the ebullition time series representing the emissions. The relevance of this issue and a suggested approach is better addressed in next section.

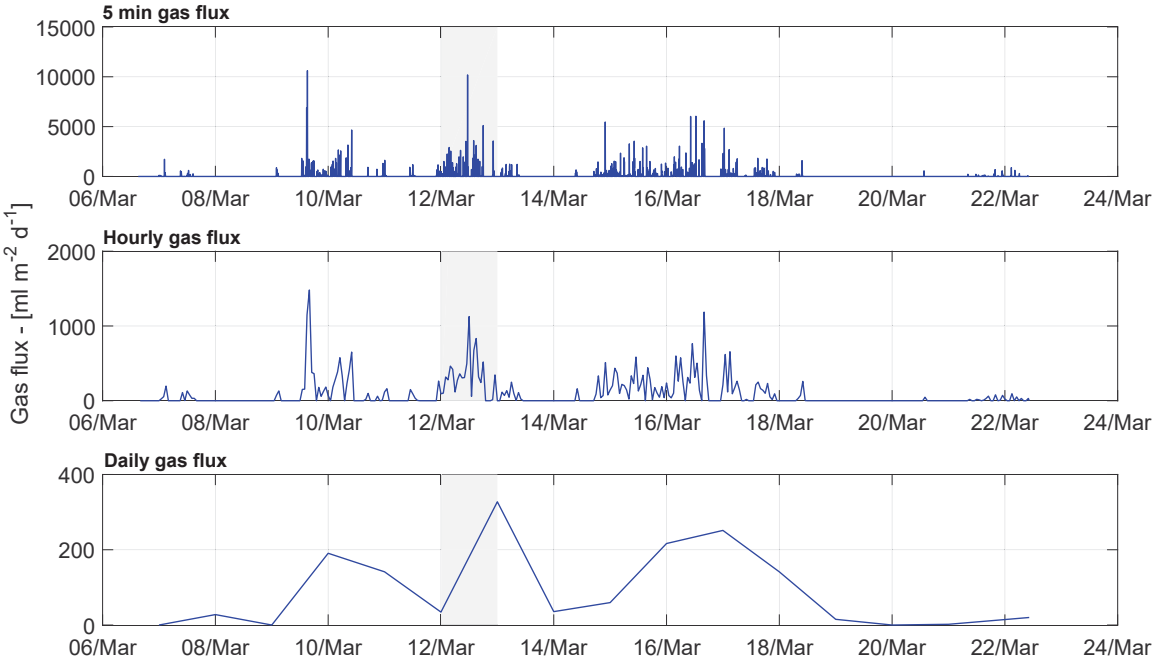


Figure 25: Ebullition flux recorded during March 2017 at location P2 with TSA of 5 minutes, 1 hour and 1 day.

## 4.4 Definition of the time step analysis

Starting from the last point mentioned in the previous section, an important question that arises when the ebullition process is analysed from high temporal resolution measurements is regarding what is the appropriate TSA (Time Step Analysis) that might be adopted. Going back to Figure 25, more specifically to the shaded areas, is verified that in larger TSA, as daily gas flux (bottom graph), all the emissions of short duration are grouped in a single ebullition event and thus, the variability occurring within a day is filtered, as a consequence hours when no emissions were recorded will have a value attributed for the gas flux.

On the other hand, the use of a very short TSA provides a time series with very detailed ebullition with a larger temporal variability observed. Nevertheless, it may turn difficult to explore the relation of ebullition to other parameters. That is because, in very small TSA or even considering the equipment time step detection (TSD), the time series may be a white noise[1] as it will be shown. Additionally, the time between the actual emission and the time recorded by the equipment differ which can mask any possible relationships among parameters. During the ABTs laboratory test, for instance, it was observed that as the battery is consumed the equipment had a delay greater than 10 seconds in the detection and gas flushing.

To better understand and to summarize the idea involving the choice of the proper TSA, an analogy can be made with the definition of continuum studied in fluid mechanics, in which we are interested in the fluid as a whole and not in its molecular characteristics. In this case, the control volume chosen to analyse any fluid property must be large enough to represent the fluid as a whole and, at the same time, must be small enough to allow for detecting spatial variations of the property of interest within the fluid (FOX; MCDONALD, 2001). In this way, the goal is to use a TSA that is small enough for representing the temporal variability of the processes, however large enough to minimize the randomness of the data.

[1] White noise can be defined as a series of independent random variables (BOX et al., 2016).

In order to support the choice of a plausible TSA, periodograms were generated for different TSAs, Figure 26, considering data recorded at P2 during March of 2017. The software used for generating the time series periodogram was STATGRAPHICS Centurion.

Periodograms, which considers that the time series is formed by sine and cosine waves with different frequencies, is applied to detect periodic patterns of time series in a background of white noise (BOX et al., 2016). Although periodograms are most of the time applied to residuals, here they are used for the purpose of reflecting whether the ebullition time series can be considered as a white noise.

In a cumulative periodogram, the white noise is represented by a straight line which has co-ordinates (x,y) as (0,0) and (0.5,1). In addition, it has limits lines about the theoretical line based on approximate probability limits of 5% and 25% (BOX et al., 2016). From the ebullition time series periodograms, it is observed that for the TSA of 30 seconds (which is two times the TSD), Figure 26, the ebullition time series represented as the blue line is very close to the limits of a white noise and as the TSA increases to TSA of 5 minutes and 1 hour the ebullition time series deviates from the white noise limits. Nonetheless, with a TSA of 1 day, the ebullition time series is a white noise as the series is short and no periodicity is detected.

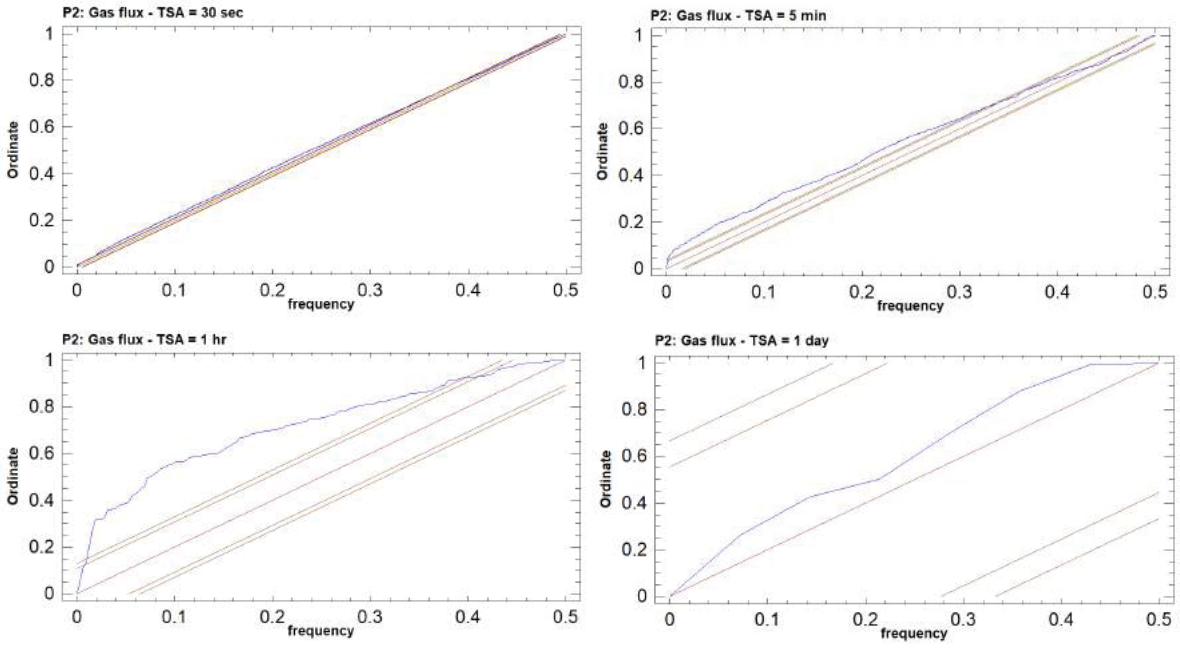


Figure 26: Periodogram calculated for ebullition time series from P2 during March with TSA of 30 seconds, 5 minutes, 1 hour, and 1 day. The blue line represents the data and the brown lines represent the white noise in the center and its 5% and 25% limits lines.

Graphs of autocorrelation were also verified for several time lags. Figure 27 shows the autocorrelation coefficients for the same ebullition time series used for the periodograms. The autocorrelation graphs indicate the dependency of actual values on the past occurrences. For a very small TSA (as 30 seconds), except for the two first lags, all the coefficients are statistically equal zero and as TSA increases is observed a dependence of occurrences for several time lags, however for larger TSA (TSA = 1day) all coefficients are statistically zero, meaning no linear dependence among the occurrences.

The use of a determined TSA also depends on the analysis that will be done. For the correlation of ebullition time series with meteorological data, for instance, might be interesting having values calculated over a large period of time, taking into account that meteorological measurements may be done with a

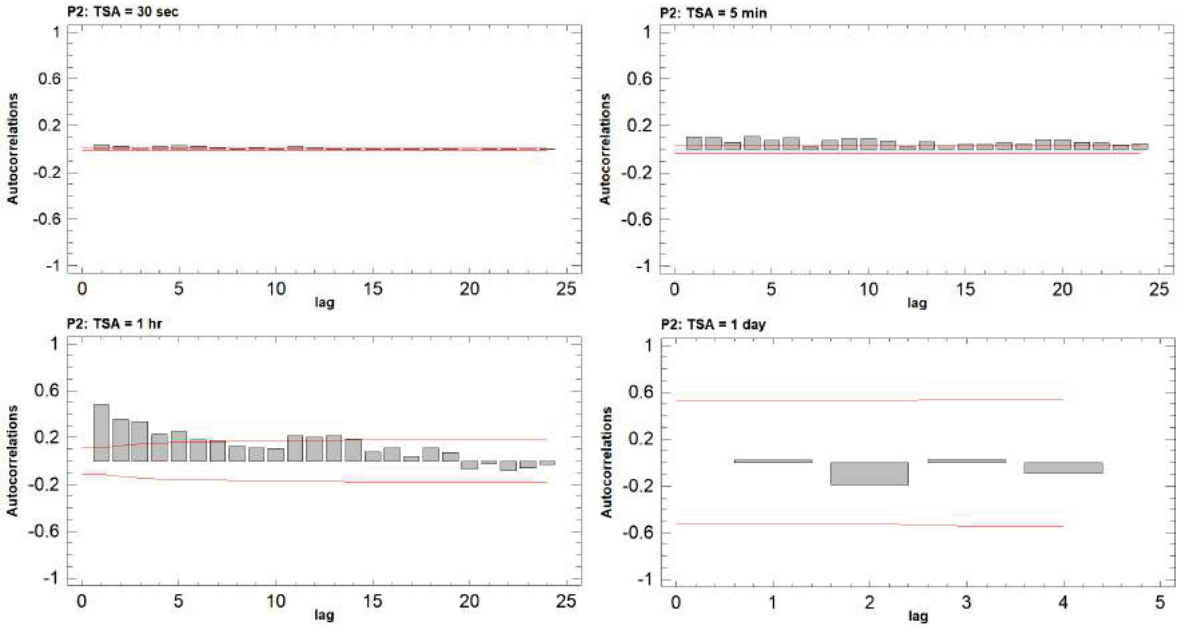


Figure 27: Autocorrelation calculated for ebullition time series from P2 during March with TSA of 30 seconds, 5 minutes, 1 hour, and 1 day. The red lines represent the 95% confidence interval.

shorter temporal resolution. On the other hand, ebullition occurrences might be analysed in terms of events. For this case, an ebullition event is referred as the amount of gas captured within a time interval. The ABTs were recording data in a time step of 15 seconds (TSD), this data was used to generate histograms with the time interval between increases of gas volume, and according to the results, Figure 28, in approximately 80% of the time interval were smaller than 10 minutes.

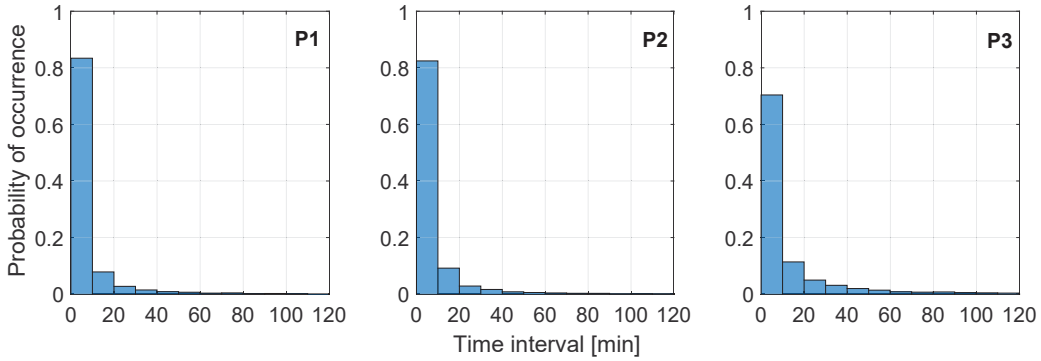


Figure 28: Probability of occurrence histogram of the time interval between increases in volume of the gas detected by the equipment with a TSD of 15 seconds. Data recorded from February 2017 to October 2017.

Considering results from the periodograms, from the autocorrelation, and from the histogram aforementioned, it was adopted a TSA of 5 minutes to be used for evaluating ebullition in terms of events and their contribution to the total amount of gas emitted, which is discussed in section 4.5.

## 4.5 Seasonal and short-term analysis

In this section, the ebullition is better explored in terms of seasonal variations and short-term variations. The daily time series of ebullition was used for a monthly box plot of the fluxes. Although

the number of days with flux measurement differs from one month to another and among locations, some observations can be made from the graphs, Figure 29. While At P2 location no ebullition data was obtained after June, at P1 measurements were continuous. The medians vary along the year with a reduction mainly from May to July. In July at P1 gas ebullition happened in one day out of 31 days of measurement, and in September ebullition occurred only in the last five days of the month.

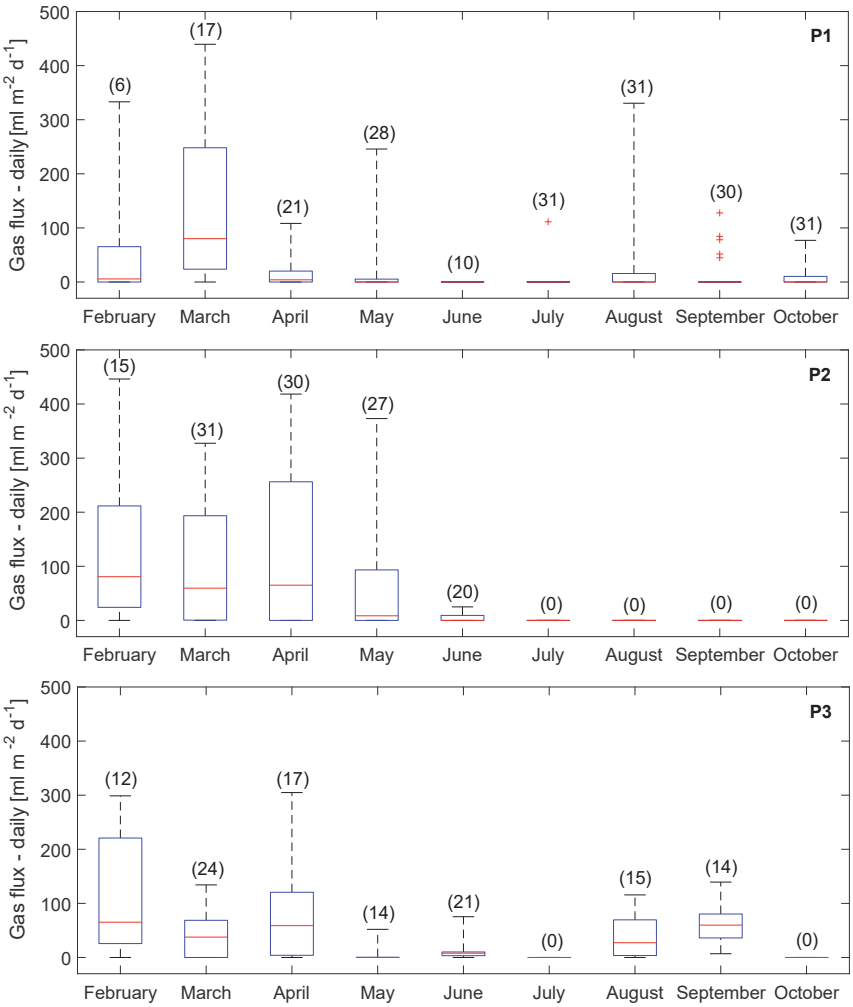


Figure 29: Box plot from daily gas flux measured in 2017, considering data presented in Figure 23. The upper and lower limits of the blue box represent the 75th and 25th percentiles respectively. The whiskers show the maximum and the minimum values, the red line represents the median, and the numbers in the top represent the number of days with measurements in each month.

A Kruskal-Wallis test was performed with the data from each location. In this test, the null hypothesis (H0) is that the data of each month has the same distribution while the alternative hypothesis (H1) is that not all data has the same distribution. The $p$-value was $1.9939 \times 10^{-9}$ for P1, $3.0231 \times 10^{-4}$ for P2, and $2.8742 \times 10^{-5}$ for P3. Therefore, in all locations the $p$-value was smaller than the significance level of 5%, meaning that at least in one month the data distribution differs from the others.

In the box-plot can be noticed the existence of seasonal variations in the gas ebullition. Either at P1 and P3 locations the emissions reduced in the period from May to July, and after August gas flux seems to rise again. In Figure 30, is represented ebullition time series recorded at P2 for two different periods: one warmer in February and another in the late fall and beginning of winter. The mean water temperature recorded by the ABT in February was 25 °C, during this period was recorded ebullition spread in all dataset with few days when no ebullition was observed whereas, during June, which had

a mean temperature of 17.2 °C, events were composed of few peaks with larger time interval among emissions. The total amount of gas emitted in both periods also varied largely. In February during the 20 days of measurements, a total of 1466.8 ml of gas was emitted which was sixteenfold the volume of gas emitted during 19 days in June which was 86.5 ml.

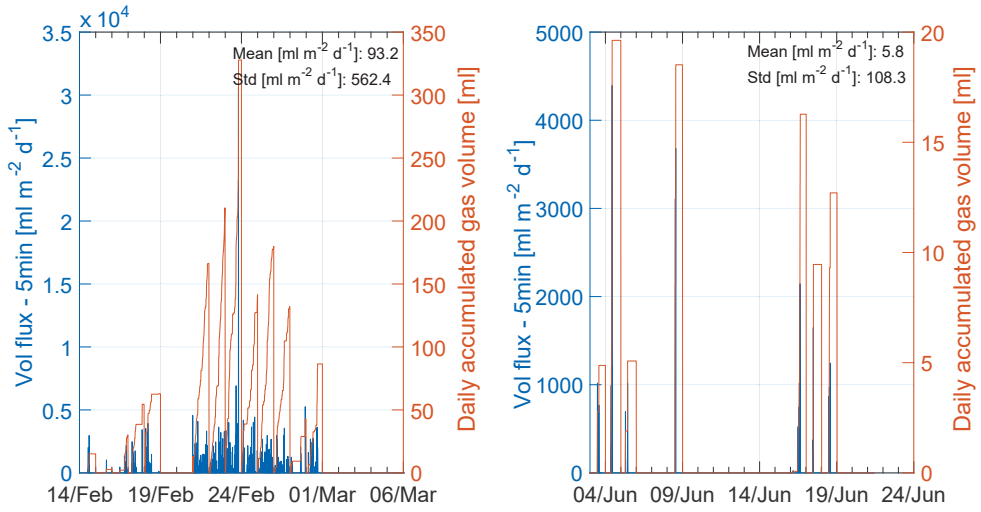


Figure 30: Ebullition flux and daily accumulated gas flux in February and June of 2017 at location P2 near water intake facility. Important to notice that both graphs have a different y-axis scale.

The amount of decrease in the mean ebullition flux from warmer to cold periods varied depending on the location. Although at P1 and P3 the reductions were smaller than at P2, the mean gas flux diminished more than twofold. Such seasonal variations are also reported in the literature in other environments. Del SONTRO et al. (2016) noticed for lakes and ponds in Canada, that while for ponds there was a correlation of methane flux with sediment temperature, in lakes this relation wasn't verified. The authors pointed out that the relationship between temperature and ebullition depended also upon other factors. In the study, they observed that the correlation of temperature and ebullition was stronger for a larger concentration of total phosphorus. Yvon-Durocher et al. (2014) observed that the dependency of methane emissions with temperature is similar to the dependency of anaerobic methane production (growth rate for cultures of methanogens) with temperature. Therefore, with a reduction in temperature there is also a decrease in methane production and as a consequence, it will take longer for having enough methane available in the sediment to form bubbles that can overcome the ambient pressure and rise in the water column.

Wilkinson et al. (2015) demonstrated seasonal flux variations caused by varying methane production as well as short-term flux variability due to changes in sediment gas storage. Liu et al. (2016) conducted sediment incubation experiments to analyse influences of sediment characteristics over methane production and its release. The tests led the researchers to classify the process into three stages. At stage one (first 6 days) bubbles started to form, at the second stage (day six to twelve) larger bubbles were verified, and at the last stage (day thirteen to twenty) bubbles increased in size and number and formed conduits with direction towards the sediment surface. Other observations made by the authors, was a depth stratification of gas content, for the case of clay the layer of 5 cm to 25 cm had the highest gas concentration, that occurs due to gas that diffuses from the lower sediment while in the very sediment top the gas diffuses to the water layer above.

Therefore, the strong seasonal variation observed in ebullition measurements might not be related with temperature and gas production only, but is a result from the influence of other factors as sediment characteristics of gas storage and gas diffusion as well. Water temperature profiles of P2 location, Figure

16, show that the bottom temperature changed from 19.2 °C in February $11^{th}$ to 19.6 °C in May $05^{th}$ (a change of 0.4 °C in 3 months), and to 16.4 °C in August $10^{th}$ (a change of 3.2 °C in 3 months). The dissolved oxygen concentration in the bottom increased 3.3 mg $L^{-1}$ from February to May, Figure 17. Some propositions can be made based on the observations and on the literature. The growth in the dissolved oxygen concentration may have resulted in the oxidation of the dissolved methane contained in the water. The increase of the methane concentration gradient between water and sediment can enhance the diffusion of the gas from the sediment to the water. That means less gas available in the sediment to form bubbles.

Results from dissolved methane measurements at different water depth in the region of P3 location presented by Schumack and Mannich (2017), show as expected the increase of dissolved methane concentration in the anoxic layer and in the bottom portion of the water column. In a discussion with the author about unpublished data of dissolved methane concentrations measured during August of 2017, was observed that methane concentration in water was smaller than the values obtained during the warmer period when the reservoir was stratified.

Another aspect, in addition to gas diffusion, is that the reduction of temperature cause an increase in gas solubility and a potential reduction in gas production. The decrease of gas content in the sediment, either due to reduction of gas production or due to its diffusion and solubility in the water, can result in a decrease of the conduits formed, and for this case bubbles would face more resistance due to sediment and might not have enough buoyancy to rise and leave the sediment. A scheme illustrating the behaviour of some parameters in the water and in the sediment is presented in Figure 31.

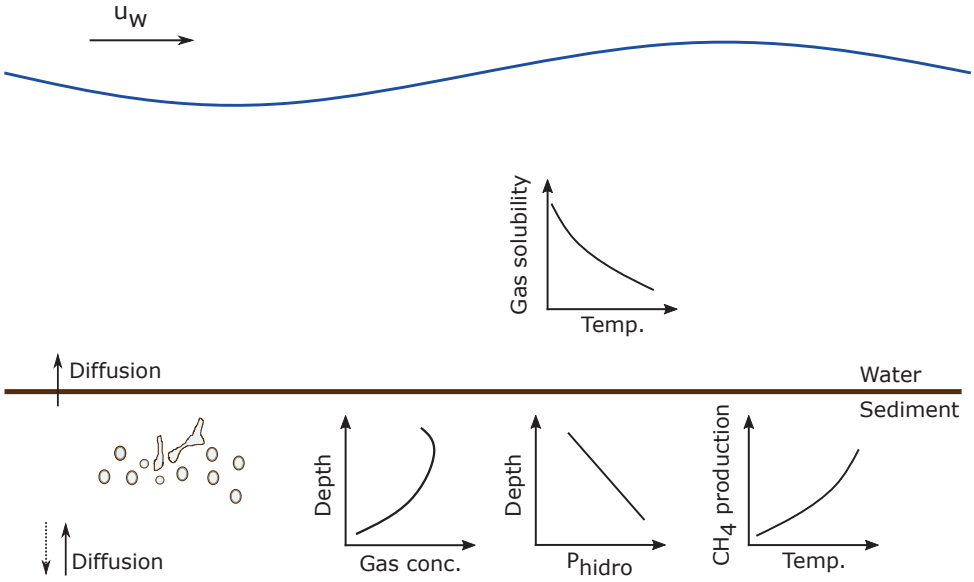


Figure 31: Conceptual representation of some parameters and their tendency regarding temperature or depth in the sediment. Gas solubility in the water decreases with temperature growth while the rate of methane production in the sediment increases with temperature; the hydrostatic pressure rises with augmenting of depth in the sediment; and gas concentration in the sediment reduces with depth, but also near the sediment surface due to diffusion to the water column above.

The Wilcoxon rank test is a nonparametric hypothesis test for comparing means of the same population (WALPOLE; MYERS, 1976). The null hypothesis is that both means are statistically equal while the alternative hypothesis is that the means are different. This statistical test was applied to ebullition data to compare the means of fluxes occurring during daytime with fluxes recorded during the nighttime. For this analysis daytime was defined from 7 a.m to 7 p.m while nighttime was determined from 7 p.m to 7 a.m. The $p$-values for all tests and the mean daily and night flux can be found in the

Appendix A. The mean day flux differed from the mean night flux considering a 5% confidence level in two data sets: at the P2 location from June $02^{nd}$ to June $21^{st}$ and at the P3 location from March $06^{th}$ to March $19^{th}$. Daytime and nighttime mean ebullition flux for two periods at P2 are presented in Figure 32.

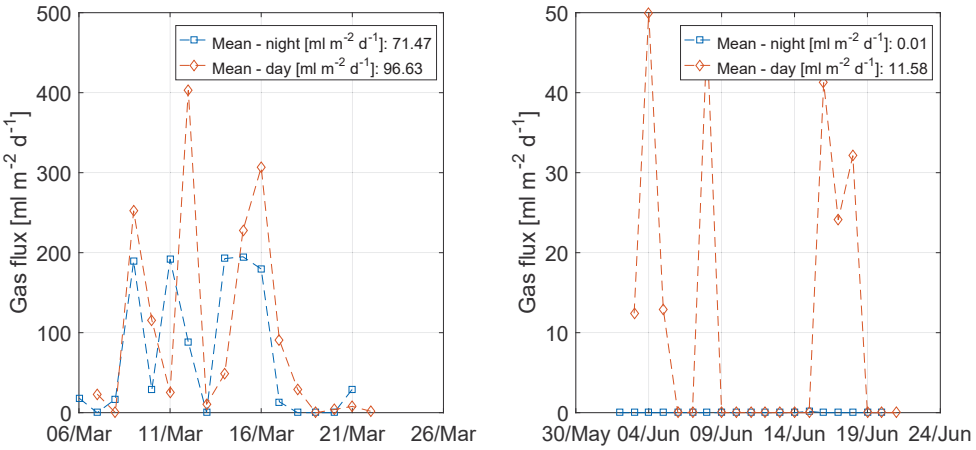


Figure 32: Day and night mean ebullition flux for two periods measured at P2 location. For the data presented in left hand side graph $p > 0.05$ while for data presented in the right hand side graph $p < 0.05$.

Although considering the Wilcoxon test results no strong daily or night pattern was observed, taking a look of the absolute mean emission values is noticed that in 70% of the cases mean day emissions were greater than mean night emissions. For the period from June $02^{nd}$ to June $21^{st}$ at P2 all the emissions recorded occurred during the daytime, and for the P3 from March $06^{th}$ to March $19^{th}$ the mean day flux was approximately twofold the mean night flux.

Day and night flux patterns can be influenced by diurnal oscillations of variables such as atmospheric pressure, wind incidence, and water level fluctuations. From the graphs of wind frequency distribution, Figure 33, It can be noticed that during the daytime, for the months showed, the wind velocity is greater than during night time and increases the occurrence of Northwest winds with a velocity greater than $3.6\,\mathrm{m\,s^{-1}}$.

The short-term variations on ebullition can also be related to other factors such as the biota which is not included in this research. However, its effect on emissions is being investigated in other studies. McGinnis et al. (2017) explored the migration behaviour of larvae *Chaoborus* spp from sediment to water. According to the authors, these organisms stay in the sediment during the daytime and use porewater methane to rise in the water column during the night to feed in the oxic layer of the water column. In addition to gas transport by the larvae itself, the authors mention that as these larvae go in and out of the sediment they cause disturbances that can facilitate bubbles to leave the sediment. Bezerra-Neto et al. (2012) applied a hydroacoustic method to identify *Chaoborus* spp in the water column of two lakes and one reservoir in Brazil. The authors also report a diurnal vertical migration of *Chaoborus* spp and from water samples the larvae density ranged from 781 to 1550 individuals per cubic meter.

In addition to seasonal variation, ebullition was also analysed in terms of its intensity distribution. For this analysis histograms were made in which the probability of occurrence was calculated from the frequency of occurrence. Histograms were obtained considering the entire ebullition flux data set for each location (Figure 34) and considering warmer and colder period separately (Figure 35). In such analysis is used TSA of 5 minutes.

The histograms for the period of February – October 2017, Figure 34, have an exponential distribution in a way that fluxes with lower intensities are more frequent, more than 25% of the flux

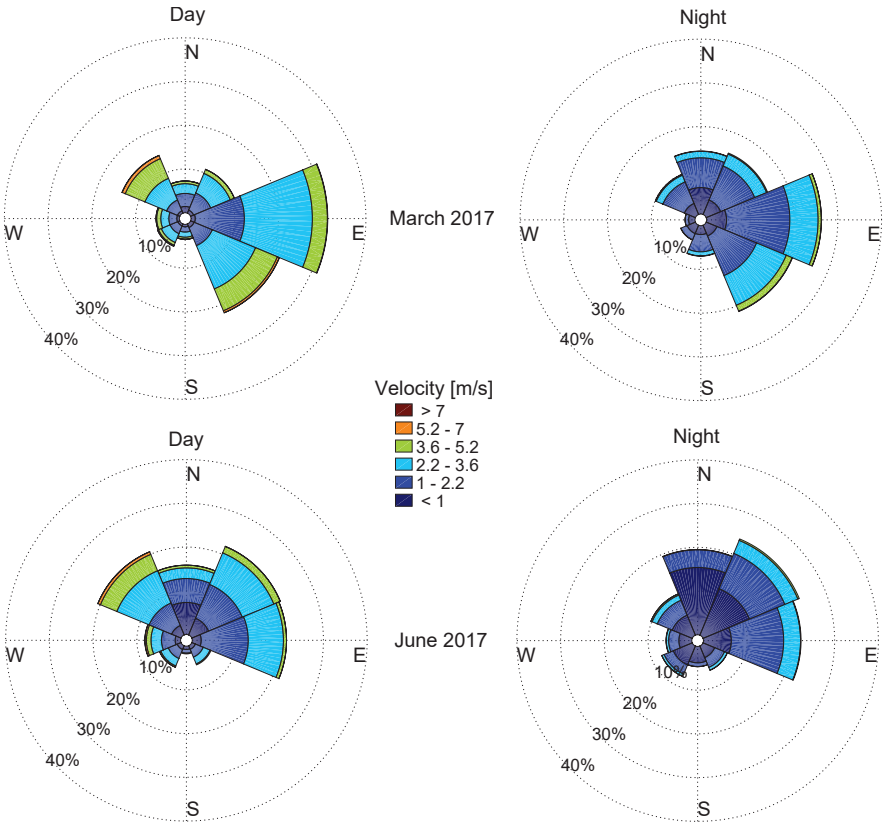


Figure 33: Day and night wind frequency distribution from Smart Energy-Tecpar data of March and June of 2017.

intensity was less than 100 ml $m^{-2}$ $d^{-1}$, Figure 34. This flux intensity distribution confirms the observed by Varadharajan and Hemond (2012).

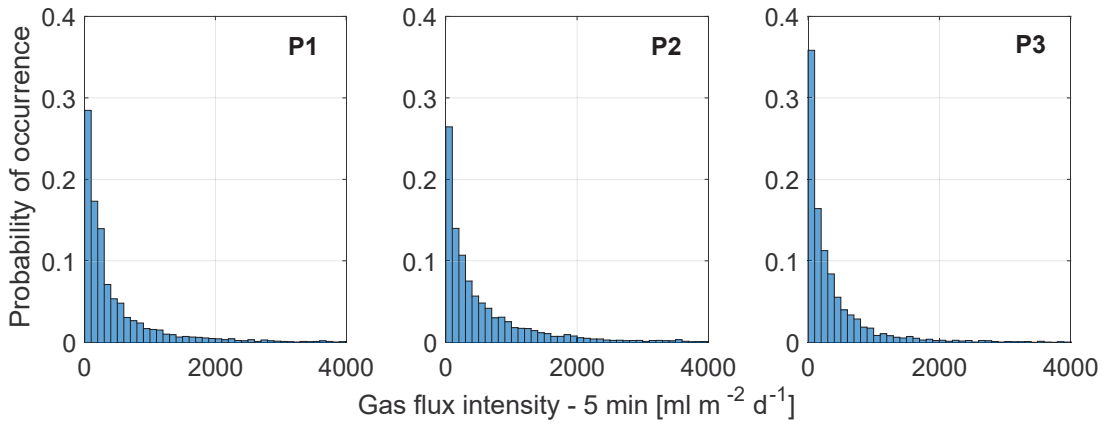


Figure 34: Probability of occurrence histograms of gas flux (5 min) in all locations for data recorded from February 2017 to October 2017. The occurrences of zero flux were removed from the histograms.

Taking into account the strong seasonal pattern observed in ebullition, histograms were made for one warm and one colder period, Figure 35. The distribution observed during February for P2 follows a similar pattern from the obtained for the entire data set whereas the distribution obtained for the colder period differs from the exponential one.

The histograms of the time interval between increases in the gas volume detected by the equipment showed that the majority (80%) is smaller than 10 minutes which is analogous to Varadharajan

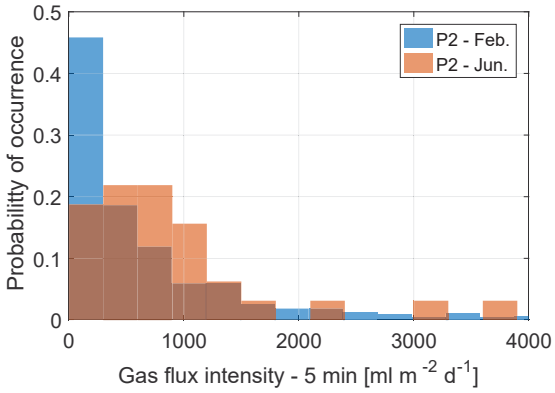


Figure 35: Probability of occurrence histograms of gas flux (5 min) at P2 location from data recorded in February 2017 and in June 2017. The occurrences of zero flux were removed from the histograms.

and Hemond (2012) whos result from wavelet analysis showed that bubbling occurred mostly within time scales less than 10 minutes. Therefore, emissions are formed mainly by fluxes of lower duration and as bubbling is triggered and the first bubbles leave the sediment matrix the next will follow within a time interval smaller than 10 minutes and after that, it may take a long time until bubbles are formed again in the sediment to be available for a new release. The next step was to quantify the number of ebullition events and their contribution to the total volume of gas emitted.

For this research, an ebullition event is defined as a single or a set of uninterrupted gas emissions, e.g when a zero flux is recorded within the 5 minutes TSA the following non zero flux value is considered a new event. This analysis allowed to quantify the ebullition events, their duration, and contribution to the total gas emitted. Tables with the information for the entire data set of each location is presented in Appendix B.

Even though the total amount of hours of data recorded is smaller at the P2 location in comparison to P1, it had the largest ebullition events. At this location occurred 2168 ebullition events from February 2017 to June 2017 and half of the events had a duration of 5 minutes and contributed to 24.4 % of the total gas emitted. At P1 and P3 a similar pattern is observed which events of 5 minutes duration had the largest contribution to the total gas emitted. Ebullition events' duration varied from 5 minutes up to 2.2 hours, however, events greater than one hour of duration represented less than 1% of the total events quantified. In the deepest region, P3, the maximum event duration was 1.1 hour and the 5 minutes events emitted 63% of the total gas captured by the ABT.

Ebullition events were analysed regarding summer versus winter variations. Recalling Figure 30 the orange curves represent the accumulated gas volume over one day. This curve shape changed considerably from summer to winter time. While during summer the curves increase gradually along the day, during winter is verified a bar-shape curve indicating that the total volume of gas emitted in each day was from fewer or even from single ebullition events. While during February begin of March occurred 335 events with durations from 5 minutes to 1 hour, in June 29 events were recorded and just 2 out of the total had a duration of 10 minutes.

## 4.6 Spatial distribution

Three periods of time when ebullition was simultaneous measured at all points were used to estimate mean ebullition flux, Table 14. The periods considered were 13 days in March, 14 days in April and 13 days in May. Except for March, the mean ebullition rate was larger at P2 than the mean ebullition

of the others locations. The deepest location which is P3 had the lowest mean ebullition flux. The highest mean emission found for P2 (Figure 36) might be related to the load of organic matter received at that location, as there is a small river inlet nearby the region. However, this strong spatial variability, mainly from P2, is still not well solved and there might be other factors, besides organic matter content in the sediment, contributing for the highest fluxes from that location.

A previous study on the organic matter content in the sediment at some points at Passaúna reservoir showed that the organic matter content at location P2 is slightly higher than in other locations. The values reported of organic matter content were 20%, 22% and 16% at locations P1, P2 and P3 [2] respectively (KNAPIK et al., 2017). In addition, the water at this location might be deep enough to prevent complete mixing of water column due to wind incidence which could contribute in keeping the bottom portion with anoxic conditions being favourable for anaerobic decomposition.

Table 14: Mean ebullition for period of mutual data in all three locations.

| | | **Mean ebullition flux** [$\mathrm{ml\,m^{-2}\,d^{-1}}$] | | | |
|---|---|---|---|---|---|
| | Depth [m] | 06/03/17 – 19/03/17 | 10/04/17 – 24/04/17 | 03/05/17 – 16/05/17 | **Mean** [$\mathrm{ml\,m^{-2}\,d^{-1}}$] |
| **P1** | 8.8 | 170.3 | 15.0 | 19.2 | 68.2 |
| **P2** | 12.3 | 102.1 | 206.9 | 112.6 | 140.5 |
| **P3** | 14.6 | 68.4 | 94.6 | 6.6 | 56.5 |

Natchimuthu et al. (2016) mention the effect of water inlet to a load of organic matter entering the system and the enhance of gas production. The author's findings suggest that the greatest emission occurs from the shallowest regions and highlight the importance of including ebullition measurements from all depths in the reservoir in order to account for the spatial variability. This spatial variability in emission fluxes was verified in this research not only among the three locations but also local variability as considering measurements from the conventional funnels, Section 4.2. This indicates that even within a short area ebullition is heterogeneous, which implies that an accurate gas emission estimation would require either to measure gas flux covering large areas or to estimate emissions based on aspects that control ebullition such as sediment characteristics for the entire system.

Considering a transversal profile all the measurements in this study are performed in the deepest regions since the equipment requires at least three meters of water column to be installed and therefore, the emissions from the shallowest portions near the reservoir banks had not been included, as a consequence a simple extrapolation of the mean for entire reservoir might result in an underestimation of the emissions.

### 4.6.1 Ebullition and water quality parameters

Water quality data obtained for NoPa-SeWaMa project and collected at different locations along Passaúna reservoir were used in the attempt to identify any relationship between water quality parameters and ebullition occurrences. Although such measurements give a snapshot of the parameters conditions, they might provide additional information for understanding ebullition processes or the conditions under which ebullition occurred. Such conditions in the water column act as boundary conditions for methane production in the sediment and bubble formation, considering that parameters such as temperature, dissolved oxygen, and other components concentrations influence the dynamics of diffusion processes between the water-sediment interface and bacterial activities.

At Figure 37 is presented the ebullition time series and the red points are the two field campaigns for water quality measurements. Results of oxidation-reduction potential (ORP), conductivity,

[2] For P3 location the sediment for determination of organic matter content was collected 800 m downstream the actual ABT-P3 location

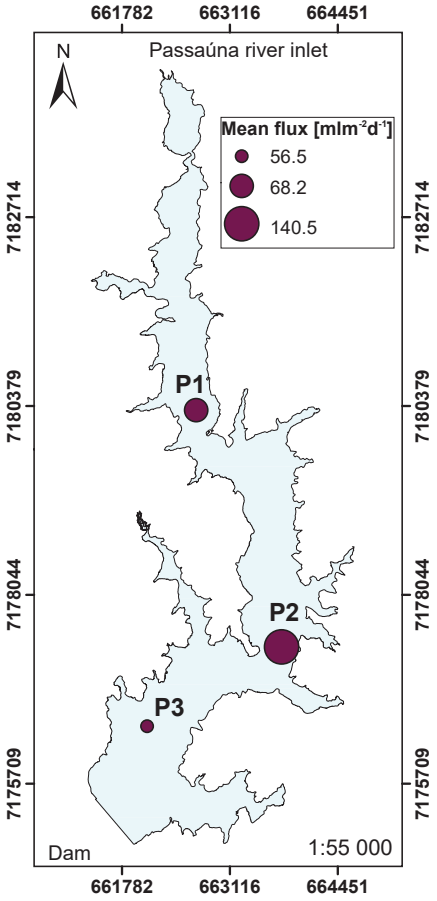


Figure 36: Spatial representation of the mean ebullition flux calculated considering months of March, April, and May when gas emission was simultaneous measured in all locations.

and potential of hydrogen (pH) for the locations are presented (unpublished data from Godoy (2017)). The measured conductivity is related to the amount of ions contained in the water and can give an idea about the primary productivity which an increase of conductivity values and a decrease of dissolved oxygen concentrations indicates that decomposition prevails, whereas a decrease of conductivity points to an augment of primary productivity (VASCONCELOS SEGUNDO; FROEHNER, 2016).

Regarding ORP, according to Lampert and Sommer (2007) in anoxic conditions, the reduction of ions ferrous and organic matter reduces the ORP. The ORP plays an important role on the solubility of elements, as examples are $Fe^{3+}$ that becomes soluble as $Fe^{2+}$ with a drop in the ORP and $SO_4^{2-}$ that is converted to $S^{2-}$ (LAMPERT; SOMMER, 2007). Taking into account that methane starts to be formed mainly after reduction of $O_2$, $NO_3^-$, $Fe^{3+}$, $Mn^{4+}$ and $SO_4^{2-}$ (SMITH et al., 2003) lower values of ORP may indicate favourable conditions for methane formation in the water column and in the sediment.

Looking at graphs in Figure 37 is observed that ORP has the lower values in the bottom portion of the water column and were smaller in February than in May. Conductivity, on the other hand, has largest values in the bottom and the greater value recorded was at P2 during February. An interesting comparison can be done with ebullition recorded which reduced from February to May. The amount of organic matter by itself might not be the limiting for methane production (as the dissolved organic carbon concentration ranged from 2–3.5 $mg\,L^{-1}$ in February and May with a small reduction in May assigned to precipitation), but also the conditions of conductivity, oxidation-reduction potential, and dissolved

oxygen in the water column.

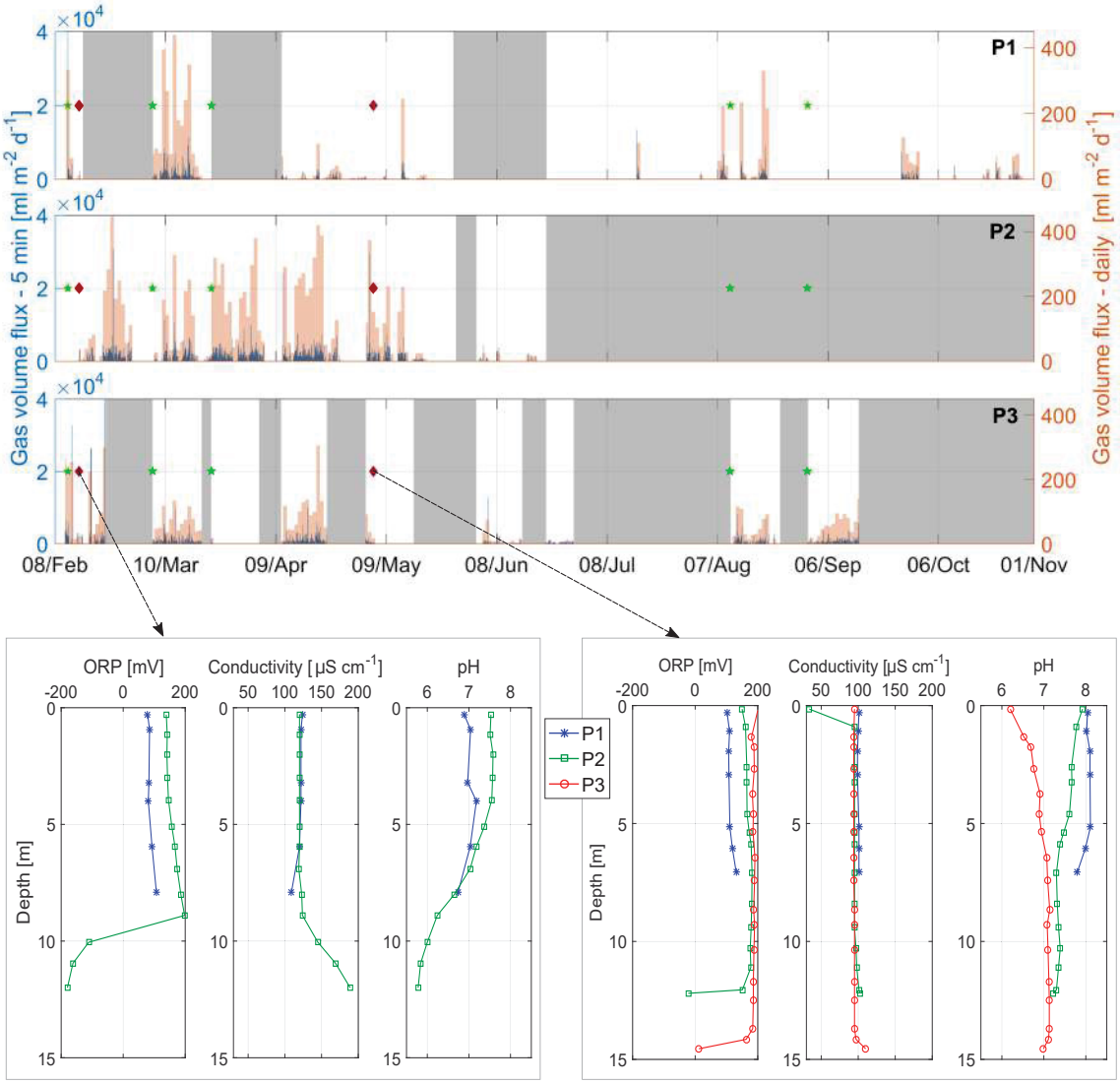


Figure 37: Ebullition time series for all three locations. The red diamond indicates days when field campaigns for water quality parameters measurements occurred (February $14^{th}$ and May $05^{th}$). The bottom graphs show profiles of oxidation-reduction potential, conductivity, and pH for ABTs' locations, except P3 which is 800 m downstream ABT-P3 – unpublished data from Godoy (2017).

With respect to the spatial variations of organic matter content in the sediment determined in October of 2016 by Knapik et al. (2017) the mean ebullition, presented in Figure 36, was higher in the location P2 where the highest organic matter content was verified, followed by P1 and P3 respectively. In addition, the nitrogen concentration determined in February $14^{th}$, Figure 20, was higher in the bottom of P2. Precipitation and allochthonous organic matter are important sources of nitrogen to reservoirs (ESTEVES, 1998) and could indicate that P2 receives a greater load of allochthonous matter. In another study conducted by Zarebska (2016) at Passaúna reservoir, loss of ignition tests were performed for sediments cores collected in February of 2016. The results showed that at P2 the organic carbon represented 27.3% of the total carbon while the inorganic carbon fraction was smaller than 1%. Therefore, as expected the largest amount of gas emitted is from the location with the largest amount of organic matter which is available for decomposition and gas bubbles formation.

## 4.7 Investigation of external forcings over ebullition

In this section, it is investigated the correlation of meteorological parameters with gas ebullition. First of all, let's take a look at the time series of ebullition for a short period of time when emissions were simultaneously recorded in all three locations. The period showed in Figure 38 is from March $06^{th}$ to March $19^{th}$ of 2017. The red ellipses in the figure highlight three largest occurrences of ebullition. Although ebullition seems to be formed of episodic events and being highly variable in time and space, the qualitative analyses of the graphs suggest that there is synchrony among events of high flux. Such synchrony of ebullition events from different locations was also reported in Varadharajan and Hemond (2012), Maeck, Hofmann and Lorke (2014). This can suggest that forcings triggering ebullition may be acting in large spatial scales in the reservoir.

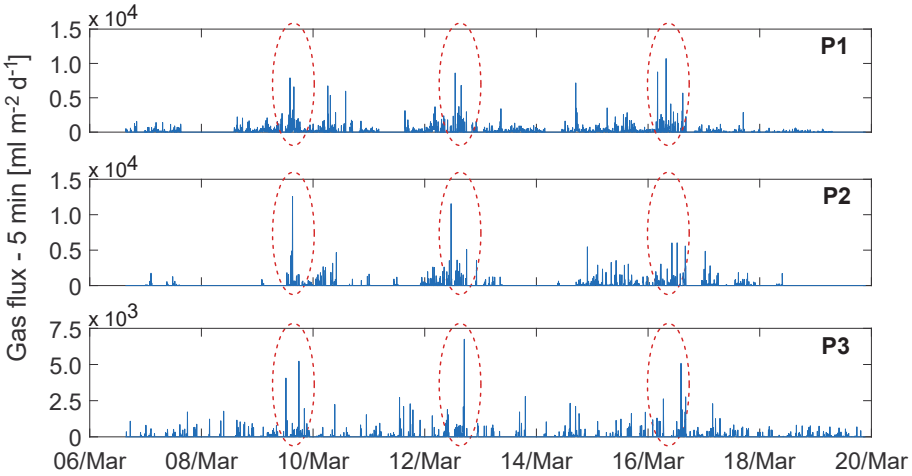


Figure 38: Gas volume flux recorded from March $06^{th}$ to March $19^{th}$ of 2017 in all three locations.

Nonetheless, it is noticed a shift of timing among the largest ebullition peaks of the three locations. A scatter graph is presented in Figure 39 for TSA of 5 minutes, 1 hour and 1 day for data recorded in March, May and April of 2017. A linear regression was applied and considering a small TSA (5 min) no clear tendency is observed. By increasing the TSA, for instance, 1 day, it can be observed a tendency of some large daily ebullition occurring at the same day. However, it is also noticed that for several points the fluxes recorded in one location (high gas flux or low gas flux) did not match to flux intensity in another location. The reason for that is due to timing difference on recording values among the ABTs and most of all due to local characteristics, such as bubbles formed in the sediment and their response to external forcings.

The possible external forcings on triggering ebullition analysed in this section are atmospheric pressure, wind incidence, air temperature and precipitation. Data of all mentioned variables from February 2017 to September 2017, except for precipitation, were obtained from the solarimetric station which is located 4 km from the ABT-P2 location and managed within the project Smart Energy - TecPar. An initial plot of daily ebullition time series recorded at P2 in March with atmospheric pressure, temperature and wind velocity (all normalized values), Figure 40, shows the possible relationships among the variables and gas ebullition. It is observed for the period plotted that for the ebullition peaks there was a combination of increased wind velocities and drop in the atmospheric pressure.

In the following paragraphs of this section, the relation of such parameters to gas ebullition are better discussed. A first parameter to be mentioned, that was not included in Figure 40 is precipitation. Daily accumulated precipitation measured at Colônia Dom Pedro rain station (located 3 km upstream the reservoir) and gas flux recorded at P2 are presented in Figure 41. The runoff occurring during rain events

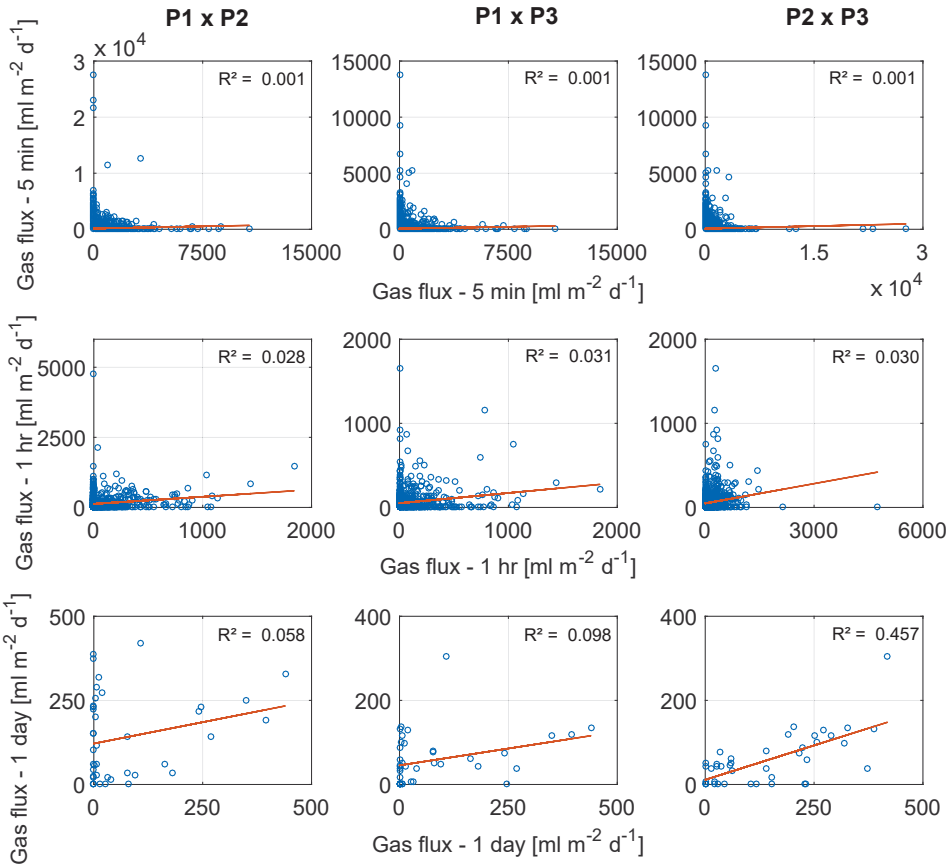


Figure 39: Linear regression of ebullition flux among the three locations for the gas flux of TSA 5 min, 1 hour, and 1 day. Data recorded simultaneously in March, May, and April of 2017.

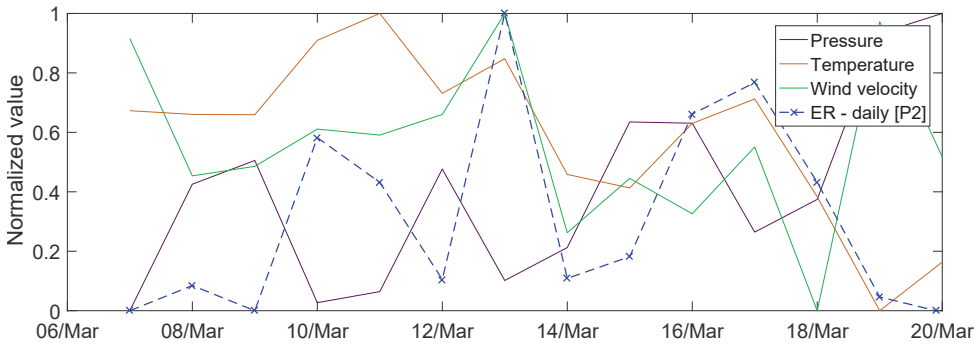


Figure 40: Ebullition rate [ER] recorded during March 2017 at P2 and secondary data (atmospheric pressure, air temperature, and wind velocity) from Smart Energy-Tecpar station. Values are daily mean and presented normalized by the maximum and minimum values from each time series: Temperature max. – min.: 24.9–15.7 °C; Atmospheric pressure max. – min.: 918.3–913.5 mbar; Wind velocity max. – min.: 2.9–1.4 $m\,s^{-1}$; Gas flux max.: 327.5 $ml\,m^{-2}\,d^{-1}$.

carries organic and inorganic components to the reservoir and in this way contributes to load of matter for decomposition and eventually to bubble formation. On the other hand, the additional amount of water entering in the system can increase the water level which results in an increment of the hydrostatic pressure that bubbles have to overcome to leave the sediment. Although precipitation itself seems not to be correlated with gas emissions, rain events are linked with low-pressure systems and therefore, result in drops of the atmospheric pressure. Some of the major ebullition events recorded, in turn, occurred during periods of reduced atmospheric pressure, as is observed in Figure 41.

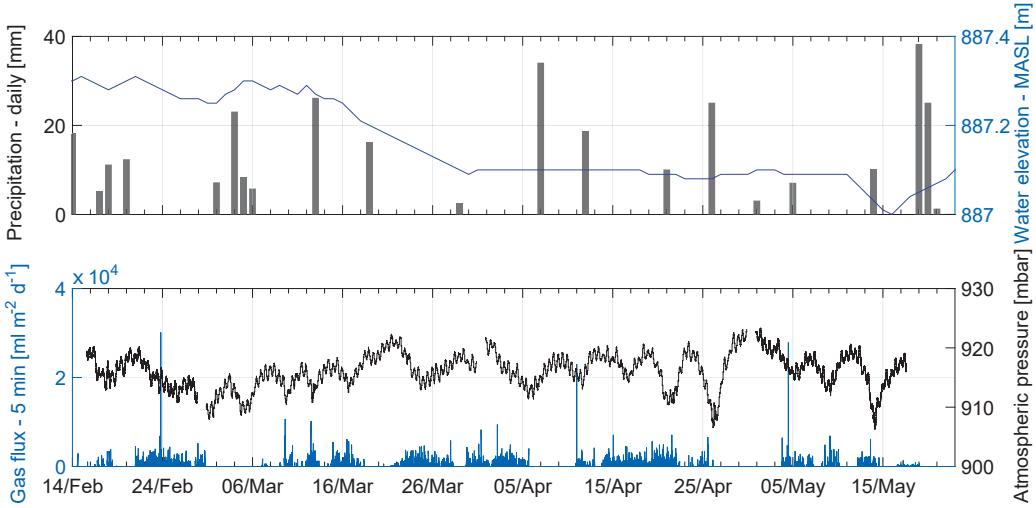


Figure 41: Top graph: daily accumulated precipitation from Colônia Dom Pedro rain station and water elevation daily measured from February to May of 2017. Bottom graph: Gas flux recorded at P2 and the atmospheric pressure measured at TecPar solarimetric station from February to May of 2017.

Reservoir's water elevation was higher in February and decreased during March, top graph of Figure 41. As the water elevation is measured daily no pattern was observed in smaller time scale. However, the literature reports the occurrence of ebullition with reduction of few centimeters in the water level, such as in Ostrovsky et al. (2008). The effect of temperature was already discussed considering a seasonal variation. Short-term variability and diurnal temperature oscillations influence mainly the conditions of the water column as its thermal vertical stratification, chemical, and biologic processes and thus has an indirect influence over ebullition. The effect observed of drops in pressure and wind incidence is addressed in the next subsection.

### 4.7.1 Correlation with pressure variation

The incidence of wind in the water surface transfers momentum from the atmosphere to the water column. Part of this momentum transferred is used for formation and maintenance of waves and the other portion is transferred to the water layer below (WÜEST; LORKE, 2003). According to Wüest and Lorke (2003) in stratified systems, a great portion of the momentum and energy is transferred to internal motions which are partially dissipated by bottom interactions (bottom currents) and a small portion dissipated in the interior shear instabilities (internal waves). There are several other processes and motions that occur either in the boundaries (bottom and surface) or in the middle portion of the water column that are not mentioned here, however it is relevant to mention that they have an influence not only in the momentum exchange but also in mixing processes, substances and particles exchange with the sediment, and pressure fluctuations (WÜEST; LORKE, 2003).

As aforementioned, the change in pressure at water-sediment interface potentially triggers the release of bubbles and as bubbles leave the sediment they form 'paths' that facilitate the movement of other bubbles through the sediment. Here, it is considered the combination of atmospheric pressure changes and surface waves to the total pressure variation at the water-sediment interface. The data was considered on a daily timescale. The atmospheric pressure change was the difference between the atmospheric pressure of actual day and the day before divided by the air density ($\rho_{air} = 1.1\,\mathrm{kg\,m^{-3}}$) times the acceleration due to gravity to have the results in meters units.

The surface waves generated by the wind were calculated considering the wind fetch at each

ABT location and the wind velocity at 10 meters high measured at the Smart Energy-TecPar solarimetric station. The procedure followed for the wind fetch calculation, the values calculated for each ABT location, the determination of the surface waves height, and the bottom pressure variation is described in the Appendix C.

The wind data available is from February to September of 2017. A scatter plot with the coefficient of determination of a linear regression for gas ebullition data of P2 with pressure variations (in meters) due to changes in the atmospheric pressure, surface waves, and the combination of both is presented in Figure 42. Looking at the top left-hand side graph is observed a tendency of the highest fluxes occurring with the greater decrease of atmospheric pressure while for the surface waves (top right-hand side graph) some of the highest fluxes occurred with the largest variations in pressure, e.g for larger surface waves due to stronger winds. However, the Spearman's correlation indicated a moderate and very weak correlation between gas flux and variation of atmospheric pressure and surface waves with coefficients of $-0.42$ ($p$-value $1.5 \times 10^{-4}$) and 0.07 ($p$-value 0.07) respectively. Similar results were verified for data of P1 and P3 location. The scatter plot with the coefficient of determination of a linear regression can be found in the Appendix C.

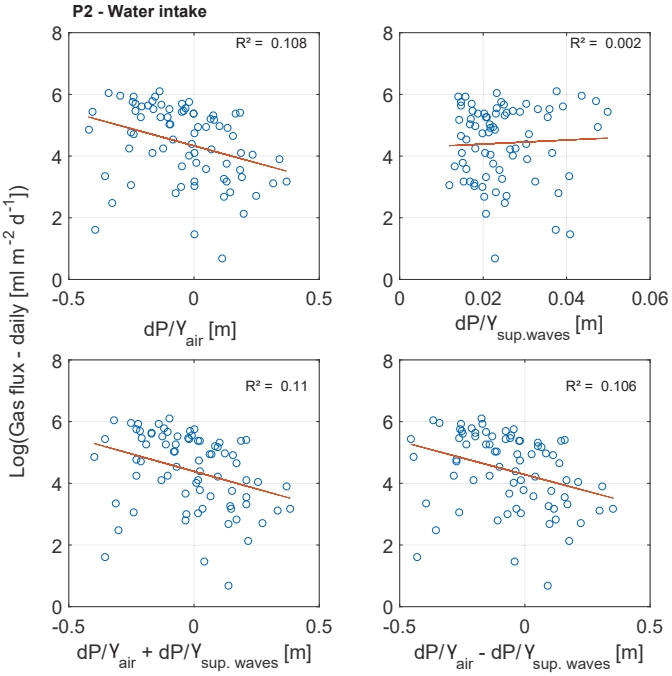


Figure 42: Linear regression of gas flux from P2 and changes in the atmospheric pressure, bottom pressure due to surface waves, and the combination of surface waves with atmospheric pressure considering daily data.

Considering Figure 41 is noticed that not all drop in atmospheric pressure resulted in an ebullition event indicating, in this way, that besides changes in the atmospheric pressure there are other factors controlling emissions. A correlation test was performed considering just the largest fluxes recorded. The criterion applied was to remove the mean ebullition flux from each value and selecting the remaining fluxes with values above zero. In the results obtained from the ebullition time series in March at P2, Figure 43, is verified an improvement in the coefficient of determination of the linear regression and a strong negative Spearman's correlation (coefficient value of -0.66 and $p$-value of 0.175) was found for gas flux and variations in the atmospheric pressure.

A similar result was verified for P2 data from April with a Spearman's correlation coefficient value of $-0.78$ ($p$-value 0.017). Nevertheless, a good correlation wasn't verified for all time series. For

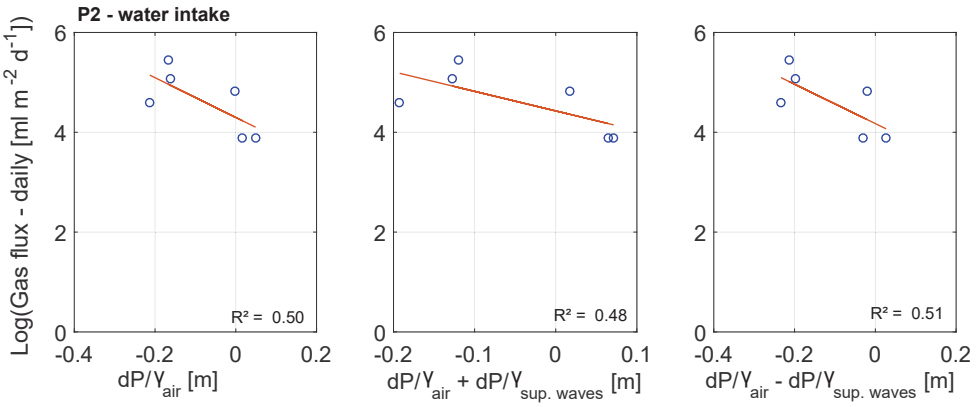


Figure 43: Linear correlation of ebullition rate and variation in atmospheric pressure in addition to surface waves applying a criterion to select gas fluxes above the mean flux value. Ebullition data recorded at P2 in March of 2017.

ebullition recorded in May in P2, for instance, the Spearman's correlation coefficient for gas flux and atmospheric pressure was $-0.25$ and $p$-value of 0.595. Two main aspects can be pointed from the low correlations obtained. The first one is regarding the equipment timing on recording variables and the system time response to any external forcing acting on it. An example is the wind incidence which leads to waves formation that depends, in turn, on the wind, and on the reservoir characteristics. The waves will propagate in the water and even with a brief break in the wind intensity, the wave propagation will continue until its energy dissipates, however, the wind sensor may record a wind velocity (in this case low velocity) that in the calculations will not reflect necessarily the existing wave conditions in the reservoir.

A second aspect is that several parameters have somehow an influence over ebullition. The effect of overlapping forcings on ebullition is difficult to determine and is still not totally understood. Varadharajan and Hemond (2012) mention that the discrepancy between measured and actual temporal and spatial scales and how variables are related, which may not be linearly correlated, can potentially mask the results. Liu et al. (2016) mention that changes in pressure in the water-sediment interface can facilitate bubbles to scape the sediment in two different ways. The increase in pressure would cause bubbles to narrow and become easier for them to move upwards, and the opposite, with a decrease in pressure, bubble expand and will have enough buoyancy to overcome the ambient pressure and sediment resistance.

## 4.8 Implications for reservoir management and monitoring strategies

Studies that aim to quantify gas emissions and the processes involved provide information to reservoir management that can support mitigation actions regarding greenhouse gases emissions. In this study is pointed that at Passaúna reservoir the largest gas emissions in 2017 occurred during the period when the reservoir was stratified, which occurred during summer time (as can be verified from the curve slope of accumulated gas in Figure 44). Observing the water temperature (Figure 44) measured by the ABT installed at P1 (shallowest location), the more intense emissions were recorded during periods of higher temperatures. However, is also noticed that there was a slight decrease in the water temperature while the emission reduction occurred abruptly after May. This is caused partially because the temperature was measured in the water column (above the thermocline) which differs from the

sediment temperature where bubbles are formed, but also due to the system response to any change in the conditions (eg. changes in ebullition due to alteration in temperature).

Additionally, this period of elevated emissions took place within higher precipitation and greater reservoir water level, whereas during the period when the most likely condition of the reservoir was mixture and uniform profile of temperature and dissolved oxygen, which was during the colder months, the mean flux had a large reduction (more than 10-fold the mean during summer).

It is also possible to identify regions of the reservoir with larger emissions. Considering the three locations where measurements were performed it is verified that the amount of gas emitted at location P2 was greater than the observed in the other locations, as is demonstrated in Figure 44. However, in this regard is important to notice that the actual amount of gas emitted must have been equal or greater than the values presented as there were gaps in the data time series.

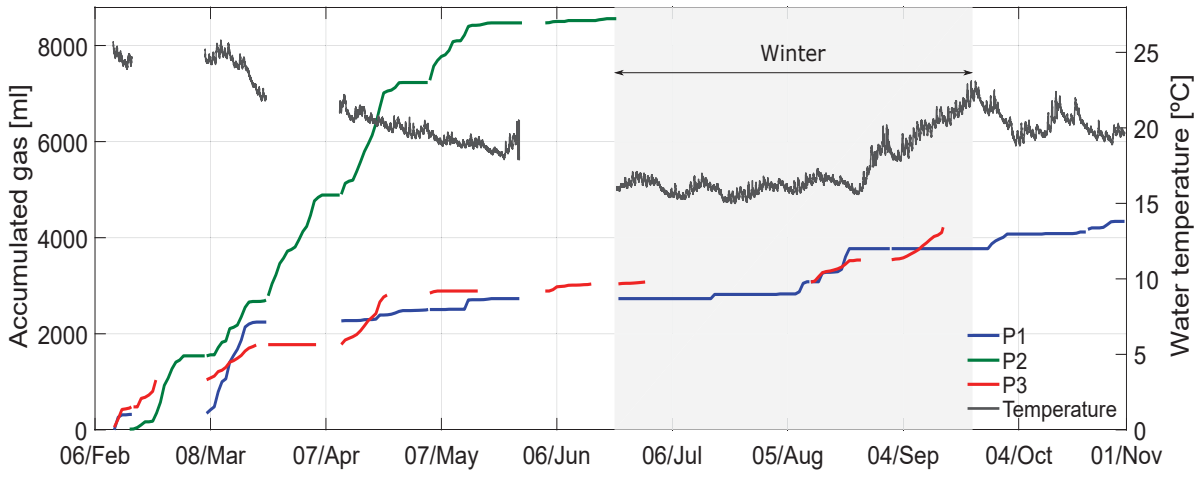


Figure 44: Accumulated volume of gas from ebullition data recorded from February to October 2017 in all ABTs location. The shaded area marks the winter period. The gaps in the curves are periods without data recorded. Thus, the actual accumulated gas volume was equal or greater than the values presented. The dark grey curve with values presented in the right hand side y axis is the water temperature measured by the ABT-P1.

According to the GHG measurement guidelines (International Hydropower Association (IHA), 2010) measurement of gas flux should be done in different regions of the reservoir from deep to shallow portions and from vegetated to non-vegetated areas to account for the spatial variability of the fluxes and in a monthly frequency to have seasonal variations. However, considering that conventional funnels are the most applied method to quantify ebullition and that measurements are mainly conducted in periods of 24 to 48 hours, it was evaluated what would be the consequence of reduced periods for the mean flux estimation.

The data applied was daily flux from P2 location measured from February to June of 2017, and was chosen because this location has fewer gaps in the time series for the period when emissions were higher. The number of days with measurement for each month were 15, 31, 30, 27, and 20 in February, March, April, May, and June respectively. The steps followed for the analysis were to randomly sample different numbers of days to calculate the mean gas flux from the samples. The number of days sampled was 2, 5, 10, 15, 20, and 30 days and the mean was calculated for ten thousand times for each number of days. The calculated flux means were then used to calculate the probability of occurrence histograms which are shown in Figure 45. The dashed red line is the mean gas flux calculated with the entire data set as $88.6\,\mathrm{ml\,m^{-2}\,d^{-1}}$.

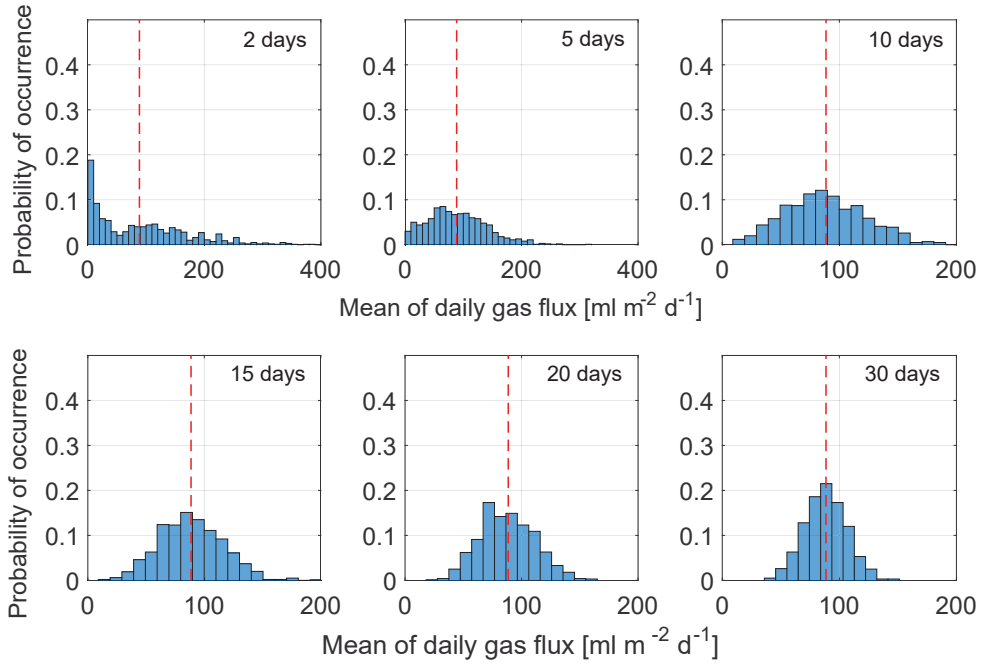


Figure 45: Probability of occurrence histograms of the mean daily flux calculated from samples of 2, 5, 10, 15, 20, and 30 days randomly chosen for P2 daily ebullition data set. The dashed red line is the mean gas flux calculated for the entire data set.

It is observed from the histograms that for 2 days sampled the probability of underestimating the mean flux by 4 times is 28%. As the number of days sampled grows the probability of having a mean sample flux close to the mean flux of the entire data set also increases. The increase of the number of days resulted in histograms similar to a normal distribution in which the probability of underestimating the mean flux is comparable to the probability of super estimating the mean gas flux. Thus, justifying the importance of continuous measurements of gas flux to quantify accurately the emissions from a reservoir.

A recent report published by the International Energy Agency (IEA) (2018) foresees the inclusion of mitigation strategies for greenhouse gas emissions in the management of reservoirs with hydropower generation purpose when is identified that emissions are relevant. Nonetheless, the accurate quantification of emissions is still challenging due to the variability surrounding the process. Thus, studies investigating the process can be used to identify the main causes of such emissions and how they could be diminished. The actions might be selected considering cost and operation feasibility, but for the case of methane bubbles formation, could be ways of oxygenating the bottom layer of water/sediment, reducing the matter that enters in the reservoir which supplies gas production, the operation of water subtraction as avoiding sediment disturbances, and so forth.

# Conclusion

The literature survey for greenhouse gas emissions from reservoirs showed that considerable emissions are reported for a few sites, however, based mainly on very short (minutes to days) and very few (3 to 20 points in a reservoir) measurements. Even though all authors reported the high and considerable temporal and spatial variations, there are only very few continuous our more resolved studies on bubbling processes present in literature, and mainly in temperate climates.

The presented study objective was to perform continuous and high temporal resolution measurement of gas emission in a subtropical reservoir using a prototype Automated Bubble Trap (ABT). The laboratory tests showed that the equipment works well for determining the volume of gas captured. The equipment could be successfully deployed at Passaúna reservoir providing original and new data for gas bubbling processes i.e. for subtropical conditions.

Gas ebullition data was recorded in more than 2500 hours in time steps of 15 seconds from February of 2017 to October 2017. On average, emissions were recorded in 10% of the time only and the time series showed a very temporal variability agreeing with the literature. Although ebullition is not continuous with days of no emissions recorded after the first bubbles leave the sediment matrix other will follow in a time interval smaller than 10 minutes. The less intense fluxes were the most frequent, in more than 25% of the flux intensity was smaller than $100\,\mathrm{ml\,m^{-2}\,d^{-1}}$ and the fluxes with short duration had the greatest share to the total amount of gas emitted.

Results furthermore showed strong seasonal variations with a reduction in the emissions during the winter period when the reservoir was not stratified. During the period of lower temperature fewer peaks of ebullition were recorded and resulted in a different probability of occurrence histogram than the exponential one obtained for the summer period. This great difference was attributed to the chemical conditions of the water column and to local physical processes that occur in the sediment.

Spatial variability of emissions was also observed. Considering mean values from March to May of 2017, the locations P2 which is near the water intake facility had the greatest emission value, followed by P1 and lastly P3 which is in the deepest region of the reservoir. Such pattern might be related to sediment characteristics and to the amount of organic matter entering the system.

A qualitative analysis of ebullition fluxes from all three locations indicated that some of the highest fluxes were synchronized, considering a daily timescale, suggesting that external forcings triggering ebullition might be acting on a spatial scale covering all the locations. The highest fluxes occurred during periods of drops is the atmospheric pressure and higher wind velocities. Nonetheless, the correlation with separated parameters hadn't good results for all time series presenting in some cases very weak correlation. Such results indicate that not only one parameter is responsible for all the variability observed in the ebullitions, but an overlapping of forcings creates the system dynamics and at some times one stands out to the others.

Lastly, it is showed that high temporal and continuous gas ebullition measurements provide information to the reservoir management regarding emissions behaviour and for quantifying the total emissions, as short-term measurement can underestimate the mean gas flux.

# Overview of field campaigns

Studies including field activities allow for a better understanding and perception of the studied site that would not be easily achieved working with the obtained data only. However, field campaigns are prone to a sort of influences and in this regard, the aim of this section is to share some of the experience gained throughout this two-year research.

A primary aspect involving field campaigns are related to logistics and time required. After defining a study area some arrangements may be necessary. In this case, the municipal water company, Sanepar, who manages Passaúna reservoir is cooperating with the NoPa-SeWaMa project and allowed for the equipment installation and the access to the reservoir.

The reservoir is located 27 km from the university campus and a car was used to transport the equipment, tools, and the boat from the campus to the reservoir at each trip to the field. For each trip, the associated costs including fuel for the car and for the boat, and equipment batteries was approximately R$112.50. This value excludes expenses with food, equipment maintenance, and any additional material needed for the activities in the field. During the year 2017, it was done 13 trips to the reservoir to collect data and for equipment maintenance resulting in total expenses of R$1462.5. In 2016 a total of 6 field campaigns were done, however, no data was collected.

Despite costs, field campaigns are also time demanding. Pre and post field tasks require at least one day for material preparation. In addition, all trips were accompanied by a professor who had available time to stay all day in the field.

In this research, the main equipment used were conventional funnels and the ABTs. After being deployed in the water for 5 months the conventional funnels had to be removed due to problems with the material. As these funnels were designed to stay submerged in the water for short period of time (one week at most), the oxidation of the iron arch and water itself damaged the canvas stitching, Figure 46. An alternative to reduce the faced problems with the material would be the use an aluminium arch instead of the iron arch to reduce material oxidation. In addition, the zipper which holds together the canvas and the iron arch could be replaced by stitched canvas.

Figure 46: Conventional funnels used for a gross estimation of gas volume. On the right hand side picture the conventional funnel removed from water after weeks deployed in water.

Another aspect related to the conventional funnels is the plastic syringe that stays attached to the top part of the funnel to allow for gas measurement, which can be seen in Figure 46. There is attached to this syringe a 3-way polypropylene stopcock to keep the syringe closed and to allow for attaching another

syringe for gas volume determination. However, this stopcock is very sensible and some samples were lost because the stopcock detached from the syringe.

With relation to the ABTs and considering that they are prototypes, some observations can be made. Laboratory tests, previous to field placement, contributes greatly to getting to know the equipment and in this way save time and costs of testing the equipment directly in the field.

The ABTs should be manipulated and installed carefully. Its placement and removal of water are crucial steps. Pressure sensors do not deal well with very large and suddenly pressure gradients and can be damaged. As the equipment is powered by batteries it requires regular maintenance which is beneficial for cleaning the equipment removing algae and dirt that accumulate in the funnel and in the head unit. A large accumulation of this material could cause a blockage of the gas flushing system and impair gas volume measurements.

Another important aspect to be mentioned is regarding the minimum water depth required for ABTs deployment. The actual version of the equipment requires a minimum of 3 m water depth to be totally submerged with a space between its base and the sediment bottom. As pointed out in studies as Rosa et al. (2016) and International Energy Agency (IEA) (2012) the ebullitive emissions from shallow regions may be considerably larger than from deeper reservoir's regions, and therefore, must be included in measurements. In this way, would be necessary to adapt the equipment to be installed in areas of reduced depth, as near the banks.

The last observation is regarding the download of the data. Not all ABTs used in this research saved data in the SD card and therefore, data was downloaded from the equipment internal memory through a USB cable which took longer, in some cases depending on the amount of data stored took more than one hour for complete download. This amount of time required for each location turn joint field activities difficult and is challenging under bad weather conditions.

## Future studies

This research brought information regarding gas ebullition in a water supply reservoir in a subtropical region and provides a small contribution towards a better understanding of the complexity surrounding ebullition process. Nonetheless, it was also pointed that several aspects are not completely understood and might have many others that were not thought about yet. And these facts open the possibility for several other studies regarding ebullition and GHG emissions from water bodies in general.

Considering that ebullition has a large temporal and spatial variability, achieving measurements with both high temporal and high spatial resolution at the same time and considering long-term scenarios still face constraints such as high costs, time demanding and requirement of qualified people for operating the technology, combining temporal and spatial information with modelling tools can contribute to understanding the processes underlying ebullition fluxes. Moreover, could provide a better estimation of emissions from water bodies considering the heterogeneities of the environment, and give emissions scenarios for changing environmental conditions.

With respect to field investigation, some aspects could be explored. Such as the influence of the biota, due to bioturbation in shallow and deep regions, to the ebullition occurrences. As the measurements of ebullition were conducted in deeper regions of the reservoir, it is also suggested to have measurements in different areas including for the case of Passaúna reservoir, measurements in the sidearms, near reservoir bank, and in the most upstream region known as 'Buffer area' at the reservoir's entrance. Additionally, there are several opened questions regarding the quantification of system time response for changing conditions, as sediment time exposure to elevated temperatures or to the oxygenated water column.

Ebullition is largely linked to methane emissions as the share of methane within the volume of gas is greater than any other gas, nonetheless, this research focused in the total volume of gas emitted rather than quantifying one component only. An estimation of the methane flux emitted from each monitoring station was obtained assuming a value from the literature for methane concentration. Considering a concentration of 80% (MAECK; HOFMANN; LORKE, 2014; WILKINSON et al., 2015) the mean methane emission for March, April, and May when the gas flux was simultaneously recorded in all locations was in the range of $0.5\,\mathrm{mmol\,m^{-2}\,d^{-1}}$–$5.66\,\mathrm{mmol\,m^{-2}\,d^{-1}}$ at P1, $3.39\,\mathrm{mmol\,m^{-2}\,d^{-1}}$–$6.87\,\mathrm{mmol\,m^{-2}\,d^{-1}}$ at P2, and $0.22\,\mathrm{mmol\,m^{-2}\,d^{-1}}$–$3.14\,\mathrm{mmol\,m^{-2}\,d^{-1}}$ at P3. Such fluxes are in the range proposed by IHA (2010) for temperate reservoirs ($-0.3$ to $8.0\,\mathrm{mmol\,m^{-2}\,d^{-1}}$).

Taking into account ebullition measurements conducted in reservoirs and lakes in Brazil, Carvalho (2015) observed that for Sinhá Mariana pond (wetland region of Mato Grosso) ebullition ranged from $0\,\mathrm{mmol\,m^{-2}\,d^{-1}}$ to $16.85\,\mathrm{mmol\,m^{-2}\,d^{-1}}$ with a mean of $6.9\,\mathrm{mmol\,m^{-2}\,d^{-1}}$. Therefore, at Passaúna reservoir, which is located in a region of the rainforest, the range of emissions were narrower than the range recorded for a pond located in a wetland region. Ebullition was also measured from 2011 to 2012 at several hydropower reservoirs located in different regions of Brazil by COPPE/RJ. According to the results presented the range of emissions varied depending on the reservoir. For reservoirs located in regions of the rainforest (Funil, Itaipu, and Segredo) the maximum emission obtained was approximately $17\,\mathrm{mgCH_4\,m^{-2}\,d^{-1}}$ at Segredo, while the mean methane emission for all three reservoirs were below $4\,\mathrm{mgCH_4\,m^{-2}\,d^{-1}}$ (BRASIL, 2014). At Passaúna the mean methane emission in terms of $\mathrm{mgCH_4\,m^{-2}\,d^{-1}}$ for the three months (March, April, and May) were $36.24\,\mathrm{mgCH_4\,m^{-2}\,d^{-1}}$, $74.69\,\mathrm{mgCH_4\,m^{-2}\,d^{-1}}$, and $30.05\,\mathrm{mgCH_4\,m^{-2}\,d^{-1}}$ at P1, P2, and P3 respectively. Such values were one order greater than the values reported for reservoirs in the same biome, nevertheless, it is important to point out that in this study the values were point measurements and thus, do not represent emissions from the entire reservoir. In addition, the sampling duration differed from the mentioned study.

To better quantify methane emissions from Passaúna reservoir instead of determining the volume of gas is still necessary to measure the methane concentration within the gas. Other parameters may also be important as measuring sediment temperature and estimating methane diffusion from sediment to the water column as both parameters control gas production and its availability in the sediment. Another field of study is to determine the actual contribution of Passaúna reservoir to gas or methane emissions to the atmosphere. For such analysis it must be included characteristics of emission of the pre-impounded area as well as the carbon burial by the reservoir formed, and emissions from different pathways (PRAIRIE et al., 2017).

# Bibliography

ALGAR, C. K.; BOUDREAU, B. P. Transient growth of an isolated bubble in muddy, fine-grained sediments. *Geochimica et Cosmochimica Acta*, Elsevier Ltd, v. 73, n. 9, p. 2581–2591, 2009. ISSN 00167037.

ALGAR, C. K.; BOUDREAU, B. P.; BARRY, M. A. Initial rise of bubbles in cohesive sediments by a process of viscoelastic fracture. *Journal of Geophysical Research: Solid Earth*, v. 116, n. 4, p. 1–14, 2011. ISSN 21699356.

ALGAR, C. K.; BOUDREAU, B. P.; BARRY, M. A. Release of multiple bubbles from cohesive sediments. *Geophysical Research Letters*, v. 38, n. 8, p. 2–5, 2011. ISSN 00948276.

ANDERSON, A. L. et al. Bubble populations and acoustic interaction with the gassy floor of Eckernforde Bay. *Continental Shelf Research*, v. 18, n. 14-15, p. 1807–1838, 1998. ISSN 02784343.

BAIRD, A. J. et al. Ebullition of methane-containing gas bubbles from near-surface Sphagnum peat. *Geophysical Research Letters*, v. 31, n. 21, p. 2–5, 2004. ISSN 00948276.

BASTVIKEN, D. et al. Methane emissions from lakes: Dependence of lake characteristics, two regional assessments, and a global estimate. *Global Biogeochemical Cycles*, v. 18, n. 4, p. 1–12, 2004. ISSN 08866236.

BASTVIKEN, D.; EJLERTSSON, J.; TRANVIK, L. Measurement of methane oxidation in lakes: A comparison of methods. *Environmental Science and Technology*, v. 36, n. 15, p. 3354–3361, 2002. ISSN 0013936X.

BEAULIEU, J. J.; MCMANUS, M. G.; NIETCH, C. T. Estimates of reservoir methane emissions based on a spatially balanced probabilistic-survey. *Limnology and Oceanography*, v. 61, n. Thornton 1990, p. S27–S40, 2016. ISSN 19395590.

BEZERRA-NETO, J. F. et al. Hydroacoustic assessment of fish and Chaoborus (Diptera-Chaoboridae) distribution in three Neotropical lakes. *Acta Limnologica Brasiliensia*, v. 24, n. 1, p. 18–28, 2012. ISSN 2179-975X.

BOX, G. E. P. et al. *Time series analysis: forecasting and control*. 5. ed. New Jersey: John Wiley & Sons, 2016. 709 p. ISBN 978-1-118-67502-1.

BRASIL. *Emissões de gases de efeio estufa em reservatórios de centrais hidrelétricas*. Rio de Janeiro, 2014. 415 p.

BRITTO, A. L.; JOHNSSON, R. M. F.; CARNEIRO, P. R. F. Water supply and hydrosocial scarcity in the Rio de Janeiro Metropolitan Area. *Ambiente & Sociedade*, v. 19, n. 1, p. 183–206, 2016. ISSN 1809-4422.

CARNEIRO, C.; KELDERMAN, P.; IRVINE, K. Assessment of phosphorus sediment–water exchange through water and mass budget in Passaúna Reservoir (Paraná State, Brazil). *Environmental Earth Sciences*, Springer Berlin Heidelberg, v. 75, n. 7, p. 564, 2016. ISSN 1866-6280.

CARVALHO, F. R. de; CARVALHO, F. R. de. *Fluxo de CO2 e CH4 em uma lagoa tropical (Pantanal, Brasil) com gradiente de turbidez*. 86 p. Tese (Master) — Universidade Federal de Juiz de Fora, 2015.

CASPER, P. et al. Fluxes of methane and carbon dioxide from a small productive lake to the atmosphere. *Biogeochemistry*, v. 49, n. 1, p. 1–19, 2000. ISSN 01682563.

CAVIGLIONE, J. H. et al. *Cartas Climáticas do Paraná*. Londrina, 2010. Disponível em: <http://www.iapar.br/modules/conteudo/conteudo.php?conteudo=597>.

COMITÊ INTERMINISTERIAL SOBRE MUDANÇA DO CLIMA. *Plano Nacional sobre Mudança do Clima - PNMC*. Comite Interministerial sobre Mudança do Clima, 2008. 1–132 p. Disponível em: <http://www.mma.gov.br/estruturas/smcq_climaticas/_arquivos/plano_nacional_mudan>.

DEEMER, B. R. et al. Greenhouse Gas Emissions from Reservoir Water Surfaces: A New Global Synthesis Manuscript. *BioScience*, v. 66, n. 11, p. 949–964, 2016. ISSN 0006-3568.

Del SONTRO, T. S. *Quantifying Methane Emissions from Reservoirs : From Basin-scale to Discrete Analyses with a Focus on Ebullition Dynamics*. 168 p. Tese (Doutorado) — ETH Zurich, 2011.

Del SONTRO, T. S. et al. Methane ebullition and diffusion from northern ponds and lakes regulated by the interaction between temperature and system productivity. *Limnology and Oceanography*, v. 61, p. S62–S77, 2016. ISSN 19395590.

Del SONTRO, T. S. et al. Spatial heterogeneity of methane ebullition in a large tropical reservoir. *Environmental Science and Technology*, v. 45, n. 23, p. 9866–9873, 2011. ISSN 0013936X.

Del SONTRO, T. S. et al. Size does matter: Importance of large bubbles and small-scale hot spots for methane transport. *Environmental Science and Technology*, v. 49, n. 3, p. 1268–1276, 2015. ISSN 15205851.

DESHMUKH, C. et al. Physical controls on CH4 emissions from a newly flooded subtropical freshwater hydroelectric reservoir: Nam Theun 2. *Biogeosciences*, v. 11, n. 15, p. 4251–4269, 2014. ISSN 17264189.

DUCHEMIN, E. et al. Comparison of Static Chamber and Thin Boundary Layer Equation Methods for Measuring Greenhouse Gas Emissions from Large Water Bodies§. *Environmental Science & Technology*, v. 33, n. 2, p. 350–357, 1999.

ESTEVES, F. D. A. *Fundamentos de Limnologia*. 2. ed. Rio de Janeiro: Interciência, 1998. 226 p. ISSN 18657125. ISBN 978-85-7193-271-5.

EUGSTER, W.; DELSONTRO, T.; SOBEK, S. Eddy covariance flux measurements confirm extreme CH 4 emissions from a Swiss hydropower reservoir and resolve their short-term variability. *Biogeosciences*, v. 8, n. 9, p. 2815–2831, 2011. ISSN 17264170.

FISCHER, H. B. et al. *Mixing in inland and coastal waters*. 1. ed. Nova York: Academic Press Inc, 1979. 483 p.

FOX, R. W.; MCDONALD, A. T. *Introdução à mecânica dos fluidos*. 5. ed. Rio de Janeiro: LTC, 2001. 519 p.

FRIEDL, G.; WÜEST, A. Disrupting biogeochemical cycles - Consequences of damming. *Aquatic Sciences-Research Across Boundaries*, v. 64, p. 55–65, 2002. ISSN 1015-1621.

FUNCEME. *Relatório técnico: Mapeamento dos espelhos de água do Brasil*. Brasilia, 2008. 108 p. Disponível em: <http://www.funceme.br/documents/Projetos/espelhos_dagua-.pdf\&usg=AFQjCNFL7yDFekPklkD5SYgbqKvbzzSkbg\&sig2=3rx5DYlcmOY>.

GODOY, R. B. *Dinâmica da qualidade da água em reservatório de abastecimento público: estudo de caso do Passaúna - PR*. Tese (Master (Qualification exam)) — Federal University of Paraná, 2017.

HILGERT, S. *Analysis of spatial and temporal heterogeneities of methane emissions of reservoirs by correlating hhydro-acoustic with sediment parameters*. Tese (phD) — Karlsruhe Institute of Technology, 2014.

HORIBA Ltd. *Multi water quality checker U-50 series*. [S.l.]: HORIBA Ltd, 2009. 45 p.

International Energy Agency (IEA). *Hydropower and the environment: managing the carbon balance in freshwater reservoirs - Volume 1: Measurement programs and data analysis*. [S.l.], 2012.

International Energy Agency (IEA). *Guidelines from quantitative analysis of net GHG emissions from reservoirs - Volume 3, Mitigation and Allocation*. [S.l.], 2018.

International Hydropower Association (IHA). *GHG measurement guidelines for freshwater reservoirs*. London: [s.n.], 2010. 138 p. ISBN 9780956622808.

IPCC. *Contribution of Working Group I to the Fifth Assessment Report of the Intergovernmental Panel on Climate Change*. Cambridge, United Kingdom and New York: Cambridge University Press, 2013. 1535 p. ISBN 9781107661820.

JAIN, A. K.; JUANES, R. Preferential mode of gas invasion in sediments: Grain-scale mechanistic model of coupled multiphase fluid flow and sediment mechanics. *Journal of Geophysical Research: Solid Earth*, v. 114, n. 8, p. 1–19, 2009. ISSN 21699356.

JOYCE, J.; JEWELL, P. W. Physical controls on methane ebullition from reservoirs and lakes. *Environmental and Engineering Geoscience*, 2003. ISSN 10787275.

KELLER, M.; STALLARD, R. F. Methane emission by bubbling from Gatun Lake, Panama. *Journal of Geophysical Research*, v. 99, n. D4, p. 8307–8319, 1994. ISSN 0148-0227.

KEPPLER, F. et al. Methane formation in aerobic environments. *Environmental Chemistry*, v. 6, n. 6, p. 459–465, 2009. ISSN 14482517.

KNAPIK, H. G. et al. *Avaliação quali-quantitativa na coluna d'água e no sedimento*. Curitiba: SeWaMa, 2017. 2 p. Disponível em: <http://www.nopa-brasil.net/en/sewama.html>.

KROOS, K. A.; POTTER, M. C. *Termodinâmica para engenheiros*. 1. ed. São Paulo: Cengage Learning, 2015. 527 p. ISBN 978-85-221-2198-4.

LAMPERT, W.; SOMMER, U. *Limnoecology: the ecology of lakes and streams*. Second. New York: Oxforf University Press, 2007. 324 p. ISBN 978-0-19-921392-4.

LEHNER, B. et al. Global Reservoir and Dam ( GRanD ) database. *European Environment*, n. March, p. 12, 2011. Disponível em: <http://www.gwsp.org/85.html>.

LIU, L. et al. The role of sediment structure in gas bubble storage and release : Sediment structure affects ebullition. n. August, p. 1–14, 2016.

LORKE, A. et al. Technical note: Drifting versus anchored flux chambers for measuring greenhouse gas emissions from running waters. *Biogeosciences*, v. 12, n. 23, p. 7013–7024, 2015. ISSN 17264189.

MAAVARA, T. et al. Global phosphorus retention by river damming. *Proceedings of the National Academy of Sciences*, p. 15603 – 15608, 2015. ISSN 0027-8424.

MAECK, A. *Understanding Methane Emissions from Impounded Rivers - A Process-based Approach to Quantify Methane Emission Rates in Space and Time*. 63 p. Tese (Doutorado) — Universität Koblenz-Landau, 2014.

MAECK, A. et al. Sediment trapping by dams creates methane emission hot spots. *Environmental Science and Technology*, v. 47, n. 15, 2013. ISSN 0013936X.

MAECK, A.; HOFMANN, H.; LORKE, A. Pumping methane out of aquatic sediments - ebullition forcing mechanisms in an impounded river. *Biogeosciences*, v. 11, n. 11, p. 2925–2938, 2014. ISSN 17264189.

MAGALHÃES, M. N.; LIMA, A. C. P. *Noções de probabilidade e estatística*. 5. ed. São Paulo: Editora da Universidade de São Paulo, 2002. 392 p.

MANNICH, M.; FERNANDES, C.; BLENINGER, T. Uncertainty analysis of gas flux measurements at air-water interface using floating chambers. *Ecohydrology and Hydrobiology*, n. 2016, 2017. ISSN 20803397.

MARQUES, M. *Modelagem paramétrica bidimensional para simulação do campo de ondas em águas continentais*. 217 p. Tese (Doutorado) — Universidade Federal do Paraná, 2013.

MCGINNIS, D. F. et al. Porewater methane transport within the gas vesicles of diurnally migrating Chaoborus spp.: An energetic advantage. *Scientific Reports*, Nature Publishing Group, v. 7, n. July 2016, p. 1–7, 2017. ISSN 20452322.

MCGINNIS, D. F. et al. Fate of rising methane bubbles in stratified waters: How much methane reaches the atmosphere? *Journal of Geophysical Research: Oceans*, v. 111, n. 9, p. 1–15, 2006. ISSN 21699291.

MINISTÉRIO DE MINAS E ENERGIA. Balanço energético nacional - BEN 2015. p. 291, 2015.

MYHRE, G. et al. Anthropogenic and natural radiative forcing. *Climate change*, v. 423, p. 658–740, 2013.

NATCHIMUTHU, S. et al. Spatio-temporal variability of lake CH4 fluxes and its influence on annual whole lake emission estimates. *Limnology and Oceanography*, v. 61, p. S13–S26, 2016. ISSN 19395590.

ODUM, E. P.; BARRETT, G. W. *Fundamentos de Ecologia*. 5. ed. São Paulo: Thomson Pioneira, 2007. 632 p. ISBN 9788522105410.

OSTROVSKY, I. et al. Quantifying gas ebullition with echosounder: the role of methane transport by bubbles in a medium-sized lake. *Limnology and Oceanography: Methods*, v. 6, p. 105–118, 2008. ISSN 15415856.

PELTOLA, O. *Field intercomparison of four methane gas analysers suitable for eddy covariance flux measurements*. 80 p. Tese (Master) — University of Helsinki, 2011.

PRAIRIE, Y. T. et al. Greenhouse Gas Emissions from Freshwater Reservoirs: What Does the Atmosphere See? *Ecosystems*, n. April, p. 1–14, 2017. ISSN 14350629.

ROHWEDER, J. et al. *Application of wind fetch and wave models for habitat rehabilitation and enhancement projects - 2012 Update*. [S.l.], 2012. 52 p. Disponível em: <https://www.umesc.usgs.gov-/management/dss/wind_fetch_wave_models_201>.

ROSA, L. P. et al. A model for the data extrapolation of greenhouse gas emissions in the Brazilian hydroelectric system. *Environmental Research Letters*, IOP Publishing, v. 11, n. 6, 2016. ISSN 17489326.

ROSA, L. P. et al. *Emissões de Dióxido de Carbono e de Metano pelos Reservatórios Hidrelétricos Brasileiros*. Brasília, 2006. 118 p.

RUDD, J. W. M. et al. Are hydroelectric reservoirs significant sources of greenhouse gases. *Ambio*, v. 22, n. 4, p. 246–248, 1993. ISSN 0044-7447.

SANTOS, E. O. dos; ROSA, L. P.; SANTOS, M. A. dos. Tecnicas De Medida E Análise De Gases De Efeito Estufa Em Reservatórios Hidrelétricos Brasileiros. *XII Congresso Brasileiro de Meteorologia*, 2002.

SANTOS, M. A. dos et al. Gross greenhouse gas fluxes from hydro-power reservoir compared to thermo-power plants. *Energy Policy*, v. 34, n. 4, p. 481–488, 2006. ISSN 03014215.

SAUNITI, R. M.; FERNANDES, L. A.; BITTENCOURT, A. V. Estudo Do Assoreamento Do Reservatório Da Barragem Do Rio Passaúna - Curitiba - Pr. *Boletim Paranaense de Geociências*, v. 54, p. 65–82, 2002.

SCHUMACK, V. V.; MANNICH, M. *Variação transversal de metano dissolvido em um reservatório subtropical*. Florianópolis: XXII Simpósio Brasileiro de Recursos Hídricos, 2017. 1–8 p.

SEGERS, R. Methane production and methane consumption–a review of processes underlying wetland methane fluxes [Review]. *Biogeochemistry*, v. 41, p. 23–51, 1998. ISSN 01682563.

SENECT. *The Automated Bubble Trap (ABT) - Continuous measurement of the gas bubble rate*. 2016. Disponível em: <http://www.senect.de/abt/>.

SMITH, K. A. et al. Exchange of greenhousegases between soil and atmosphere: interactions of soil physical factors and biological processes. *European Journal of Soil Science*, v. 54, n. December, p. 779–791, 2003.

SOBEK, S. et al. Extreme organic carbon burial fuels intense methane bubbling in a temperate reservoir. *Geophysical Research Letters*, v. 39, n. 1, p. 2–5, 2012. ISSN 00948276.

SONTEK. *CastAway CTD User's Manual 1.5*. San Diego: SonTek, 2012. 83 p.

SOTIRI, K. *Investigation of urban mass fluxes to river systems through the use of reservoirs as validation points*. 68 p. Tese (Master) — Karlsruhe Institute of Technology, 2016.

ST. LOUIS, V. L. et al. Reservoir Surfaces as Sources of Greenhouse Gases to the Atmosphere: A Global Estimate. *BioScience*, v. 50, n. 9, p. 766, 2000. ISSN 0006-3568.

SUDERHSA; RDR. *Plano de Bacia do Alto Iguaçú e afluentes do Alto Ribeira: Relatório de Diagnóstico*. Curitiba, 2007.

TANG, K. W. et al. Paradox reconsidered: Methane oversaturation in well-oxygenated lake waters. *Limnology and Oceanography*, v. 59, n. 1, p. 275–284, 2014. ISSN 00243590.

TEODORU, C. R. et al. The net carbon footprint of a newly created boreal hydroelectric reservoir. *Global Biogeochemical Cycles*, v. 26, n. 2, p. 1–14, 2012. ISSN 08866236.

TREMBLAY, A. et al. *Greenhouse gas emissions - fluxes and processes: Hydroelectric reservoirs and natural environments*. [S.l.]: Springer Science & Business Media, 2005. v. 1. 743 p. ISSN 1098-6596. ISBN 9788578110796.

VALENTINE, D. L. et al. Carbon and hydrogen isotope fractionation by moderately thermophilic methanogens. *Geochimica et Cosmochimica Acta*, v. 68, n. 7, p. 1571–1590, 2004. ISSN 00167037.

VARADHARAJAN, C.; HEMOND, H. F. Time-series analysis of high-resolution ebullition fluxes from a stratified, freshwater lake. *Journal of Geophysical Research: Biogeosciences*, v. 117, n. G02004, p. n/a–n/a, jun 2012. ISSN 01480227.

VARADHARAJAN, C.; HERMOSILLO, R.; HEMOND, H. F. A low-cost automated trap to measure bubbling gas fluxes. *Limnology and Oceanography: Methods*, v. 8, p. 363–375, 2010. ISSN 15415856.

VASCONCELOS SEGUNDO, E. H. de; FROEHNER, S. Conductometric model for the determination of dissolved carbon dioxide concentration in Vossoroca reservoir, Brazil | Modelo condutométrico para determinação da concentração de dióxido de carbono dissolvido no Reservatório Vossoroca, Brasil. *Engenharia Sanitaria e Ambiental*, v. 21, n. 3, p. 479–487, 2016. ISSN 14134152.

VÖRÖSMARTY, C. J. et al. Anthropogenic sediment retention: Major global impact from registered river impoundments. *Global and Planetary Change*, v. 39, n. 1-2, p. 169–190, 2003. ISSN 09218181.

WALPOLE, R. E.; MYERS, R. H. *Probability and statistics for enginneers and scientists*. New York: Macmillan Company, 1976. 505 p.

WIK, M. et al. Multiyear measurements of ebullitive methane flux from three subarctic lakes. *Journal of Geophysical Research: Biogeosciences*, v. 118, n. 3, 2013. ISSN 21698961.

WILKINSON, J. et al. Continuous Seasonal River Ebullition Measurements Linked to Sediment Methane Formation. *Environmental Science and Technology*, v. 49, n. 22, p. 13121–13129, 2015. ISSN 15205851.

WÜEST, A.; LORKE, A. Small-scale hydrodynamics in lakes. *Annual Review of Fluid Mechanics*, v. 35, n. 1, p. 373–412, 2003. ISSN 0066-4189.

XAVIER, C. d. F. *Avaliação da influência do uso e ocupação do solo e de características geomorfológicas sobre a qualidade das águas de dois reservatórios da região metropolitana de Curitiba – Paraná*. 167 p. Tese (Master) — Universidade Federal do Paraná, 2005.

XAVIER, C. d. F. et al. *Qualidade das águas: reservatórios do estado do Paraná 2005 a 2008*. Curitiba, 2009. 124 p. Disponível em: <http://www.iap.pr.gov.br/arquivos/File/boletins/RELATORIO_AGUA-/relatorio_RESERVATORIOS_2005>.

YVON-DUROCHER, G. et al. Methane fluxes show consistent temperature dependence across microbial to ecosystem scales. *Nature*, Nature Publishing Group, v. 507, n. 7493, p. 488–91, 2014. ISSN 1476-4687.

ZAREBSKA, Z. *Small scale sediment analysis in a Brazilian reservoir*. 57 p. Tese (Master) — Karlsruher Institute of Technology, 2016.

ZARFL, C. et al. A global boom in hydropower dam construction. *Aquatic Sciences*, v. 77, n. 1, p. 161–170, 2014. ISSN 14209055.

# Appendix

# APPENDIX A – Day and night fluxes comparison

For the day versus night mean flux comparison a Wilcoxon test was applied. All the ebullition time series, recorded in all three locations were separated between day and night fluxes for each day, after that the test was done. For all steps MatLab was used. The $p$-values as well the mean flux is presented in Table 15. The periods highlighted in red are the data set which mean day flux is statistically different from mean night flux for a 5% confidence level ($p$ <0.05).

Table 15: Results $p$-values of Wilcoxon rank test to compare mean flux recorded during day (7 a.m to 7 p.m) and mean flux recorded during night (7 p.m to 7 a.m).

| **Period** | ***p*-value** | **Mean day flux** $[\mathrm{ml\,m^{-2}\,d^{-1}}]$ | **Mean night flux** $[\mathrm{ml\,m^{-2}\,d^{-1}}]$ |
|---|---|---|---|
| **P1 - Park** | | | |
| Feb.$10^{th}$–Feb.$15^{th}$ | 0.257 | 144.52 | 14.77 |
| Mar.$06^{th}$–Mar.$22^{nd}$ | 0.316 | 169.80 | 107.74 |
| Apr.$10^{th}$–May$03^{rd}$ | 0.805 | 14.39 | 11.36 |
| May$04^{th}$–May$27^{th}$ | 0.821 | 13.03 | 10.01 |
| Jun.$21^{st}$–Aug.$10^{th}$ | 0.501 | 8.29 | 8.07 |
| Aug.$11^{th}$–Aug.$31^{st}$ | 0.420 | 32.34 | 38.67 |
| Sep.$01^{st}$–Oct.$21^{st}$ | 0.864 | 6.21 | 10.62 |
| Oct.$21^{st}$–Oct.$31^{st}$ | 0.791 | 13.85 | 26.99 |
| **P2 - Water intake** | | | |
| Feb.$14^{th}$–Mar.$06^{th}$ | 0.917 | 91.67 | 93.17 |
| Mar.$07^{th}$–Mar.$22^{nd}$ | 0.428 | 96.63 | 71.47 |
| Mar.$23^{rd}$–Apr.$10^{th}$ | 0.860 | 124.49 | 140.33 |
| Apr.$11^{th}$–May$03^{rd}$ | 0.639 | 126.07 | 115.13 |
| May$04^{th}$–May$27^{th}$ | 1.000 | 59.52 | 56.57 |
| Jun.$02^{nd}$–Jun.$21^{st}$ | 0.013 | 11.6 | 0.01 |
| **P3 - Dam** | | | |
| Feb.$10^{th}$–Feb.$15^{th}$ | 0.257 | 176.55 | 51.29 |
| Feb.$16^{th}$–Feb.$21^{st}$ | 0.238 | 218.30 | 29.06 |
| Mar.$06^{th}$–Mar.$19^{th}$ | 0.036 | 86.62 | 48.31 |
| Mar.$22^{nd}$–Apr.$04^{th}$ | - | 0 | 0 |
| Apr.$10^{th}$–Apr.$24^{th}$ | 0.601 | 101.62 | 82.84 |
| May $03^{rd}$–May $16^{th}$ | 0.655 | 3.84 | 6.10 |
| Jun.$02^{nd}$–Jun.$14^{th}$ | 0.245 | 20.31 | 7.97 |
| Jun.$21^{st}$–Jun.$28^{th}$ | 0.231 | 7.84 | 5.31 |
| Aug.$10^{th}$–Aug.$24^{th}$ | 0.586 | 45.06 | 37.58 |
| Aug.$31^{st}$–Sep.$14^{th}$ | 0.959 | 77.46 | 48.69 |

# APPENDIX B – Gas ebullition events analysis

The tables contained in this appendix, Tables 16, 17, and 18 present the number of ebullition events, their duration, and the volume of gas emitted. For the calculation was considered the entire data set of ebullition flux for a TSA of 5 minutes (e.g dt = 5 minutes).

Table 16: Gas ebullition events from data recorded at P1-Park location

| Duration [number of dt] | Number of events | Gas volume emitted [ml] | Fraction in relation to the total gas volume [%] |
|---|---|---|---|
| 1 | 680 | 1101.06 | 27.76 |
| 2 | 253 | 846.40 | 21.34 |
| 3 | 139 | 494.18 | 12.46 |
| 4 | 63 | 295.53 | 7.45 |
| 5 | 43 | 228.57 | 5.76 |
| 6 | 29 | 217.24 | 5.48 |
| 7 | 20 | 192.22 | 4.85 |
| 8 | 11 | 94.79 | 2.39 |
| 9 | 9 | 147.22 | 3.71 |
| 10 | 2 | 37.93 | 0.96 |
| 11 | 2 | 71.05 | 1.79 |
| 12 | 3 | 27.37 | 0.69 |
| 13 | 2 | 18.59 | 0.47 |
| 14 | 1 | 13.93 | 0.35 |
| 15 | 0 | 0.00 | 0.00 |
| 16 | 1 | 13.18 | 0.33 |
| 17 | 2 | 42.47 | 1.07 |
| 18 | 0 | 0.00 | 0.00 |
| 19 | 1 | 47.48 | 1.20 |
| 20 | 0 | 0.00 | 0.00 |
| 21 | 0 | 0.00 | 0.00 |
| 22 | 1 | 53.35 | 1.34 |
| 23 | 0 | 0.00 | 0.00 |
| 24 | 0 | 0.00 | 0.00 |
| 25 | 0 | 0.00 | 0.00 |
| 26 | 0 | 0.00 | 0.00 |
| 27 | 1 | 24.28 | 0.61 |
| **Total** | **1263.00** | **3966.81** | **100.00** |

Table 17: Gas ebullition events from data recorded at P2-Water intake location

| Duration [number of dt] | Number of events | Gas volume emitted [ml] | Fraction in relation to the total gas volume [%] |
|---|---|---|---|
| 1 | 1102 | 1939.24 | 24.44 |
| 2 | 503 | 1732.47 | 21.84 |
| 3 | 235 | 1187.72 | 14.97 |
| 4 | 138 | 970.79 | 12.24 |
| 5 | 69 | 619.32 | 7.81 |
| 6 | 43 | 439.37 | 5.54 |
| 7 | 24 | 216.46 | 2.73 |
| 8 | 23 | 269.56 | 3.40 |
| 9 | 10 | 117.46 | 1.48 |
| 10 | 7 | 108.17 | 1.36 |
| 11 | 4 | 92.40 | 1.16 |
| 12 | 2 | 38.52 | 0.49 |
| 13 | 4 | 69.26 | 0.87 |
| 14 | 0 | 0.00 | 0.00 |
| 15 | 1 | 16.50 | 0.21 |
| 16 | 2 | 47.95 | 0.60 |
| 17 | 0 | 0.00 | 0.00 |
| 18 | 0 | 0.00 | 0.00 |
| 19 | 0 | 0.00 | 0.00 |
| 20 | 0 | 0.00 | 0.00 |
| 21 | 0 | 0.00 | 0.00 |
| 22 | 0 | 0.00 | 0.00 |
| 23 | 1 | 68.60 | 0.86 |
| **Total** | **2168** | **7933.79** | **100.00** |

Table 18: Gas ebullition events from data recorded at P3-Dam location

| Duration [number of dt] | Number of events | Gas volume emitted [ml] | Fraction in relation to the total gas volume [%] |
|---|---|---|---|
| 1 | 1190 | 1321.86 | 33.80 |
| 2 | 391 | 962.39 | 24.61 |
| 3 | 149 | 799.35 | 20.44 |
| 4 | 82 | 422.40 | 10.80 |
| 5 | 31 | 136.81 | 3.50 |
| 6 | 27 | 144.08 | 3.68 |
| 7 | 11 | 56.62 | 1.45 |
| 8 | 4 | 16.62 | 0.42 |
| 9 | 1 | 13.21 | 0.34 |
| 10 | 1 | 17.80 | 0.46 |
| 11 | 0 | 0.00 | 0.00 |
| 12 | 1 | 11.21 | 0.29 |
| 13 | 1 | 7.93 | 0.20 |
| **Total** | **1889** | **3910.30** | **100** |

# APPENDIX C – Reservoir fetch and superficial waves calculation

The wind fetch for the the ABTs location was determined using the model developed by the US Army Corps of Engineers. The model was developed for the software ESRI ArcGis and requires as input parameters for the fetch field a raster file of the reservoir and a csv file containing wind directions and its percentage of occurrence. As output is generated raster files of fetch field for each wind direction and a weighted wind fetch considering all wind directions and their percentage of occurrence. Detailed information can be found at Rohweder et al. (2012).

The fetch for each wind direction is calculated from the arithmetic mean of nine radial measurements that are distributed around the direction of interest at three degrees increment (ROHWEDER et al., 2012). The wind fetch obtained for Passaúna reservoir is showed in Figure 47. The model has limitations as it does not consider the surrounding topography neither processes as refraction, diffraction, and reflection (ROHWEDER et al., 2012).

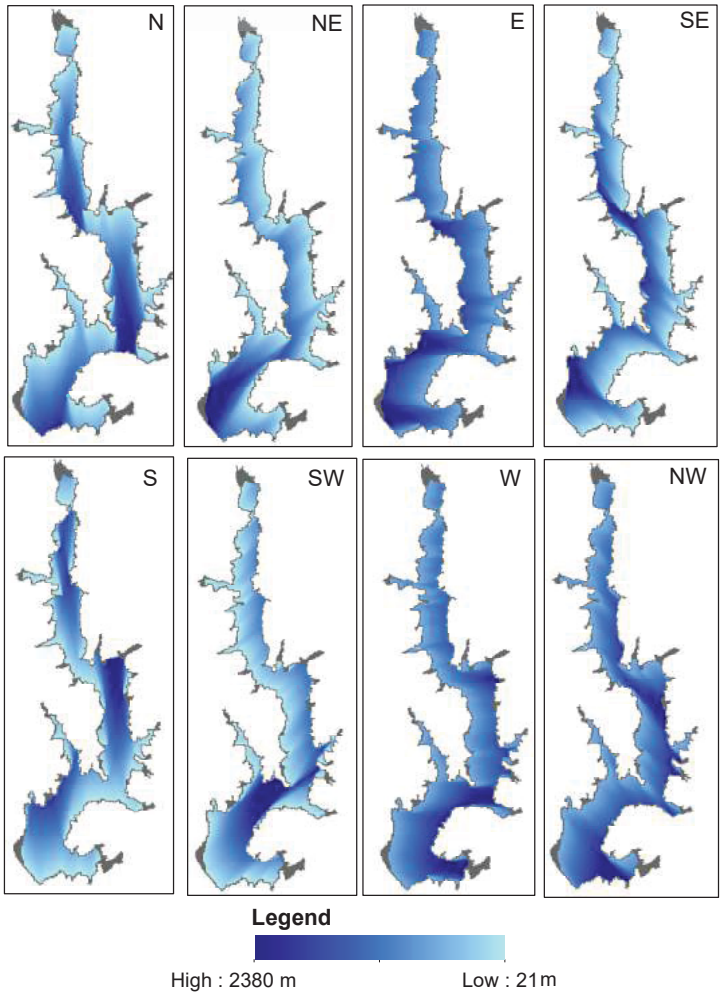


Figure 47: Wind fetch field for Passaúna reservoir for 8 wind directions.

From the wind fetch maps was obtained the fetch values for each wind direction and for each ABT's location. The values are presented in Table 19. The value of the longest wind fetch for all ABT's location is greater than 1500 m; at P1 and P2 is from North winds and at P3 is from Northeast winds.

Table 19: Wind fetch for each ABT's location and for each wind direction.

| | **Fetch [m]** | | | | | | | |
|---|---|---|---|---|---|---|---|---|
| | **N** | **NE** | **E** | **SE** | **S** | **SW** | **W** | **NW** |
| **P1** | 1522.0 | 286.0 | 270.0 | 298.0 | 652.0 | 306.0 | 358.0 | 630.0 |
| **P2** | 2043.0 | 463.0 | 203.0 | 160.0 | 568.0 | 975.0 | 353.0 | 647.0 |
| **P3** | 423.0 | 1543.0 | 609.0 | 592.0 | 1324.0 | 829.0 | 482.0 | 518.0 |

The surface waves generated due to wind incidence were calculated through equation proposed by Saville *et al.* (1962) *apud* Marques (2013),

$$H_s = \frac{0.0026}{g}\left(\frac{gF}{U_{10}^2}\right)^{0.47} U_{10}^2, \tag{C.1}$$

where $H_s$ is the surface wave height, $g$ is the acceleration due to gravity, $F$ is the wind fetch, and $U_{10}$ is the wind velocity at 10 m high.

The height of the surface wave generated was applied to calculate the variation of the hydrostatic pressure considering a point placed in the bottom portion of the reservoir at the sediment-water interface. The hydrostatic pressures in the a point (P) considering the wave peak over it and the wave trough are calculated as

$$P_P = \rho_w g\left(H_{total} + \frac{H_s}{2}\right) \tag{C.2}$$

and

$$P'_P = \rho_w g\left(H_{total} - \frac{H_s}{2}\right), \tag{C.3}$$

respectively, where $\rho_w$ is the water density and $H_{total}$ in the water column depth.

The variation in pressure is determined as the difference between both equations as,

$$\Delta P = P_P - P'_P = \rho_w g H_s \tag{C.4}$$

or just equal to $H_s$ in meters units.

Linear regression for P1 and P3 data are presented in Figures 48 and 49.

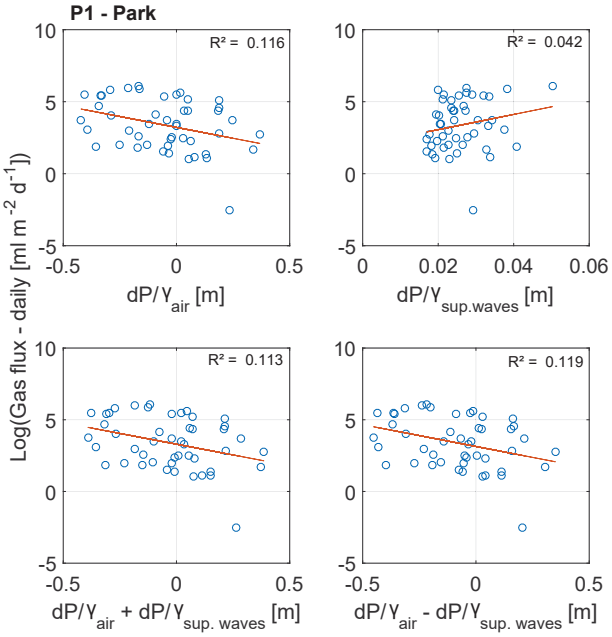


Figure 48: Linear regression of gas flux from P1 and changes in the atmospheric pressure, bottom pressure due to surface waves, and the combination of surface waves with atmospheric pressure considering daily data.

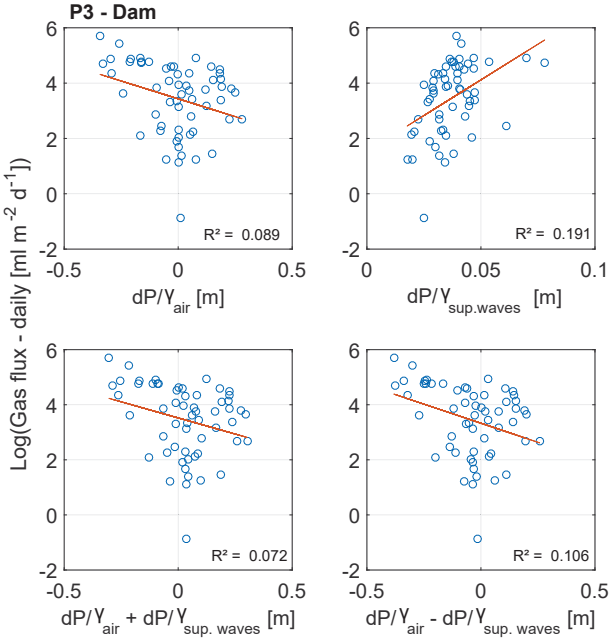


Figure 49: Linear regression of gas flux from P3 and changes in the atmospheric pressure, bottom pressure due to surface waves, and the combination of surface waves with atmospheric pressure considering daily data.